INVESTIGATION OF FRACTURE BEHAVIOR OF
STEEL/STEEL LAMINATES

A THESIS SUBMITTED TO
THE GRADUATE SCHOOL OF NATURAL AND APPLIED SCIENCE
OF
THE MIDDLE EAST TECHNICAL UNIVERSITY

BY

MEHMET ŞİMŞİR

IN PARTIAL FULFILLMENT OF THE REQUIREMENTS FOR THE DEGREE OF

DOCTOR OF PHILOSOPHY

IN

THE DEPARTMENT OF METALLURGICAL AND MATERIALS ENGINEERING

MARCH 2004

Approval of the Graduate School of Natural and Applied Sciences.

<div style="text-align: center">

Prof. Dr. Canan ÖZGEN
Director

</div>

I certify that this thesis satisfies all the requirements as a thesis for the degree of Doctor of Philosophy

<div style="text-align: center">

Prof. Dr. Bilgehan ÖGEL
Head of Department

</div>

This is to certify that we have read this thesis and that in our opinion it is fully adequate, in scope and quality, as a thesis for the degree of Doctor of Philosophy.

<div style="text-align: center">

Prof. Dr. Tayfur ÖZTÜRK
Acting Supervisor

</div>

Examining Committee Members.

Prof. Dr. Mustafa Doruk

Prof. Dr. Tayfur Öztürk

Prof. Dr. Ahmet Avcı

Assoc. Prof. Dr. M. Uğur Polat

Assoc. Prof. Dr. Cevdet Kaynak

ABSTRACT

INVESTIGATION OF FRACTURE BEHAVIOR OF STEEL/STEEL LAMINATES

Şimşir, Mehmet

Ph.D., Department of Metallurgical and Material Engineering

Acting Supervisor: Prof. Dr. Tayfur Öztürk

March 2004, 99 pages

A study is carried out into fracture behavior of steel/steel laminates both experimentally and through finite element analysis (FEM). The laminates produced by hot pressing consisted of low carbon and medium carbon steels with two volume fractions; 0.41 and 0.81. Fracture toughness, J_{IC} has been measured using partial unloading technique assuming a critical value of crack extension. The technique is initially applied to monolithic material and then to the laminates in crack divider orientation. Evaluation of fracture toughness of laminates indicates that there is a substantial improvement of J_{IC} with increase in the volume fraction. The systems under study were also evaluated by FEM modeling with the use MARC package program. To evaluate J_{IC}, the problem has been evaluated in several steps; first two-dimensional plane strain problem is considered. This is followed by three-dimensional case and then by an artificially layered system, all for monolithic materials. Values of J_{IC} derived were close to one another in all cases. Following this verification, the method, as implemented in layered monolithic system, was applied to laminates. This has shown that J_{IC} of laminates can be predicted using FEM analysis, including the delamination. Values of J_{IC} varied in the

same manner as the experiment verifying that fracture toughness in the current system increases with increase in volume fraction. It has been concluded that modeling as implemented in this work can be used for useful composite systems incorporating hard/brittle reinforcements both in crack divider and crack arrester orientation.

ÖZ

ÇELİK-ÇELİK LAMİNE KOMPOZİTLERİN KIRILMA DAVRANIŞININ İNCELENMESİ

Şimşir, Mehmet

Doktora, Metalurji ve Malzeme Mühendisliği Bölümü

Tez Yöneticisi(vekaleten):Prof. Dr. Tayfur Öztürk

Mart 2004, 99 sayfa

Bu çalışmada, çelik/çelik lamine kompozitlerin kırılma davranışları deneysel olarak ve sonlu elemanlar yöntemi ile inclenmiştir. Kompozit düşük ve orta karbonlu çelik plakalardan sıcak presleme yöntemi ile farklı hacim oranlarında 0.41 ve 0.81 üretilmiştir. Deneysel olarak, Kırılma tokluğu J_{IC}, kritik çatlak büyümesi esas alınarak, kısmi yük boşalma yöntemi ile ölçülmüştür. Yöntem önce monolitik malzemeye takiben de çatlak bölücü oriantasyonlu tabakalı malzemeye uygulanmıştır. Çalışma tabakalı malzemede kırılma tokluğunun artan orta karbonlu çeliğin oranı ile arttığını göstermektedir. Tabakalı malzemede kırılma tokluğu sonlu elemanlar yöntemi MARC paket programı kullanılarak incelenmiştir. Kırılma tokluğunu tespit etmek için, monolitik malzemeler için birkaç step uygulanmış ve önce iki-boyutlu düzlemsel gerinme durumu dikkate alınmış sonra üç boyutlu durum ve son olarakta suni olarak tabakalı malzeme sistemine geçilmiştir. Kırlma tokluğu değerleri her durum için bir birlerine yakın olduğu bulunmuştur. Bu doğrulamadan sonra tabakalı sistem monolitik sistem, tabakalı malzemelere uygulanmıştır. Tabakalı malzeme sisteminin kırılma

tokluğu, tabaka ayrılmasınıda içine alarak sonlu eleman yöntemi ile hesaplanmıştır. Bulunan sonuçlar deneyle uyumlu olarak kırılma tokluğunun artan orta karbonlu çeliğin oranı ile arttığını göstermektedir. Bu çalışmada uygulanan model çatlak bölücü ve çatlak engelleyici oriyantasyonlu sert/kırılgan takviyeli kompozit malzemelere uygulanabilirliği sonucu elde edilmiştir.

Anahtar Kelimeler: Tabakalı malzemeler, Kırılma tokluğu, Tabaka ayrılması, Sonlu Eleman Methodu, Kısmi yük boşalma yöntemi, Tabakalı malzemeyi oluşturan fazların hacim oranı, Arayüzey dayanımı.

To My Son, Wife, and Parents...

ACKNOWLEDGEMENTS

TABLE OF CONTENTS

CHAPTER I

INTRODUCTION

Unexpected failure in systems and parts is quite common. A number of these failures have been due to poor design. However, it has been discovered that many failures have been caused by pre-existing flaws in materials that initiate cracks that grow and lead to fracture. This discovery has lead to concept of fracture mechanics. The process of fracture can be considered to made up of two parts; crack initiation and crack propagation, which may occur either in brittle or ductile manner

The basic idea of fracture mechanics is to predict the load caring capabilities (i.e. energy absorb capability) of structure and components containing cracks. Almost all designs and standard specifications require the definition of tensile properties for a material, these data are only partly indicative of inherent mechanical resistance to fracture in service. Except for the situations where the large yielding or highly ductile fracture represent limiting fracture condition, tensile strength and yield strength are offer insufficient for the design of failure resistance structures. The fracture mechanic approach is based on a mathematical description of the characteristic stress field that surround any crack in a loaded body. When the region of the plastic deformation around a crack is small compared to, the size of the crack (as is often true for large structures and high strength materials) the magnitude of the stress field around a crack is related to the stress intensity factor, K.

In general, when the material thickness and the in-plane dimensions near the crack are large enough relative to the size of the plastic zone, then the value of K at which growth begins is a constant and is at its minimum. This is referred to as the plane strain fracture toughness factor, K_{IC} of the material. K_{IC} is particularly important in material selection because, unlike other measures of the toughness, it is independent of the material configuration.

Originally, the field of the fracture mechanics was limited to relatively high strength materials, i.e. materials that behave nearly linear elastic manner. Recent advancements in the field, such as R-curve and J integral methods have extended the use of fracture mechanics to elastic-plastic conditions. Thus, the evaluation of stable crack growth was possible in lower strength materials and smaller section sizes. J integral is simply the change in energy stored when the crack advances a unit length. J_{IC} refers to a critical value of this energy so that the crack grows in a stable manner, before catastrophic failure. In the elastic case, J integral is the strain energy release rate.

In this study, fracture toughness, J_{IC} of steel-steel laminates is investigated. Since J_{IC} is normally used where fracture involves substantial plastic deformation the laminates prepared involved soft and hard layers each with sufficiently high ductility. The study involves two parts. In one, the fracture toughness was evaluated experimentally with the use of partially unloading compliance technique. In the other, a predictive study was carried out for toughness of first monolithic material and then for the laminates based on finite element analysis. The study aims to determine the applicability of FEM modeling for prediction of J_{IC} in layered composite systems.

CHAPTER II

MODELING OF FRACTURE TOUGHNESS WITH FEM

2.1. Modeling of Fracture Toughness of Monolithic Material

From a micromechanics viewpoint, simple models were proposed by Mc Clintock (1968), Rice and Tracy (1969) for crack initiation and propagation. From a macromechanics viewpoint, first modeling of crack tip blunting followed by propagation was given with node release technique for 2D analysis Kobayashi (1973), De Koning (1975), Light et al (1975) and with stiffness reduction technique for 2D analysis by Andersson (1974,1975), and Newman and Armen (1974).

J-integral method was first proposed by Rice 1968. Since then many studies have been carried out that concerned with adaptation and application of this technique to finite element method. Using either incremental plasticity or deformation plasticity theory (Kishimoto et al (1980), Dadkhah and Kobayashi (1989), Fraisse and Schmit (1993), Freg and Zhang (1993) have shown that J line integral is path independent provided that integration path was located far from crack tip. The studies by McMeeking (1977), Sivaneri et al. (1991), Stump and Zywicz (1993) have shown when the path is within the plastic zone J integral is path dependent

A variety of techniques has been proposed over the years for numerical evaluation of various parameters of fracture mechanics, i.e. Stress intensity, J integral, Strain

Energy Release Rate. Chan et al (1970) used Direct Displacement Extrapolation Method to calculate the stress intensity factor. Parks (1974) proposed Virtual Crack Extension Method (VCEM) to calculate J integral values for elastic case. In this method, the growth of crack front was calculated from a change in potential energy. This method was extended by Parks (1977) to non-linear material behavior in terms of finite element method. De Lorenzi (1982) gave a derivation of this in terms of continuum mechanics. Irwin (1957) proposed Crack Closure Integral Method (CCIM) to calculate strain energy release rate. In this method, strain energy release rate is expressed in terms of the stresses (nodal forces) ahead of the crack tip and the displacement behind it. Rybicki and Kanninen (1977) calculated stress intensity factor by Modified Crack Closure Integral Method to get simple formula for the 2D four-node element. Raju (1987) applied Virtual Crack Closure Method to calculate the strain energy release rate for isotropic materials. Roeck and Wahab (1995) derived expressions based on Irwin's crack closure integral method to calculate strain energy release rate for 3D singular and nonsingular elements. A comparison of these methods was given by Bleackley and Luxmoore (1983), Wahab and Roeck (1994).

Satisfaction of equilibrium conditions and derivation of shape function of elements are important especially for the higher order element in the application of FEM (Lamain, 1985). Nagtegaal et al. (1974) derived the incompressibility constraints for commonly used elements. Nagtegaal et al. (1974) pointed out that if the number of elements is increased, the solution convergences more easily. This is the case if the number of degree of freedoms in a mesh increases faster than the number of incompressibility constraints.

Meshing can be carried out either manually or through automatic mesh generator. Manual meshing takes long time and increases the possibility of mistake. Therefore, the details of meshing are important in the finite element analysis. The mesh modification strategy is based on a minimization of interpolation error (Demkowich and Oden (1986). This method was applied to conformal map type mesh generation for quadrilateral mesh only. Sandhu and Liebowitz (1995) worked on the

hierarchical adaptive meshing for 4-node Reissner-Mindlin plate bending element. It was stressed that the automatic adaptive algorithm can be effective in achieving a high level of accuracy. An optimal mesh according to Sandhu and Liebowitz is one, which the discretization errors are of the same order for all elements, so that the total error is equidistributed between all elements in the mesh.

Lee and Lo (1995) presented an adaptive mesh refinement procedure for triangular and quadratic elements in 2D elasticity problems. According to this procedure, only size of the elements is allowed to change during successive refinement steps while the order of polynomial for the shape function used is kept constant. It was concluded that if the domain geometry is simple and regular, mixed and quadrilateral meshes are more efficient than triangular mesh. If the domain geometry was complex, the use of quadrilateral element in the mesh might not improve the accuracy of the solution. Liebowitz (1995) applied adaptive mesh algorithm for crack tip in 2D analysis to calculate the stress intensity factor. It was determined that applying adaptive mesh refinement increases the accuracy of stress intensity factor.

The choice of crack tip element; type and the size is important in calculation of stresses and strains in the plastic region ahead of the crack. Crack tip can be modeled by singular or nonsingular elements or by collapsed degenerated element. Nagtegaal (1974) showed that conventional 4-node element is not suitable for the analysis of the fully plastic region. De Lorenzi and Shih (1977) concluded that 8-node isoparametric element is suitable for fully plastic analysis. Barsoum (1976) presented singularity in the strain field by quarter point technique. For 2 D analysis, 8-node isoparametric quadratic element and 8-node collapsed elements were used in this study. For 3D analysis, the elements were 20-node brick and 20 node collapsed brick. Quarter point technique was applied to all models. The best results were obtained with 8-node collapsed element for 2D analysis and 20-node degenerated collapsed brick element for 3D analysis. Raju (1987) examined the effect of element type for a fixed size element (1/16 th of crack length) for center crack tension specimen using 8-node parabolic and 12 node cubic elements. The specimen was

analyzed in a variety of elements; regular parabolic elements everywhere, regular parabolic element with quarter point technique at the crack tip, cubic elements everywhere and cubic elements with singularity elements at the crack tip. Comparisons with reference solutions from the literature showed that strain energy release rate was calculated more accurately from the models with singularity elements.

Shivakumar and Newman (1989) modeled crack tip element size as 0.4 mm for constant strain triangular element. This element size was selected because previous studies had shown that this mesh size provides accurate modeling of stable crack growth behavior for a variety of materials. DeGiorgi et al. (1989) modeled crack tip with elements of a size of 4 10^{-3} of total crack length. 8-node continuum element was used. The finite element mesh was more refined in regions surrounding the crack tip than remaining portion of the model. No crack tip singularity was used in this model. Fernando et al. (1995 a, b) presented a methodology for crack tip mesh design, which compares the geometric parameters against the accuracy of the finite element solution. Degenerated quadrilateral with quarter point element was used for crack tip element. Meshing was carried out based on semi circular rings centered on the crack tip element. Optimal mesh was obtained in terms of the ratio of uncracked ligament/crack length, and the number of rings, the number of elements in the ring. It was concluded that for optimal design the use of at least five semi circular rings, each comprising at least 8 elements were necessary with the ligament ratio between 0.91 to 1.01. Kuang and Chen (1996) using 8-node plain strain element with collapsed node have examined element sizes of 8 10^{-3}, 4 10^{-3}, 2 10^{-3} and 4 10^{-4} of total crack length in concentric rings. The element size as well as the size of the ring was increased gradually in regions away from the crack tip.

The crack will initiate and start to propagate when the material reaches a defined fracture criterion. A various criteria have been proposed over the years; crack tip opening displacement (CTOD), crack opening displacement (COD), crack opening angle, strain energy release rate, work density over a process zone, J integral in the elastic plastic behavior etc. Shih et al. (1979) suggested fracture parameters based

on J integral and CTOD for the characterization of crack initiation and growth. Yagawa et al. (1984) used experimental relationship between load line displacement verses crack extension data as a fracture criterion for J integral evaluation. The relation between load line displacement and crack extension was formulated as second order polynomial equation determined from the experimental data with least square technique. Newman (1985, 1988,) and Shivakumar and Newman (1989) used a critical value of CTOD as fracture criterion.

Shivakumar and Newman (1989) in the above study used 3-point bend specimen to evaluate the fracture toughness of HY 130 steel. Samples with a variety of initial crack length (i.e. a0/W ranging from 0.1 to 0.8) were used. The critical CTOD value was selected for a_0/W=0.6 sample corresponding to a maximum load on the load-TOD curve. The J value determined experimentally as well as through FEM analysis, which gave a value of 83 kJ/m2, was close to each other. De Giorgi et al. (1989) used critical strain energy density as a fracture criterion to predict the stress intensity factor and J integral values for HY 100 steel at crack initiation for compact tension specimen. 2D and 3D analysis were carried out. Difference between the experiments and the analysis were small. Cordes and Yazıcı (1993) used a critical value for energy release rate determined experimentally, and inserted this into finite element analysis. Shan et al. (1993) used a value of the crack opening angle as critical value to predict crack initiation and growth. Elangovan (1991) formulated a method for generating resistance curves that requires two parameters: the critical stress intensity factor K_c and its value at crack initiation K_o. Amini and Wnuk (1993) postulated that energy dissipated incrementally during fracture is invariant to during the crack growth. Cordes et al. (1995) have used a critical value of CMOD for determination of K_{IC} for experiments and for FEM analysis. The value taken corresponds to 5% deviation from initial slope of load-crack mouth opening displacement (CMOD). This criterion is consistent with ASTM E399 under brittle fracture condition. It was stated that at the 5% deviation, sufficient amount of irreversible work has been introduced into the specimen to cause crack initiation. Cordes et al state that the criterion may be applicable to a variety of materials both high strength and low strength. Kuang and Chen (1996) used a fracture criterion

based on plastic zone size. In the study, the value of J integral was evaluated along various paths around the crack tip. J integral would be path dependent if the selected path cannot fully enclose the plastic zone. Otherwise, the J integral will be path independent. Therefore, the critical size of plastic zone is that of plastic zone of minimum radius yielding path independent J value. Dhar et al. (2000) proposed a criterion based on the initiation of local crack growth. Two parameters were defined critical damage as a continuum parameter and average austenite grain size as a characteristic length. The critical length parameter denotes the distance ahead of the crack tip where the continuum parameter has to reach its critical value for micro crack initiation. In the study, AISI 1095 spherodised steel was used. J_{IC} values were predicted 72.44 kN/m for 3-point bend specimen, 73.78 kN/m for compact tension specimen. The values were slightly higher than the experiments

Sakata et al. (1983) examined the variation of J integral across the thickness of the sample. It was found that J integral increases from surface to the center reaching its maximum value at the midsection. Dodds et al. (1988) in a similar analysis found that J integral values at the midsection are slightly higher than experimental J values.

2.1.1. Modeling of Crack Growth

Lamain (1985) used three techniques to examine crack growth; nodal release, nodal stiffness reduction and the node shifting. In the nodal release technique, the crack is extended by releasing the nodes in the crack plane. The sign of reaction forces were reversed on the newly surfaces. The smallest amount of growth is equal to the length of the element at the crack tip. The node release will cause a severe loading situation at the crack tip, so increment of the load should not be kept quite small. If higher order elements are used, the corner node and the midside node should be released at the same time. It was found essential that the elements in the crack plane should be small compared to the crack length. Nodal stiffness reduction technique is similar to nodal release technique and differs from it the way that nodes are released. The displacements in the crack plane are not prescribed in the direction of the crack

plane, but the stiffness is increased in the diagonal term of the stiffness matrix where a new surface is created. The practical way of doing this to add spring elements of required stiffness. In the node shifting technique, if the node at the crack tip is displaced to the node of the next element in the plane of the crack, it can be released. After releasing the node, stress is redistributed in an iterative manner over the elements and the find the acceptable distribution. First two methods can be used for 2D but not for the 3D models. Node shifting can be used for 2D as well as for 3D analysis. According to Lamain (1985), if large crack extension is modeled, node shifting can be combined with node release or nodal stiffness reduction techniques.

2.2. Modeling of Fracture Toughness of Composite Materials

Modeling of fracture behavior of composite materials is more complex than monolithic materials. Differences in the mechanical behavior of each phase must be incorporated into the model. Additionally, interfaces and the size and shape of constituent phases must be taken into account.

Williams (1959) was the first to study the problem of a crack in the plane of the interface between two dissimilar isotropic materials. He found that this geometry leads to oscillations of stress and strain in the crack tip and as a result, crack faces interpenetrate or overlap with each other. Rice (1988) proposed two concepts, mode mixity and small-scale contact zone. If the contact zone is small scale, complex stress intensity factor could be used in Linear Elastic Fracture Mechanics. Parhizgar et al. (1982) examined the application of Linear Elastic Fracture to orthotropic composite materials by finite element method. Stress intensity factor was calculated by using Wastergard's equation.

Gdoutos et al. (1999) carried out modeling that takes into account the debonding of interface in a tough fiber reinforced composite with a brittle matrix. K_I, K_{II} and strain energy release rate, G were calculated using Airy function proposed by Zak and Williams (1963). Chen and Sih (1980) developed Laminated Plate Theory by

application of minimum complementary energy theorem in variation calculus. Normalized stress intensity factor was predicted for three-layered composite system.

Oscillatory singularity causes difficulty in the analysis of fracture behavior of composite materials. Therefore, recent work concentrated on the strain energy release rate for characterizing the composites. Malyshev and Salganik (1965) was the first to derive the expression for total strain energy release rate, G_T. Rice and Sih (1965), Comninou (1977) Hutchinson et al. (1987), Sun et al. (1987, 1989), Monaharan and Sun (1990) described G_T and in terms of its components, G_I and G_{II}. Sun and Jih (1987) calculated strain energy release rate using Virtual Crack Closure Integral Method (VCCIM) by neglecting the oscillatory singularity terms where they are present. It was found that G_I and G_{II} depend on the choice of assumed crack extension. When small crack extensions are used, G_I and G_{II} approach to half of G_T. Minimum crack extension can be the size of crack tip element. Raju et al. (1988) calculated strain energy release rates for edge delaminated composites using Virtual Crack Closure Integral Method (VCCIM). It was found that when oscillatory term is taken zero, G_I and G_{II} converge as well as G_T. Dattaduru et al. (1994) calculated G_I, G_{II} and G_T of the interface crack by Modified Crack Closure Integral technique. The same techniques is also used by other workers; Rybicki and Kaninnen (1977), O'brien (1982), Buchholz (1984), Krishnamuthy et al. (1985), Raju (1987), Sethuraman and Maiti (1988).

Dattaguru et al. (1994) considered he crack lying in one of the material near and parallel to the interface. The distance between the crack and the interface is reduced to zero at the limiting case. It was concluded that with decrease of the distance G_{II} becomes a more dominating term in G_T Buchholz et al. (1997) modeled the fracture behavior of composite taking into account the effect of delimitation. G_I, G_{II} and G_T were predicted. When the interface was friction free G_I approaches almost zero and G_{II} equals almost G_T. When the friction coefficient is increased, G_I increases, G_{II} decreases but it is still dominant in G_T. Han et al. (2002) worked on fracture behavior of honeycomb core composite taken into account the effects of delamination. Applied loads at a given crack length from computational results were

10 to 30% higher, but the growth of delamination were close to the experiments. Simha et al. (2003) found that that if the interface is flat and the crack is initially parallel to the interface, material inhomogeneity has less effect on crack driving force. Thus, the interface does not have an immediate influence on crack growth. However, if the strain field is perturbed the interface influences the crack growth.

Studies above refer to crack parallel to the interface. Chen and Wu (1980) considered crack perpendicular to the interface, i.e. crack arrester orientation. Crack being placed at interface between two dissimilar materials. Crack was pressurized. Nonhomogeneous structure was divided into three different homogeneous regions. Stress intensity factors were determined by adding J integral values, using concept proposed by Karlsson and Backlund (1978), of the three homogeneous regions. Gdoutos et al. (1999) investigated fiber debonding when the annular crack was placed perpendicular to the fiber orientation. Loading was applied parallel to the fiber direction. K_I, K_{II} and strain energy release rates were calculated. Simha et al. (2003) modeled the perpendicular cracks in two modes; in one, the crack is placed far away from the interface and the other the crack is placed near the interface. Two conditions were compared with respect to energy considerations.

In terms of modeling of interface, Raju et al. (1988) used Bare Interface for the analysis of isotropic and orthotropic materials. In this model, the thickness of the interface is zero. The same method was also used by Dattaguru et al. (1994). Raju et al. (1988) modeled the interface by Resin Layer Model. In this model, the interface consists of a resin layer between the two dissimilar materials. The thickness of the resin layer is adjusted in relation to the element size used for crack tip. Han et al. (2002) modeled the interface with cohesive element with the use of 8-node 3D element of zero thickness. Similar elements were used by De Andres (1999), Ortiz and Pandolfi (1999). Simha et al. (2003) modeled the interface by a Gradient Layer that is a transition region between two dissimilar materials. The properties change linearly in this model so that, continuous transition was satisfied between the two homogeneous materials.

The effect of interfacial strength or energy on fracture toughness of composites was investigated by Yang and Qin (2001). Interfacial energy was used as fracture criteria for fiber debonding. When interfacial energy is low, debonding takes place easily. When the energy is high, fracture process is dominated by fiber fracture. It was found that as volume fraction of fibers is increased, the average stress increases in the composite. Han et al. (2002) for modeling of delamination in the honeycomb core composites used a critical interfacial energy as fracture criterion

Effect of layer thickness on the fracture toughness of composite was investigated by Chen and Sih (1980). Three-layered system consisting of a different mid layer was investigated. The crack was located along the thickness in the mid layer. The stresses were found to change parabolically along the thickness of the mid layer and reaches maximum at the center plane. When thickness of the mid layer is increased relative to crack length, there is an increase in stress intensity factor. Gdoutos et al. (1998) examined the effect of fiber length on the fracture toughness.

The effect of fiber orientation on the fracture toughness of the composites was investigated by Parhizgar et al. (1982). It was concluded that when the fiber and the crack are parallel i.e. $\alpha=0^o$, K_{IC} has the lowest value and the crack grows in the same plane. When $\alpha=45^o$, K_{IC} increases and reaches its highest at $\alpha=90^o$.

The effect of material properties on the fracture toughness of a three layered composite was modeled by Chen and Sih (1980). The stress intensity was high at $E_{mid}/E_{outer}=0.5$ whereas with $E_{mid}/E_{outer}=2$ stress intensity was found to be low. Simha et al (2003) examined the crack tip driving force for crack arrester orientation in a bimaterial composite (Al/Steel). When the crack was located in the soft layer, the crack driving force as found to be negative and J_{tip} is less than J_{far}, then the interface inhibits the crack growth and vise versa.

2.3. Experimental Measurement of Fracture Toughness

In Linear Elastic Fracture Mechanics, the measurement of plain strain fracture toughness K_{IC} is a standard method to investigate the material behavior of brittle materials. To determine the K_{IC}, load- load line displacement curve is obtained from a standardized test piece such as compact tension, three point bend (Kaufman, 1977, Zhao and Tuler, 1994). Typical load –load line displacement curve is shown below, Fig.2.1. In the method, it is assumed that there is a very small plastic zone at the crack front and the crack grows in the same plane with the initial crack. According to the standard, P_Q, i.e. load determined given by a line drawn parallel to the initial slope at a prescribed offset is the basis for the calculation of stress intensity coefficient K_Q. This coefficient evaluated in a manner described in the relevant standard (e.g. ASTM E-399) is considered equal to K_{IC} provided that the validity criteria are satisfied, $P_{max}/P_Q \leq 1.1$ and thickness of the specimen, B or uncracked ligament, $b_o \geq 2.5 (K_Q/\sigma_y)^2$.

Morozov (1979) reexamined the validity criterion and stated that the factor of 2.5 should be varied between 0.5 and 5 depending on the condition. He proposed an evaluation procedure based on P_{max} instead of P_Q in the calculation of K_{IC}. Zaho and Tuler (1994), Balton and Gant (1998) have evaluated K_{IC} of metal matrix composites with reinforced particles. Osman et al. (1997) in an investigation on laminated composites, noting that the crack did not grow in the same plane, calculated the fracture toughness in terms of three parameters, K_Q based on P_Q, K_C based on P_{max}, K_{ee}, (equivalent energy toughness) based on P_e (defined in ASTM E992).

Hwu and Derby (1999) determined K_{IC} of laminated composites both for crack divider and crack arrester orientations. For the crack arrester orientation, there was serration in the load-load line displacement curve beyond the maximum load. This was attributed to renucleation of crack in soft and hard phases. The minimum is that of renucleation of crack in the soft phase and the maximum is due to renucleation of crack in the hard phase. For crack divider orientation, there was no serration and P_Q

could be determined quite easily. Chung et al. (2002) evaluated the investigated crack initiation toughness K_c for metal/intermetallic laminated composites for crack divider and crack arrester orientations. Rohatgi et al. (2003) in a similar system measured K_{IC} based on P_Q and K-resistance curve using acquisition system to collect the load, load line displacement data and the crack lengths were measured using video analyzing system
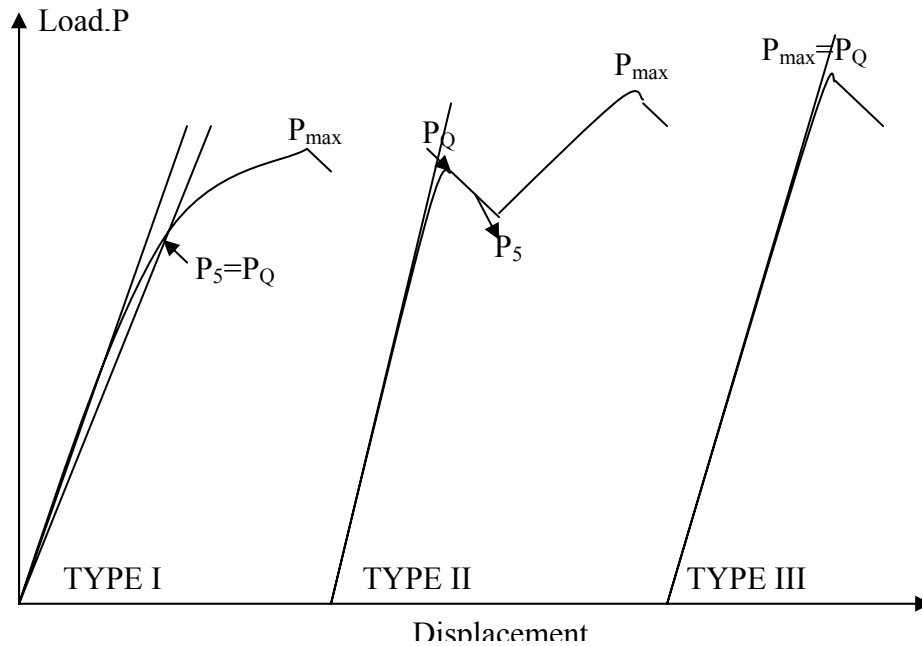

Figure 2.1. *Typical load-displacement curves for K_{IC} tests. P_Q is the basis for the calculation of K_{IC}, see text and ASTM E399 standard for details.*

Jeng et al. (1991) calculated critical crack initiation energy and total work of fracture energy experimentally for fiber metal matrix composites. Chevron notched the three point bend specimens was used, so that crack grew in the same plane. Load-deflection curve was obtained under a constant crosshead speed. The critical crack initiation energy was defined as the area under load–deflection curve at up to a discontinuity in the curve. The total work of fracture energy was considered to be equal to the total energy absorbed during the entire fracture process i.e. total area in the load-deflection curve.

Papanicolous and Bakos (1995) measured interlaminar fracture toughness in terms of G_{IC} by a new approach. In this approach, maximum displacement δ_{max} was found

based on P_{max}. An offset line parallel to initial slope was drawn at $0.1\delta_{max}$. G_{IC} was calculated based on the load P_c given by this offset line.

In studies referred to above, different specimens were used for fracture toughness testing. Bend specimens were used in a variety of studies, e.g. Balton and Gant (1998), Hwu and Derby (1999), Rohatgi (2003) Chung et al. (2002) for particulate metal matrix, metal/ceramic, and metal/intermetallic laminated composites In some of the other studies compact tension specimens were used e.g. Osman et al. (1997) for metal/intermetallic laminated composite.

Testing may be varied out with load control Lou et al. (2002) or displacement controlled condition. The latter in some studies were in the form of stroke control, Balton and Gant. (1998). Testing under displacement control is more common Hwu and Derby (1999), Chung et al. (2002), Rohatgi (2003). The rate varies from 0.01 mm/min up to 0.5 mm/min. In the case of stroke control, the rate may be as high 10 mm/min. The tests with the displacement control or stroke control can be continued beyond the maximum load whereas under the load control the testing is limited up to the maximum in the load.

In elastic-plastic fracture mechanics, the use of J-Integral and strain energy release rate, G is more common. Detailed description of J-Integral testing will be given in Chapter IV and therefore will not be described here.

Experimental procedure for the determination of fracture toughness in terms of J-integral was first developed by Begley and Landes (1972). He proposed two procedures one is based on the use of several specimens, i.e. multiple specimen technique, and the other is based on the testing of a single specimen, i.e. single specimen technique. In order to establish their reliability, two Round Robin test programs were carried out. Materials in these test programs were monolithic, namely HY 130 and A533B Class1. Various aspects of the test program have been reviewed in a number of papers by Clarke et al. (1979a, 1979 b, 1980 and by Gudas and Davis (1982). It has been concluded that the procedure proposed by Begley and

Landes (1972) for fracture toughness testing of J_{IC} or crack resistance curve, J-R with the use of either multiple specimen technique or single specimen yield results, which are quite reliable. The value of J_{IC} for HY 130 was given as 210-140 kJ/m^2 with 95% confidence band

A typical load-displacement curve for multiple sepecimen technique is given in Fig.2.2. J integral value refers to area under the curve as depicted in Fig. 2.2(b). The method requires the use of at least five identical samples that are loaded to different displacement values. The method requires the measurements of crack growth, Δa, at each value of displacements. Each specimen delivers only one J-Δa data point of the J_R curve. From all data, collected J_{IC} is derived as described in ASTM E813 standard.

(a) **(b)**
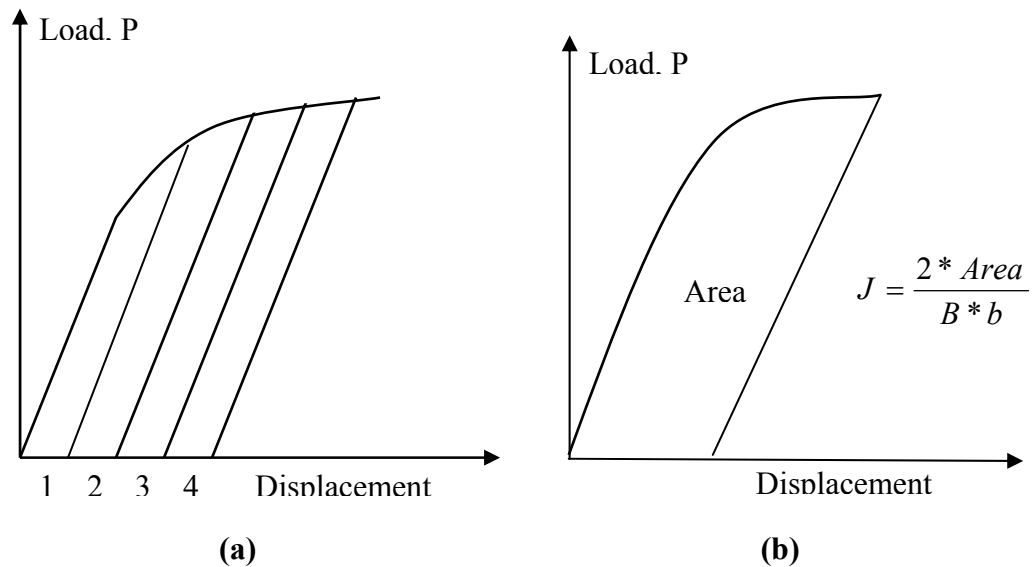
Figure 2.2. a) *Typical load-displacement curves for each specimen in multiple specimens test b) calculation of J-Integral*

In the case of single specimen technique, crack growth is normally measured indirectly via a variety of methods; electrical potential drop, ultrasonic testing and resonant frequency or compliance method. In electrical potential drop, constant current is applied to the test specimen. As the crack advances, this causes a change in the electrical resistance. Change in resistance is a measured as an increase in potential between the two measurement points. The output, i.e. the potential can be

monitored a typical curve is given in Fig. 2.3, while the load-LLD curve is recorded. If correctly interpreted the potential output gives an instantaneous measure of crack length as a function of displacement. A disadvantage of this method is plastic deformation and the void formation ahead of the crack tip, which increases the material's resistivity. Schwalbe et al (1985) has used this technique to follow the stable crack growth in a number of steel and aluminum alloys
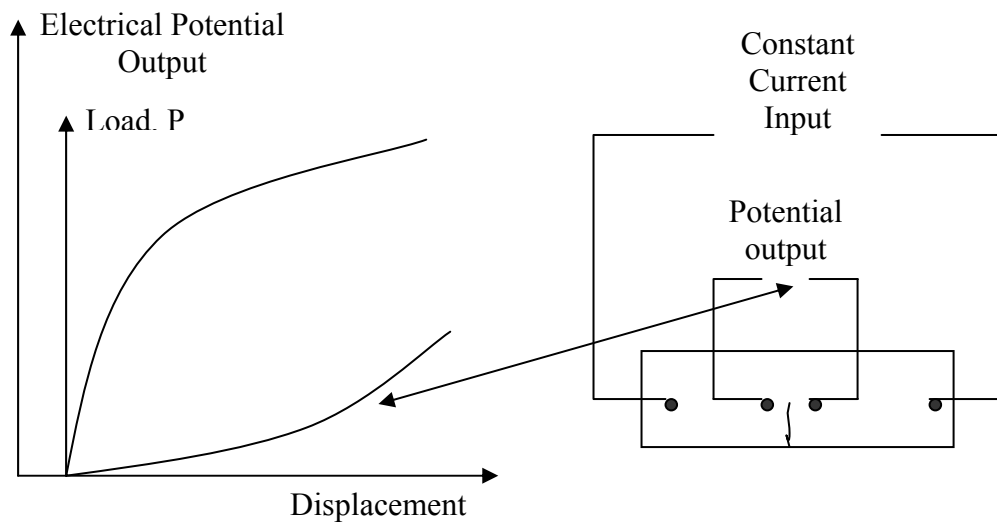

Figure 2.3. *Typical load-displacement and electrical potential-displacement curves for potential drop test method for 3 point bend specimen.*

Another test method is ultrasonic testing. As given by Underwood et al. (1976), this involves transmitting an ultrasonic wave from the back of the specimen parallel to the crack plane. The blunting tip of the crack during a J_{IC} tests can be monitored by the transducer. A disadvantage of this method is some false indications that are caused by large geometry changes during the plastic portion of the loading. Clarke et al (1980) used to this method to measure the crack advance in HY 130 steel for four point bend test.

Resonant frequency method involves the monitoring crack advance via measurement of small changes in the resonant frequency of the test specimen. Hickerson (1976) has used this method to develop curves of J versus Δa.

The most widely used method to determine the crack growth is the compliance method in partial unloading. A typical load-displacement curve that involves partial unloading is given in Fig. 2.4. The method is based on a change in compliance of the sample during successive unloading. Details of the procedure are given in the Chapter IV. Gudas and Davis (1982) reported the result of the round robin test program for compliance method. They have concluded that the ratio of actual crack extension to those measured by compliance method varies from 0.42 to 2.918. Futato et al. (1985) has show that accuracy of the compliance method depends on the linearity and accuracy of load transducer and of clip on gage, as well as on how precisely the dimensions of the test piece and its elastic modulus is measured.
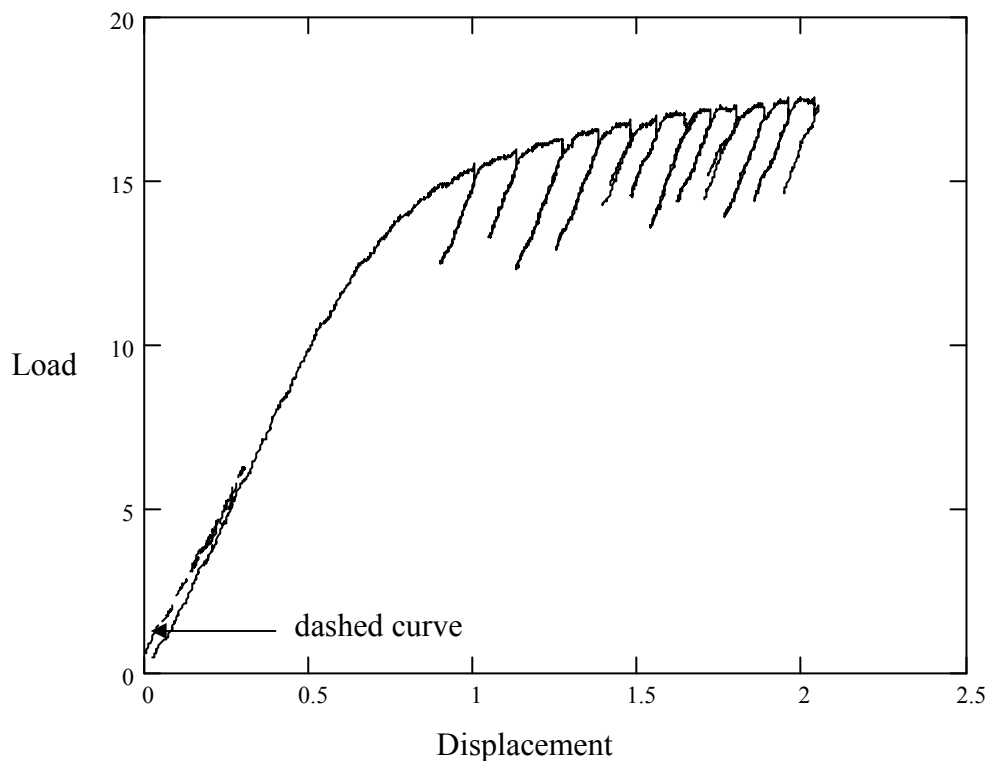
Figure 2.4. Typical load-displacement curve for partial unloading compliance test method for J integral testing. Dash curve for a_o, the others for different crack lengths.

Hollstein et al. (1985), in determining the J initiation and J–R curve, have compared compliance method with potential drop method. They have concluded that both methods underestimate the crack growth.

Monaharan, et al. (1990, b) and Pandy et al. (2001) have applied the compliance method to laminated composites. In the former, the test was carried out under stroke control at a crosshead speed of 25 μm/min, and displacements were measured across the crack mouth using clip-gage. J resistance curve was constructed following the standard procedure for plain strain J-integral estimation, ASTM E 813. Pandy et al. (2001) used compact tension specimen with constant 0.002 mm/min displacements. COD values, measured by a clip on gage placed on the crack were transformed to load line displacement values by a suitable formulation. J_{IC} for 0.2 mm crack extension was determined. Pandy et al. (2001) in this study also compared crack extension values physically measured from the fracture surface with those derived from the compliance method. The difference was 5-10%.

CHAPTER III

FRACTURE TOUGHNESS OF METAL MATRIX COMPOSITES

Metal matrix composites may be in the form of particulate or fiber reinforced or in the form of laminates. Here, fracture toughness of composites is briefly reviewed with emphasis on physical parameters, e.g. volume fraction, thickness of the reinforcement.

3.1. Particle Reinforced Metal Matrix Composites

Xia (2002) examined the effect of the volume fraction on fracture toughness of Al2O3 reinforced Al (2xxx or 6xxx) composites Using Three point bend test he derived crack opening forces (peak of the curve) and energy absorption levels (area under the curve) from Load-displacement curves. For 6xxx series composites he obtained values of 1180 N and 250 KJ for the crack opening force and the energy. These values refer to the volume fraction of V=0.1. When the volume fraction is doubled, the values were higher by 8% and by 53 % respectively. Thus, the effect of the volume fraction on crack opening force was not very pronounced.

In the case of Al reinforced with steel and stainless steel powders, Baron et al (1997) observed a decrease in fracture toughness with increase in the volume fraction of the reinforcements. They attributed this to the formation of brittle phases between matrix and particles that fail at low stresses. Bolton and Gant (1998) worked on fracture toughness of high-speed steel reinforced with hard ceramic particles. Best results were obtained with NbC reinforcement. They obtained a value of K_{IC}=25.2

MPa.m$^{0.5}$ at a volume fraction of V=0.077 NbC. However, fracture toughness was decreased to lower values with increase in the volume fraction. Similar results are reported for Nb alloys reinforced with Cr2Nb Davidson (1999). K_{IC} value of 25 MPa.m$^{0.5}$ obtained at V=0.1 was reduced to half of its value when the volume fraction is increased to V=0.4.

Zhao and Tuler (1994) studied on the effect of particle size on the fracture toughness of SiC reinforced Al (2xxx) alloys at V= 0.10 and V=0.15. The particle size of 5.31 micron (at V=0.15) yielded a value of K_{IC}=17.2 MPa.m$^{0.5}$. When the particle size was increase to 9.88 micron, there was a slight increase (10%) in the fracture toughness. They attributed this to an increase in local plastic strains around the particles of larger sizes. They also found that the use of reinforcement with low aspect ratio leads to an increase in the fracture toughness.

Effects of interfacial strength on the mechanical properties of SiC whisker reinforced Mg composites were investigated by Zheng et al (2001). The composite produced with binders had higher values for the interfacial strength as well as better mechanical properties (ultimate tensile, yield stress, elastic modulus and elongation) than those manufactured without binders. Based on these, as well as from the examination of fracture surfaces they suggest that fracture toughness of the composite may be improved by increasing the interfacial strength.

3.2. Fiber Reinforced Metal Matrix Composites

Antolovich, et al. (1971 a) studied the effect of volume fraction in continues fiber reinforced maraging composite. The fibers were tough maraging steel and the matrix were also maraging steel but relatively brittle. When the volume fraction is increased from V=0.03 up to 0.16, the fracture toughness measured in terms of K_{IC} and G_{IC}, increases but beyond that point there was a decrease in the value. The fracture toughness of the composite was not higher than that of the matrix tested on its own. Since the fracture of the fibrous composites occurred in a stable manner, the

load displacement data were converted into crack growth resistance curves. The crack resistance was improved with the increase in the volume fraction. The R curve exhibited a serration at G_{IC}. It was showed that the increase in crack growth resistance could not be attributed to plastic deformation of the fibers and the local debonding between the fibers and matrix.

Gent and Wang (1992 and 1993) studied the effect of fiber diameter on fracture behavior of polymer composites. It was found that even for the samples with perfect adhesion between the matrix resin and fiber, interfacial failure would occur if the fiber radius was less than about one-fifth of the matrix thickness. For fibers of large radius, either fiber pull-out or matrix cracking can take place; the cracking mechanism depends on the relative level of interfacial fracture energy and the fracture resistance of the resin.

Fu and Lauke (1997) worked on the fiber pull-out energy of a composite reinforced with discontinuous fiber. The fiber pull-out energy was derived as a function of fiber length distribution, and fiber orientation distribution, as well as in terms of the interfacial properties. It was concluded that high strength fiber, a large fiber volume fraction and a large fiber diameter at a comparatively large mean fiber length were favorable for achieving a high fiber pull-out energy.

Chiang (2000) in a study on glass fiber reinforced polymeric composite examined the effect of fiber length on the fracture toughness. He concludes that fiber pull out is a dominant mechanism and therefore the fracture toughness increases with increase in the fiber length up to values less than the ineffective length.

Jeng et al (1991) considered the interfacial shear strength in Ti alloys reinforced with continues fibers in terms of a normalized crack initiation energy and fracture energy. It was concluded that the energies were higher when the matrix was tough and the interfacial energy was high. Qin and Zhang (2002) in a study on Al alloy reinforced with continuous rods of different interfacial energies arrived to the same conclusion, i.e. fracture toughness was higher with high interfacial energy. The rods

themselves were composite SiC reinforced aluminum. Also they found that the fracture toughness of the composite measured in terms of K_{IC} were higher than that of the conventional SiC reinforced Al, but lower than that measured for the aluminum without reinforcement.

3.3. Laminated Metal Matrix Composites

Chen and Winchell (1977) examined the toughness and mechanical properties in a steel/steel laminated composite combining soft and hard layers. It was suggested that toughness decreases with increase in the volume fraction of the hard layer. In addition, they conclude that two requirements should be met to optimize the strength and toughness of the composite. One is the necessity of allowing the soft layer to deform independently, i.e. weak bonding between hard and soft layers. The other is the necessity of making the soft layer thick enough so that the crack through one hard layer can not produce cracking in the next hard layer without first fracturing the soft layer in between.

Laminated composite studied by Antolovich, et al. (1971 b) contain V=0.25 tough steel plates as reinforcement in a brittle steel matrix. It was concluded that the plain strain fracture toughness of the laminates was slightly higher than K_{IC} of the monolithic brittle constituent and was independent of either crack length or the dimensions of the reinforcement. The toughness as a function of thickness exhibited a relative maximum when the tough layer was 1.02 mm thick and relative minimum when the tough layer was 1.52 mm thick.

Facture toughness of metal-intermetallic laminated composites were examined by a number of authors, Bloyer, et al. (1997), Lou et al (2002), Chung, et al (2002), Rohatgi et al. (2003). Rohatgi et al. (2003) investigated Ti-Al$_3$Ti metal/intermetallic laminated composites and measured the R-curve and fracture toughness for crack arrester and crack divider orientation. The volume fraction is varied between V= 0.65 to up to 0.8. Crack initiation toughness both at crack divider and crack arrester

orientation decreased with an increase in the volume fraction. Similar results were reported by Bloyer et al (1997) and Chung, et al. (2002) for Nb- Nb aluminides, and Lou et al (2002) for V-NiAl.

Fracture toughness of SiC-Al composite laminated with Al alloy layers were examined by Osman et al (1997). They found that the inclusion of Al layer improves the toughness as compared to that of the SiC-Al tested on its own. They also found that by modifying the thickness of Al layer from 0.45 to 1.5 mm did not produce a significant change in fracture toughness.

A similar system was investigated by Zhang and Lewandowski (1997). In this study, the laminate was in the form of SiC reinforced 7xxx Al alloy with an interlayer of 7xxx aluminum. Different interfacial strengths were obtained by changes in the heat treatment. The laminate had higher toughness than SiC reinforced Al. When the interfacial strength is low, delamination takes place before crack reaches the interface. When the strength was intermediate, the crack deflected along the interface after reaching the interface. Catastrophic propagation of primary cracks was retarded because of this delamination. When the strength was high, the crack crosses the interface and fracture continues in the neighboring layer.

Alic, (1975) worked on adhesively bonded 7xxx series aluminum alloys. He derived crack growth resistance curves both for bonded alloy and for the monolithic alloy. It was concluded for equivalent nominal stresses, that lamination could give an improvement in fracture resistance of about 50 %. A combination of 2xxx and 7xxx alloys in a similar context was examined by Alic and Danesh (1978).

The R-curve of fiber reinforced composite combined with Al layers was investigated by Macheret, and Bucci, (1993). The laminates are bonded arrangements of thin, high strength aluminum sheets alternated with plies of reinforced-reinforced epoxy adhesive. It was concluded that fiber/metal laminates behave like metal i.e. laminates exhibit slow stable crack extension before rapid

fracture, like metals. They found that the crack growth resistance was higher in the laminate based on 2xxx alloy then that based on 7xxx alloy.

CHAPTER IV

EXPERIMENTAL AND NUMERICAL PROCEDURES

4.1. Experimental Procedure

In this work, fracture toughness of two materials was studied in terms of J integral. A monolithic medium carbon steel with 0.5 %C and a laminated composite of medium carbon steel (0.6 %C) with low carbon steel (0.12 %C). Chemical composition of the materials is given in Table 4.1.

Table 4.1. *Chemical composition of the materials*

	%C	%Mn	%P	%S	%Si	%Cr	%Fe
AISI 1112	0.12 Max	0.6 Max	0.045 Max	0.045 Max	-	-	Bal.
AISI 1060	0.61	0.84	0.017	0.004	0.203	0.367	Bal.
AISI 1050	0.45-0.54	0.6-0.9	0.04	0.05	0.15-0.35	-	Bal.

4.1.1. Mechanical Properties of Materials

4.1.1.1. Tensile Test

In order to characterize the steel plates, standard tension test specimens were prepared from longitudinal (rolling) direction. Tensile tests were carried out in accordance with ASTM E 8M-93. Monolithic medium carbon steel was used as received, i.e. as –hot rolled condition. For laminates, sheets of medium carbon and low C steel were heat treated with the same procedure as the laminate (see below). This involved, for medium carbon steel, austenitizing at 830 °C for 15 min. followed by quenching in oil, and subsequent tempering at 550 °C for 6 hours. The treatment for low carbon steel involved annealing at 550 °C, for 4 hours.

Tensile tests were carried out in a hydraulic test machine. Yield stress and UTS values of the materials are given in Table 4.2. In heat-treated condition, the strength of the constituents in the laminate medium differed by a factor of nearly 4. True stress- true strain diagrams are given in Figs 4.1. Data were fitted into an equation of the form $\sigma = \kappa \varepsilon^n$, by plotting the corresponding log true stress-log strain curves, Fig.4.2. Values of strength coefficients, κ and strain hardening exponent, n are included in Table 4.2.

Table 4.2. *The Mechanical Properties of Materials*

Materials	E GPa	σ_{ys} MPa	$\sigma_{UTS,}$ MPa	ν	κ MPa	n	%Elongation at fracture
Medium carbon steel (AISI 1060)	200	858	959	0.3	1244	0.0722	10.4
Low carbon steel (AISI 1112)	200	232	328	0.3	557	0.212	42.4
Monolithic medium carbon steel (AISI 1050)	200	409	641	0.3	1163	0.2144	33.8
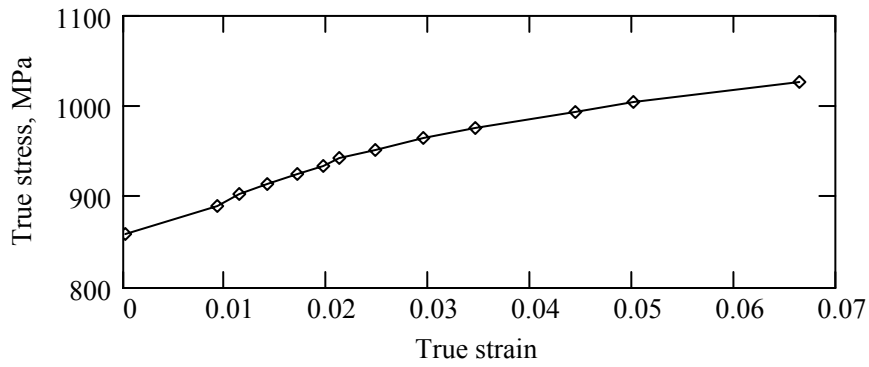
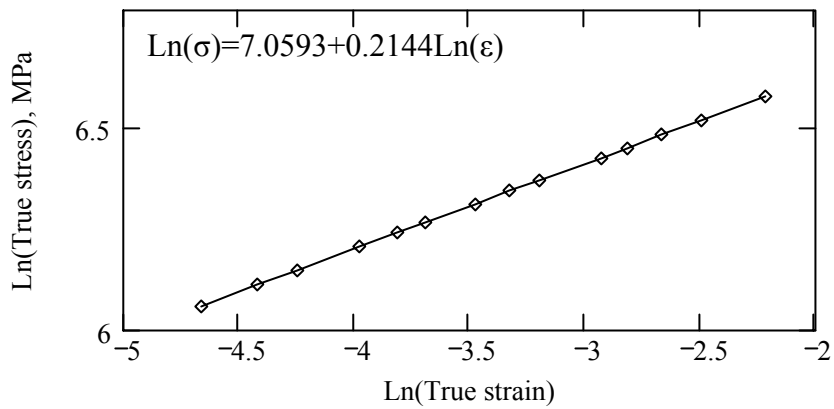**(a)**
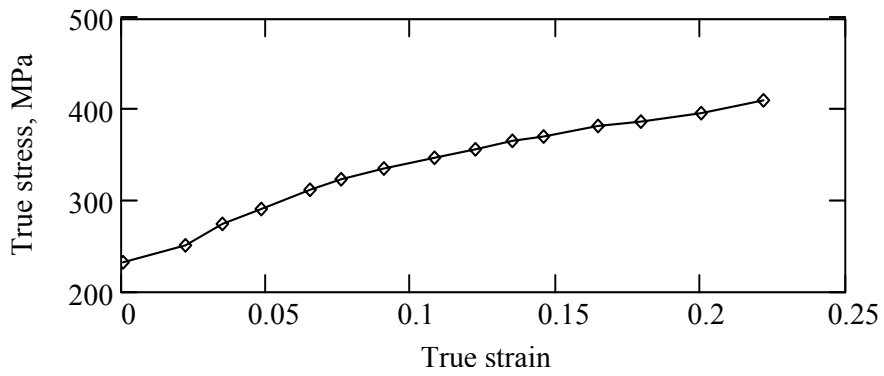
(b)
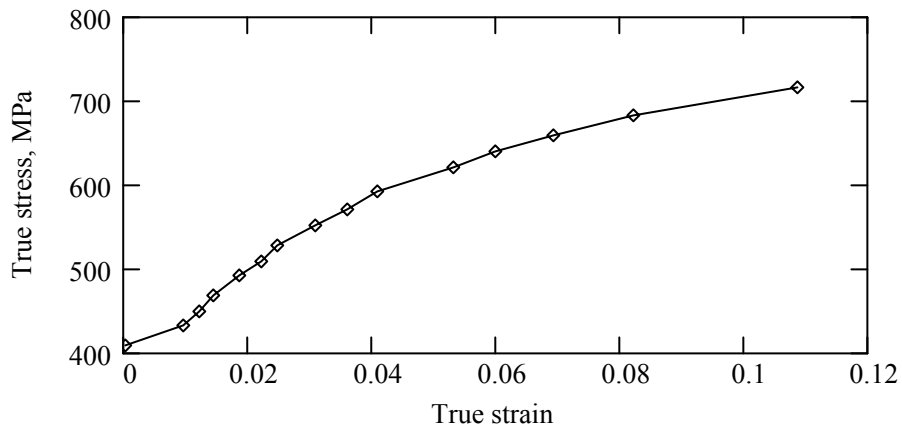
(c)

Figure 4.1. *True stress–strain curves for a) Medium carbon (AISI 1060) b) Low carbon (AISI 1112) c) Monolithic medium carbon (AISI 1050) steels.*
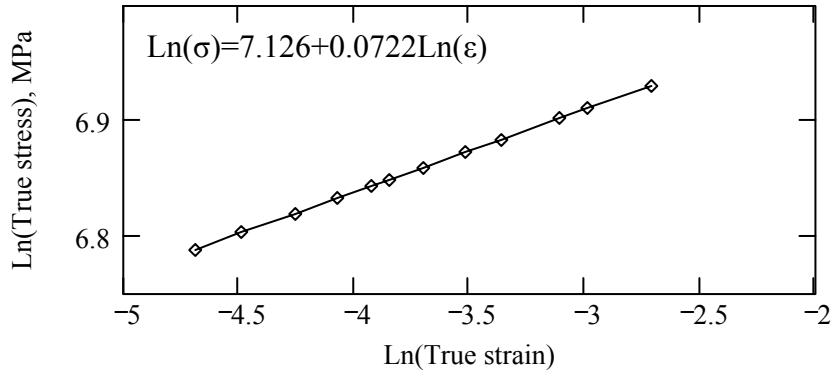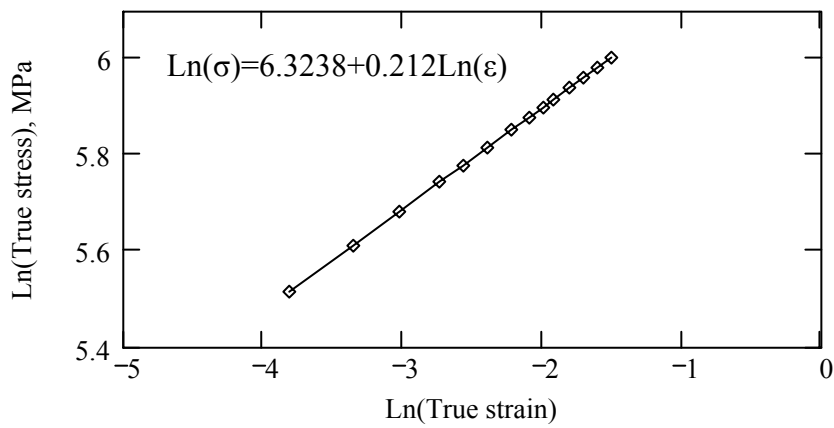
Figure 4.2. *Log true stress-log strain curves for a) Medium carbon (AISI 1060) b) Low carbon (AISI 1112) c) Monolithic medium carbon (AISI 1050) steels.*

4.1.1.2. Measurement of Interfacial Strength

Interfacial strength in the laminate was measured both by a bend test for polymer matrix composites and via a direct shear test. Test samples were cut from hot pressed laminates in different heat treatment conditions

The bend was carried out according to ASTM D 2344-76 "horizontal short beam shear test". For this purpose, three point bend tests were used. The samples were in dimensions 12 x 12 x 84 mm, Fig.4.3. Span to depth ratio was 4.125. This was slightly less than the recommended ratio (5) in the ASTM D2344-76. The crosshead speed was 1.3 mm/min.

Load- deflection data were used to calculate the "apparent horizontal shear strength", given by

$$SH = \frac{0.75 * P_B}{b * d} \qquad\qquad (4.1)$$

Where   SH = apparent interfacial shear strength

P_B = load causing interfacial failure

b   = width of specimen

d   = thickness of specimen

In the calculation, P_B, was taken in the load-deflection curve, as the load at which the first deviation from linearity occurred.

Interfacial shear strength was evaluated as a function of time for the "final heat treatment" of the laminates, i.e. bonding time at 550 ^{o}C. Results are given in Fig. 4.4. It is seen that the interfacial shear strength first increases with bond/annealing time reaches a maximum at 4 hrs and then decreases. As a result, the treatment was fixed at 4 hours for laminate production.
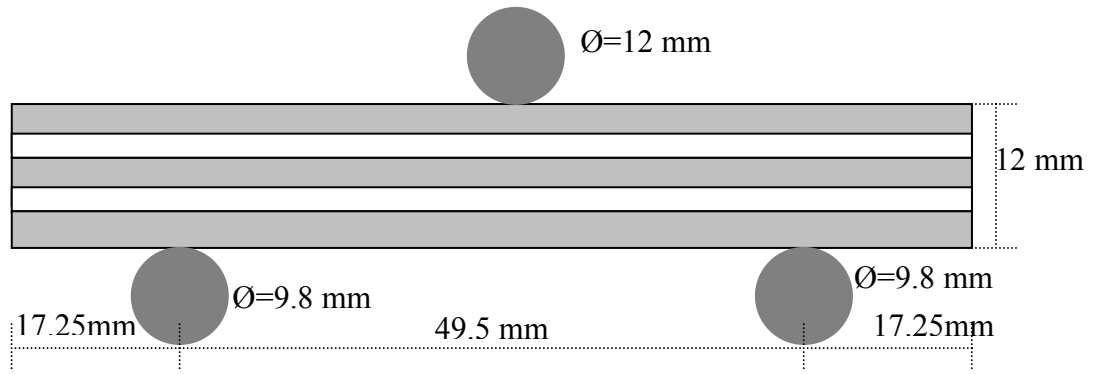
Figure 4.3. *The schematic representation of 3 point bend test, width=12 mm.*
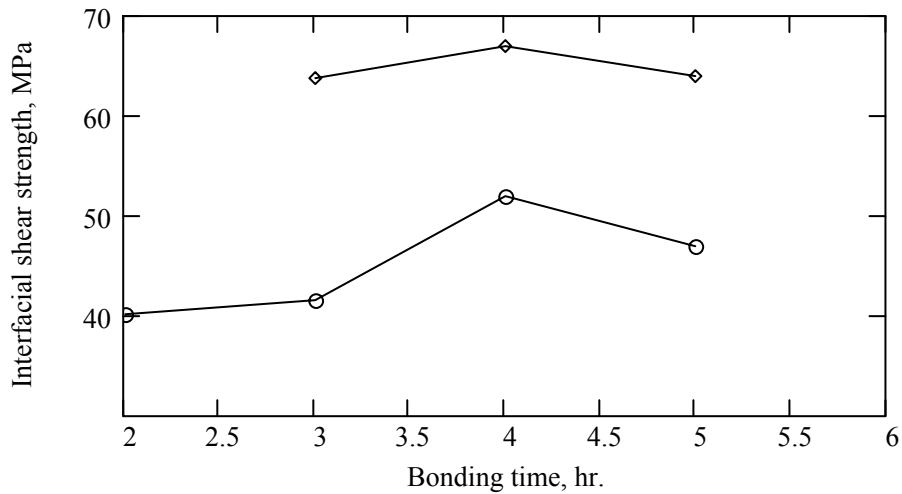
Figure 4.4. *Interfacial shear strength versus bonding /annealing time at 550 ^oC.*

For 4 hours annealing/bond time, the interfacial strength was also determined by a direct shear test. Dimension of the test piece is shown in Fig 4.5. As seen in the figure the sample is notched from opposite sides, both terminated at the same interface. The piece was subjected to tensile testing and failure load was recorded. In this test, the sample fails by shear of the interface between the notches. Shear strength is similarly calculated by dividing the failure load by the area of ligament between the notches.
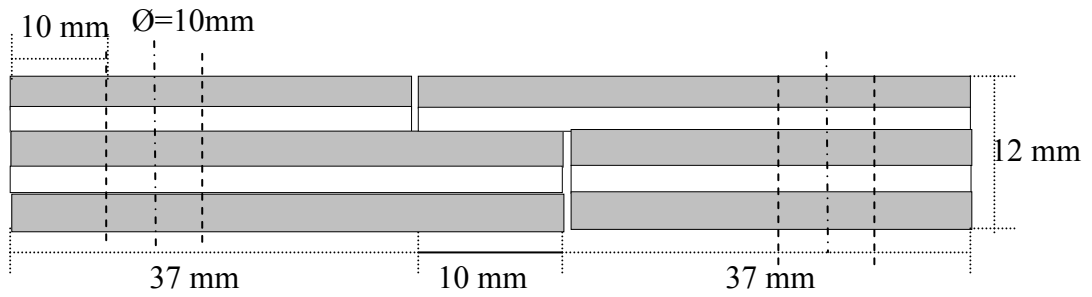
Figure 4.5. *The schematic representation of direct shear test specimen, width=12mm.*

Results of bend test and direct shear test are given in Table 4.3. The results obtained by both tests are close to each other. As a result, all were averaged yielding a value of 59 MPa for the interfacial strength.

Table 4.3. *Interfacial shear strength values for direct shear test for 4 hr holding/annealing time.*

Specimen no	Interfacial shear strength MPa
Direct shear test-1	60.00
Direct shear test-2	56.54
3 point bend test -1	66.92
3 point bend test-2	51.91
Average	58.84

4.1.1.3. Production of Laminates

For the production of laminated composite, coupons of 80X85 mm were cut from steel sheets of medium carbon and low carbon steel. The medium carbon steel sheet was 2.5 mm thick and that of low carbon steel was 1.5 mm.

Medium carbon coupons were subjected to the same heat treatment as described above, i.e. austenitizing at 830 ^{o}C for 15 min, oil quenching and tempering at 550 ^{o}C for 2 hours.

Steel coupons were then cleaned by immersing into a solution of 3.7 g hexamethylenetetramine, 500 ml hydrochloric acid and 500 ml pure water for 10-15 min. Then, the surfaces of the coupons were grinded sequentially 320, 600, 800 and 1200 emery paper, and washed by water and dried by alcohol.

Cleaned coupons were than alternately stack and hot pressed in a hydraulic press. Schematic representation of hot pressing setup is shown in Fig. 4.6. The set-up contained two heating plates made up of hot work tool steel, DIN XCrMoV33. The plates contained channels for heating element, i.e. resistance wire. A "ceramic paper" 3 mm thick was used to isolate the wire in the channels from the metallic block.

Stack of metallic coupons were wrapped around by a copper foil and placed into rectangular steel frame. The frame was placed in the set-up between the heating plates and hot pressed at 550 ^{o}C for 4 hours. Two types of laminates were produced. Figs.4.7 (a, and b) shows the stacking sequences of laminates for Vr=0.41 and Vr=0.81.

Typical microstructures in the laminate are given in Fig. 4.8. The structure in medium carbon layer consisted of tempered martensite and that of low carbon layer is ferrite. At the interface, there is a transition of microstructures. In addition, there were some pores, see Fig. 4.8 (c and d). Hardness profile across the interface measured in terms of Knoop hardness is given in Fig. 4.9. It is seen that the transition layer is typically ~1 mm thick.
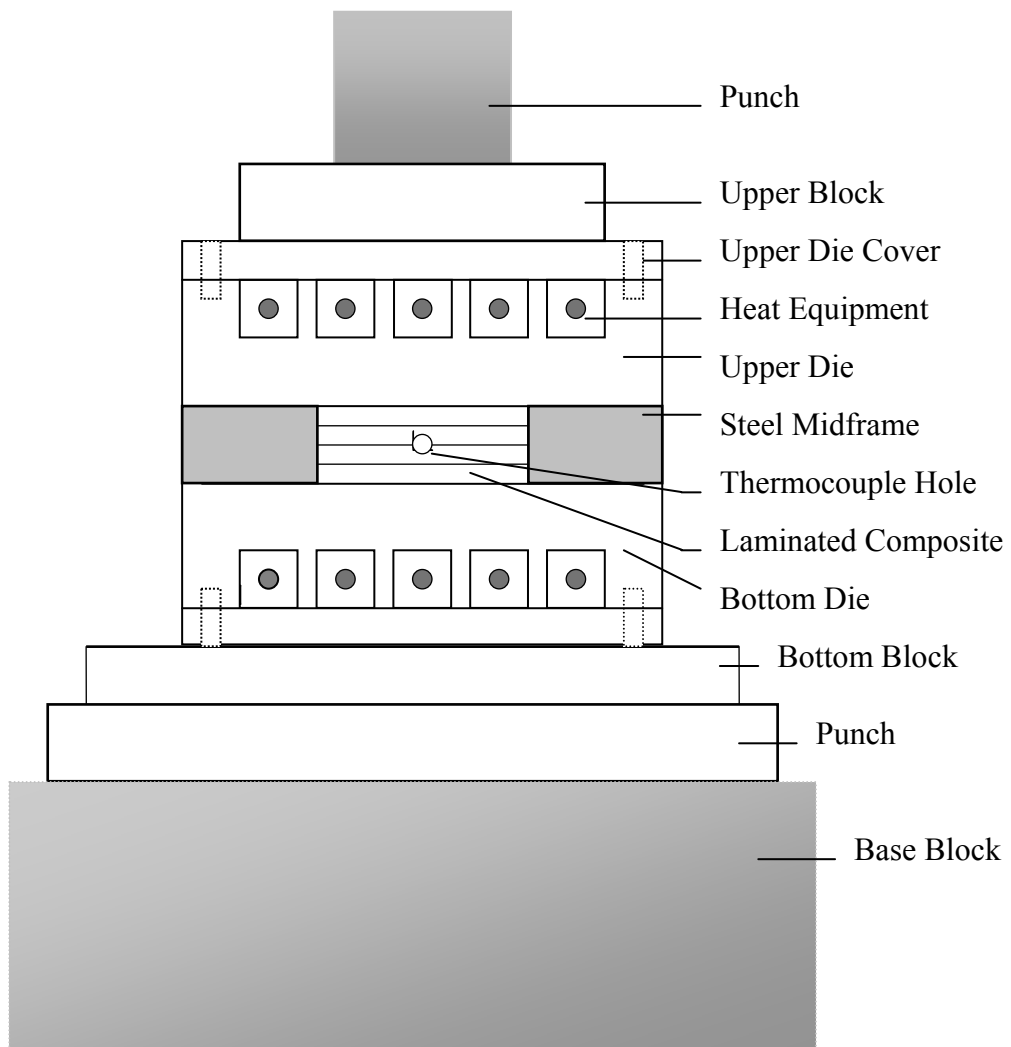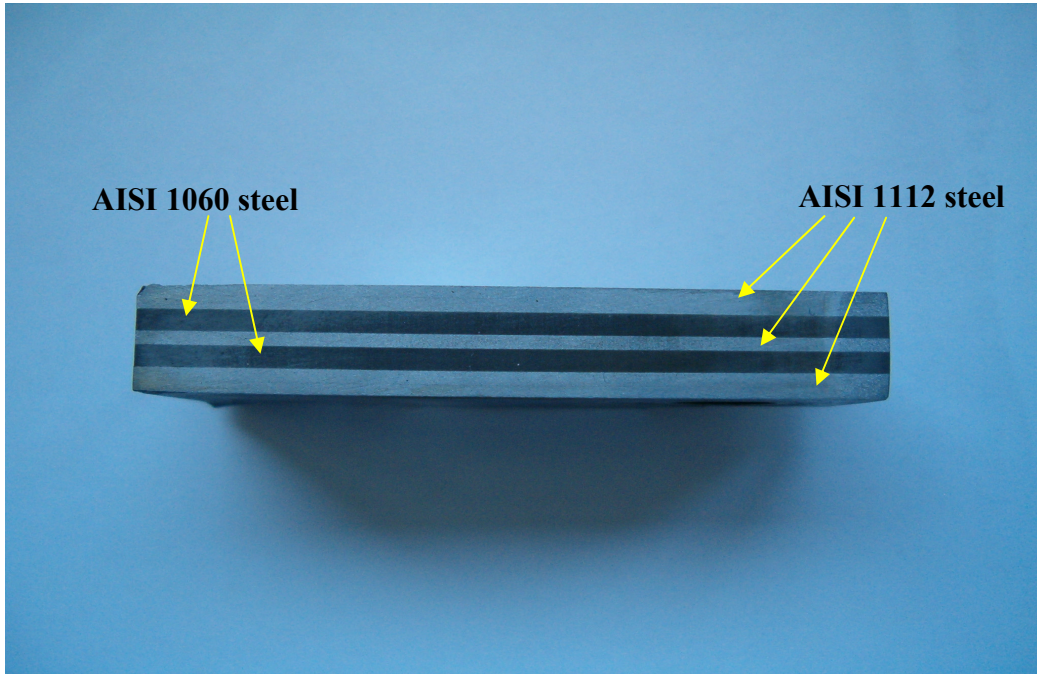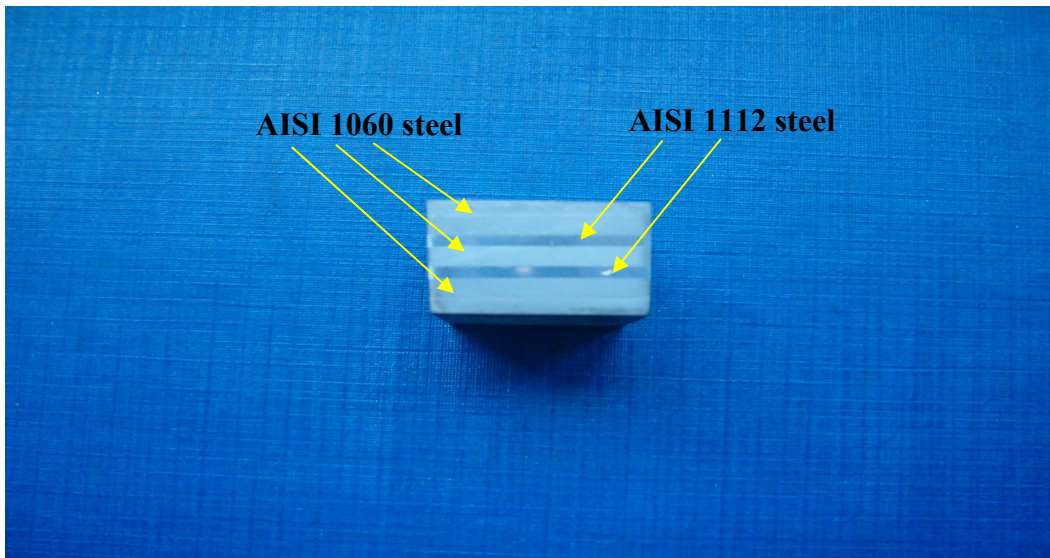
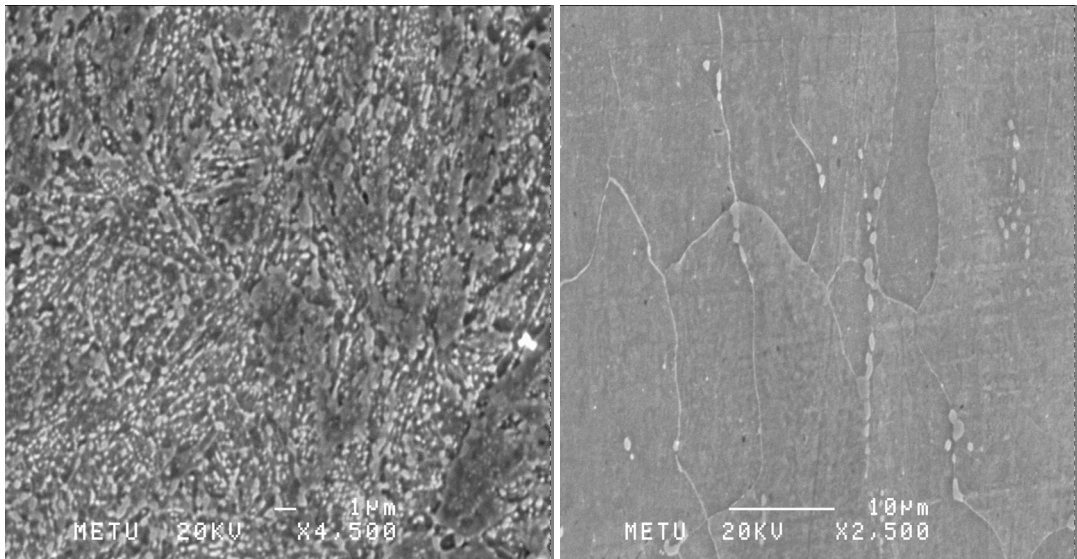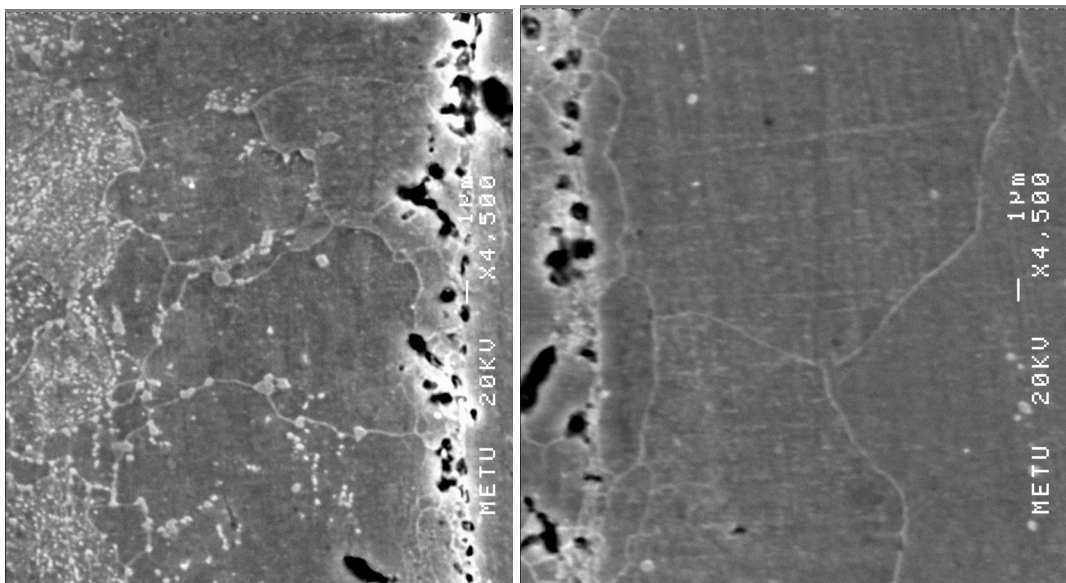*Figure 4.6.* *Hot pressing set-up (schematic) used for production of steel*

(a)

(b)

Figure 4.7. *Stacking sequences; a) 5 layers with ASTM 1112 and 2 layers ASTM 1060 steels for Vr=0.41, b) 5 layers ASTM 1060 and 2 layers ASTM 1112 steels for Vr=0.81*

(a)

(b)

(c)

(d)

Figure 4.8. *Typical microstructures in steel laminates.*
  a) Medium carbon layer away from the interface.
  b) Low carbon layer away from the interface,
  c and d) refers to the structure at the interface. Note the transition of
   microstructure across the interface.
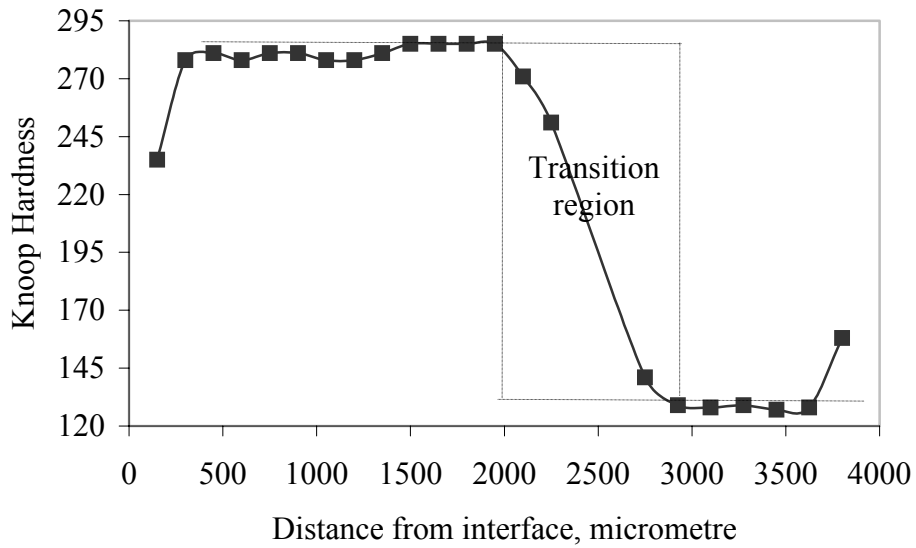
Figure 4.9. *Variation of Knoop hardness as function of distance from the interface in the laminated composite. Data on the left refers to locations across the medium carbon layer and those at the right refer to those in low carbon layer. Note that the transition layer is ∼ 1 mm thick.*

4.1.2. Measurement of Fracture Toughness, Jıc

For measurement of fracture toughness, J_{IC} single specimen (compact tension) technique was used. For this purpose, ASTM E 813 standard was followed. Dimensions of the compact tension specimen are shown in Fig.4.10. The sample had a thickness of typically 13 mm (varied from 10 to 13 mm) with chevron notch, with details as depicted in the Fig.4.10.

The sample was first loaded under fatigue to generate a sharp crack. For this purpose, the load was alternated between 300 N and a value which was less 0.4 PL defined in ASTM E 813;
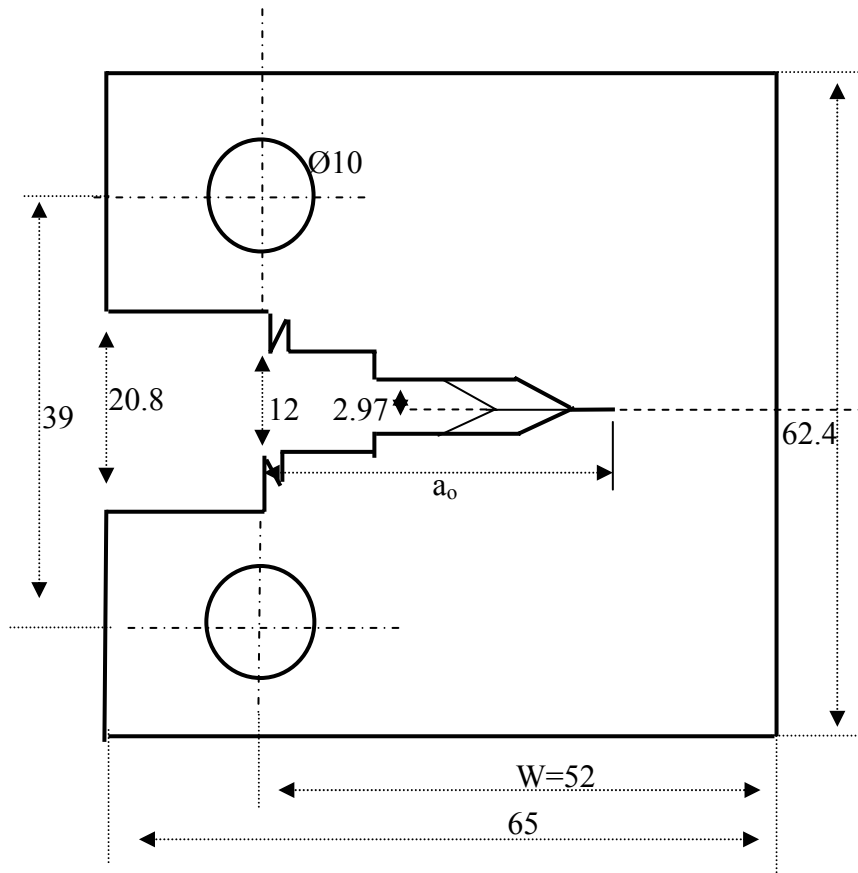
(a)
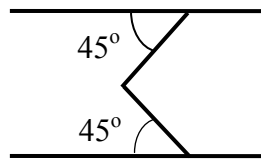
(b)

Figure 4.10. *a) compact tension specimen for $a_o/W=0.65$, $B=13\text{-}10$ mm*
b) details of chevron notch, all dimensions in mm.

$$P_L = \frac{Bb_0^2\sigma_Y}{(2W+a)}$$

Where B is the specimen thickness, b_o is the uncracked ligament; W is the width of the sample.

Fatigue loading was stopped when the crack length, a_o, reached a value of $a_o/W=0.65$ where W is the width of the sample.

Following fatigue cracking, samples were tested in DARTEC servo hydraulic test machine under stroke-controlled condition. The sample is mounted on the machine as shown in Fig. 4.11. The test involves a sequence of loading and partial unloading of the sample. Load line displacement values were read directly from the stroke. As a result, load- load line displacement curve was obtained.
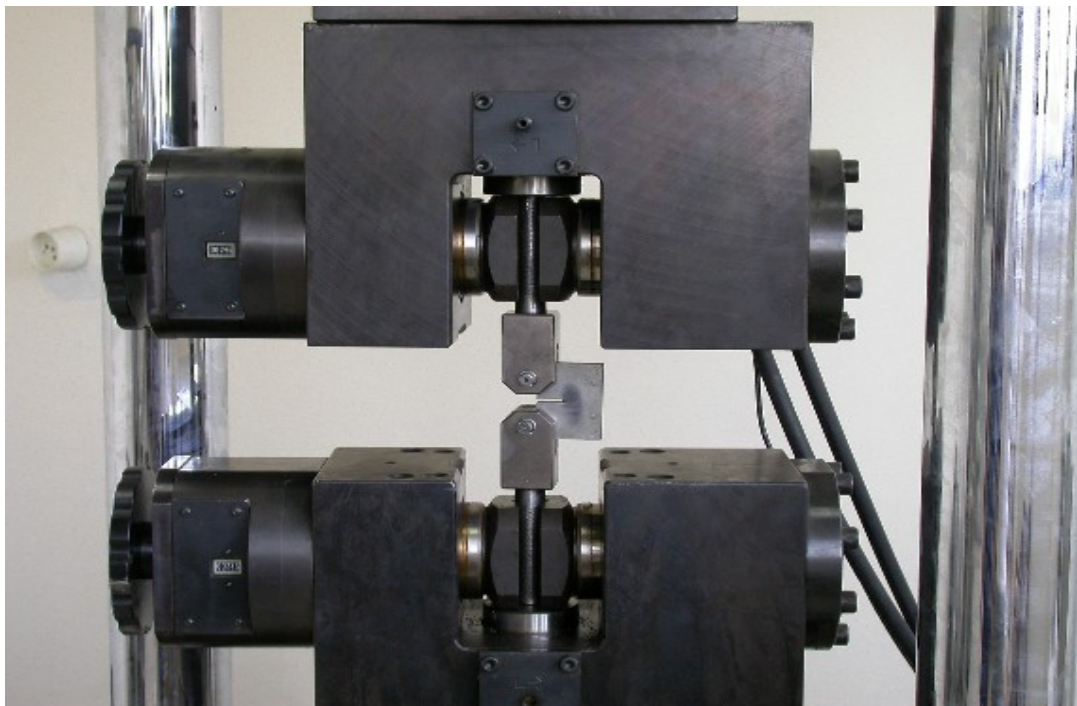

Figure 4.11. *Compact tension specimen, as mounted on hydraulic test machine.*

The first step in this test is the estimation of the original crack length, a_0, i.e. crack length form line of loading up to the tip of the fatigue crack. For this purpose, the specimen was loaded <0.4PL and unloaded to >0.1P_L three times with a constant crosshead speed of 0.008 mm/sec. The crosshead was stopped for about 10 sec before unloading as well as for reloading.

After having measured the data for a0, the load was decreased to lowest possible load value while maintaining the fixture alignment. The sample is then loaded at unloaded repeatedly at a crosshead speed of 0.008 mm/sec. At each step load line displacement/the stroke value was 0.1 mm higher than the previous loading. At unloading the displacement was -0.15 mm from the current position. While unloading, the minimum load was always greater than half of the level of previous loading. The crosshead was stopped for 10 sec before each unloading/reloading and load relaxation was observed.

Having gone beyond a maximum in the load- load line displacement curve, the test is stopped and the sample is removed. To determine the length of crack growth a heat tint method was used. For this purpose, the sample was heated to 300 ^{o}C and held for 10 min. The sample was fatigued in MTS until a growth of the crack was observed then it was overloaded and broken by tension. Broken surfaces are examined and distance between the original the final fatigues were measured.

For monolithic samples, crack growth length is determined 9 point averaging technique, i.e. 9 length measurements across the thickness of the sample (Clarke et al. 1980). For the laminates, crack extension was measured from the edge and the middle of each layer and then the values were averaged for the laminate as whole.

The method requires crack growth data as the sample is progressively loaded. This is determined via a compliance method. The compliance, C_i is defined as

$$C_i = \frac{\Delta \delta}{\Delta P} \hspace{4cm} \textbf{(4.3)}$$

Where is the change in load line displacement ($\Delta\delta$) and is the change in load (ΔP) measured during unloading. After C_i values were calculated at each unloading, crack length, a_i, normalized with respect to the width, W, relevant to each step was calculated as

$$\frac{a_i}{W} = 1.000196 - 4.06319u_{LL} + 11.242u_{LL}^2 - 106.043u_{LL}^3 + 464.335u_{LL}^4 - 650.677u_{LL}^5$$

(4.4)

U_{LL} is defined as

$$u_{LL} = \frac{1}{\left[BEC_i\right]^{1/2} + 1} \tag{4.5}$$

Where B is the sample thickness, E is Elastic Modulus.

The same equations were used for calculation of the original crack length. The of amount crack extension was determined as;

$$\Delta a = a_i - a_o \tag{4.6}$$

Values found for the original crack and the final lengths were compared with physically measured data.

J integral values were determined from load-load line displacement data. For this purpose;

$$J = J_{el} + J_{pl} \tag{4.7}$$

Where J_{el} is the elastic J integral and J_{pl} is the plastic J integral.

At a point of loading, P_i, corresponding to displacement value of δ_i, Elastic part of the J-integral is given by

$$J_{el(i)} = \frac{\left(K_{(i)}\right)^2 \left(1 - v^2\right)}{E} \qquad (4.8)$$

Where v Poisson ratio and $K_{(i)}$ is defined by

$$K_{(i)} = \left[\frac{P_i}{BW^{1/2}}\right] * f\left(a_0 \Big/ W\right) \qquad (4.9)$$

$$f\left(a_0 \Big/ W\right) = \frac{\left(2 + (a_0/W)\right)}{(1 - a_0/W)^{3/2}} \qquad (4.10)$$

Plastic component of J integral;

$$J_{pl} = \frac{\eta A_{PL(i)}}{Bb_0} \qquad (4.11)$$

Where b_0 is uncracked ligament, B is the thickness of the sample and

$$\eta = 2 + 0.522\left(b_0 \Big/ W\right) \qquad (4.12)$$

$A_{PL(i)}$ is the plastic work. To determine this, the total area under load-load line displacement curve (combining both elastic and plastic work), A_T was determined by using trapezoidal rule. The Elastic part, A_{el} was determined, based on the value of elastic displacement given by construction as depicted in Fig.4.12, i.e. by extending the unloading slope to P=0. The elastic displacement is then given by;
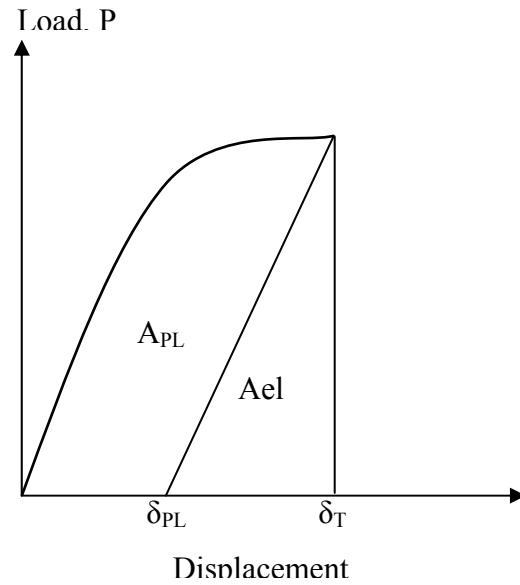
Figure 4.12. Load-load line displacement curve. δ_T and δ_{PL} are the total and plastic *displacements respectively.*

$$\delta_{el\,(i)} = \delta_{T(i)} - \delta_{PL(i)} \tag{4.13}$$

A_{el} is the area of the triangle and APL described in units of energy Joule, is derived from the total area A_T as;

$$A_{PL\,(i)} = A_T - A_{el} \tag{4.14}$$

J values and crack extension data determined following the procedure described above is collected together in a curve, Fig. 4.13. A power law curve fitting procedure was used to describe J integral-Δa data, Fig. 4.13.

As seen in Fig. 4.13, a blunting line passing through the origin was drawn with a slope, $2\sigma_f$

$$\sigma_f = (\sigma_{ys} + \sigma_{UTS})/2 \tag{4.15}$$

Where σ_{ys} is the yield stress, and σ_{UTS} is the ultimate tensile strength.

This yields a main reference line with an equation of J=2σ$_f$Δa.

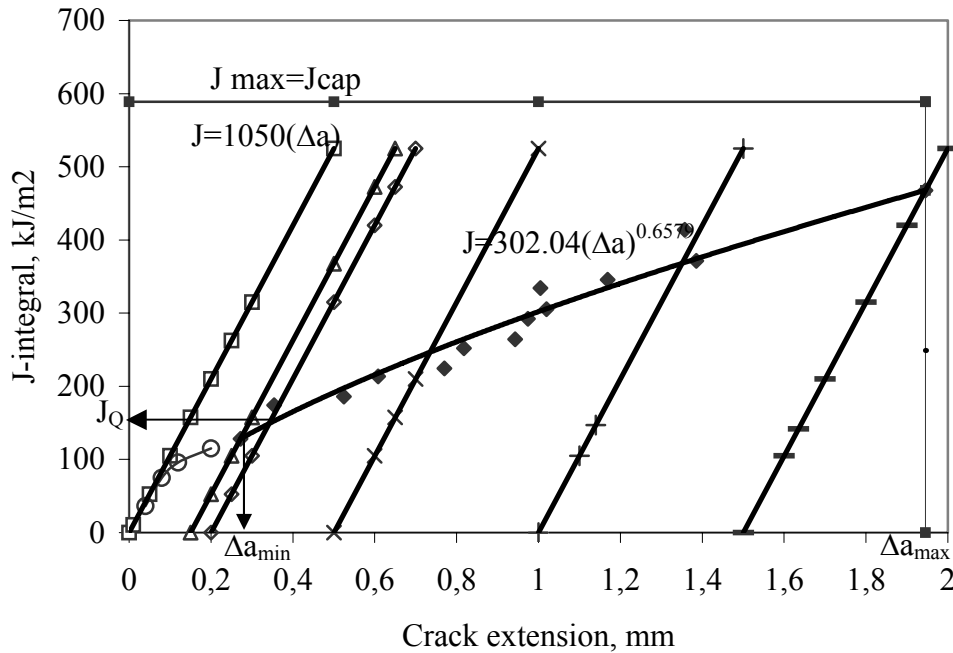*Figure 4.13. Validations of data in J$_Q$ evaluation. Data in-between exclusion lines of 0.15 and 1.5 are considered valid. ○-invalid data ◆-valid data*

After plotted this line, parallel lines (exclusion lines) were drawn at crack extension values of 0.15 mm and at 1.5 mm. The area enclosed in-between the parallel lines is given by

$$J_{max}=b_o\sigma_y/15 \qquad\qquad (4.16)$$

The intercepts of the exclusion lines with the power law curve were projected vertically down yielding values of Δa$_{min}$, and Δa$_{max}$, respectively. Data that do not fall between Δa$_{min}$, and Δa$_{max}$, and J values greater than J$_{max}$ cap were eliminated. Thus a region of valid data is obtained that can be used for J$_{IC}$ determinations.

For this purpose, an offset line at a value of $\Delta a = 0.2$ mm was drawn parallel to the blunting (and exclusion lines). A linear regression line was fitted to data in between at $\Delta a = 0.15$ and 1.5 using a method of least squares;

$$\text{Ln }(J) = \text{Ln }(C_1) + C_2 \text{ Ln }(\Delta a) \qquad \textbf{(4.17)}$$

The intersection of the regression line with the offset line at $\Delta a = 0.2$ defines J_Q and Δa_Q. The value of J_Q determined in this manner is equal to J_{IC} provided that

$$B \text{ and } b_o > 25 \; J_Q/\sigma_y \qquad \textbf{(4.18)}$$

Certain precautions are necessary to measure the fracture toughness, J_{IC} accurately. One is related to the minimization of friction in the pinholes so that the pin is free to rotate while loading. Plastic deformation in the pin as well as in the pinhole must be avoided since this increases the friction at the interface, which may cause the rotation of clevises). Formulation of J_{IC} given above assumes that data refer to loading along the center of the pinholes. If the real load line is displaced because of the clevis rotation then the compliances are underestimated. A sign of this is negative values for the crack extension. The other is related to relaxation time, i.e. holding time at loading and unloading. The time should be sufficiently long so that the sample relaxes fully. With insufficient time, compliances are underestimated and therefore crack growth data may have negative values.

4.2. Numerical Procedures

Finite element modeling (FEM) as implemented in MARC package program was used throughout this study. Details of FEM formulation can be found form various sources (Mac Neal, 1994, Braess, 1997) as well as from MARC documentation (MARC 2001), and will not be given here. The method is applied to compact tension specimen with essentially the same geometry as that used in the experiments.

In sections below, first 2-D analysis is considered. This is followed by 3-D and finally by layered 3-D analysis. The method is verified with data from literature, specifically for HY130 steel for which a large volume of data was available (Clausing, 1970, Clarke, et al.1980, Gudas and Davis, 1982).

4.2.1. Two Dimensional (2-D) Analysis

The geometry of the compact tension specimen as used in 2-D analysis is shown in Fig. 4.14. One half of the test piece is shown together with the symmetry line. Here the reference direction x, y (and z) are parallel, in the respective order, to line of loading, crack direction (and the thickness). Typically, the crack is located at the symmetry line AA' and extends from point B (-33.8,in the x- axis; load line) to point C (0 in x-axis; crack tip), i.e. BC=33.8. The total width of the model is from point B to point D (18.2 in the x-axis), i.e. BD=52. This corresponds to $a_0/W=0.65$ (i.e. BC/BD). The model is loaded at "pinholes" placed in positions in accordance with ASTM E813 Standard. Loading was applied in terms of displacements of nodes at the pinhole in y direction. Because of the symmetry, displacement in y-direction of nodes in between C and D at the symmetry line AA' was set to zero. To ensure equilibrium, the node at the very edge of the symmetry line, D, was stationary, i.e. displacements in x and y directions were set to zero.

Meshing was done manually; since different mesh sizes were necessary at the crack tip region and elsewhere. 8-node quadrilateral plain strain element was used[1]. In the model a total of 64 elements and 242 nodes were used. The crack tip element had the smallest size which had nearly $5 \ 10^{-4}$ the size of the crack length, a_0. At the crack tip the element was modified in accordance with "one quarter method "(Barsoum, 1976, Raju, 1987, 1988), Fig.4.15. The size of elements were increased gradually away from the crack tip both in x and y directions. The crack front of the model is shown in Fig.4.16.
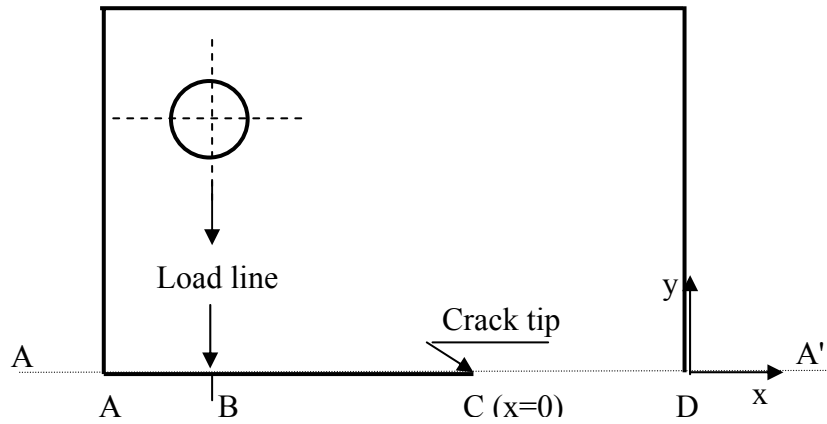
---

[1] Element 27 in MARC Package program

Figure 4.14. *Schematic representation of one half of the 2-D model. AA' is the symmetry axis. Point B (x=-33.8) is the location of the load line, and point C (x=0) is the crack tip and point D (x=18.2) is the end of the uncracked ligament. a_o/W (BC/BD)=0.65.*

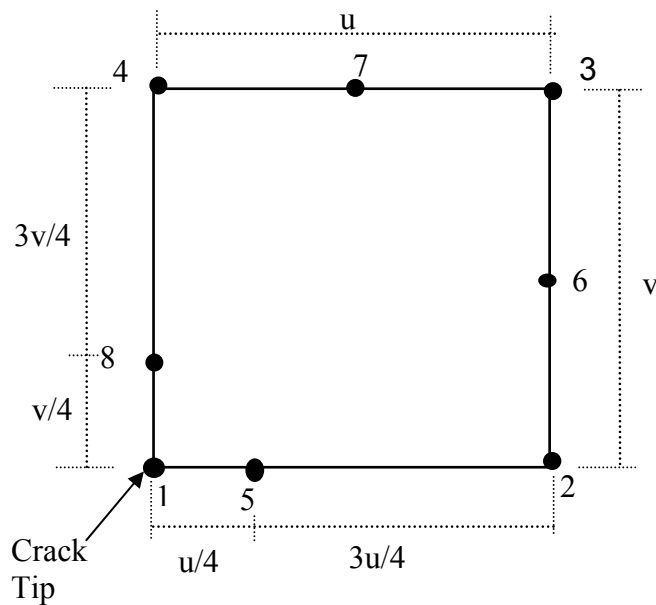
Figure 4.15. *8-node quatralaterial plain strain element used in 2-D Medelling. Mid nodes as shown in the fure are modified with one quarter technique .*

Material properties, assumed to be isotropic, were specified. The model was loaded in terms of displacement at the pinhole along y direction. Typically, the total displacement was one hundredth of the crack length a_o which was imposed typically over 100 increments. In the evaluation, finally, in the mechanical analysis option, Updated Lagrange and Large Strain Additive approaches were chosen for the formulation the elastic-plastic analysis especially plastic deformation region in front of the crack tip. Convergence is checked by Newton-Raphson Iteration Method
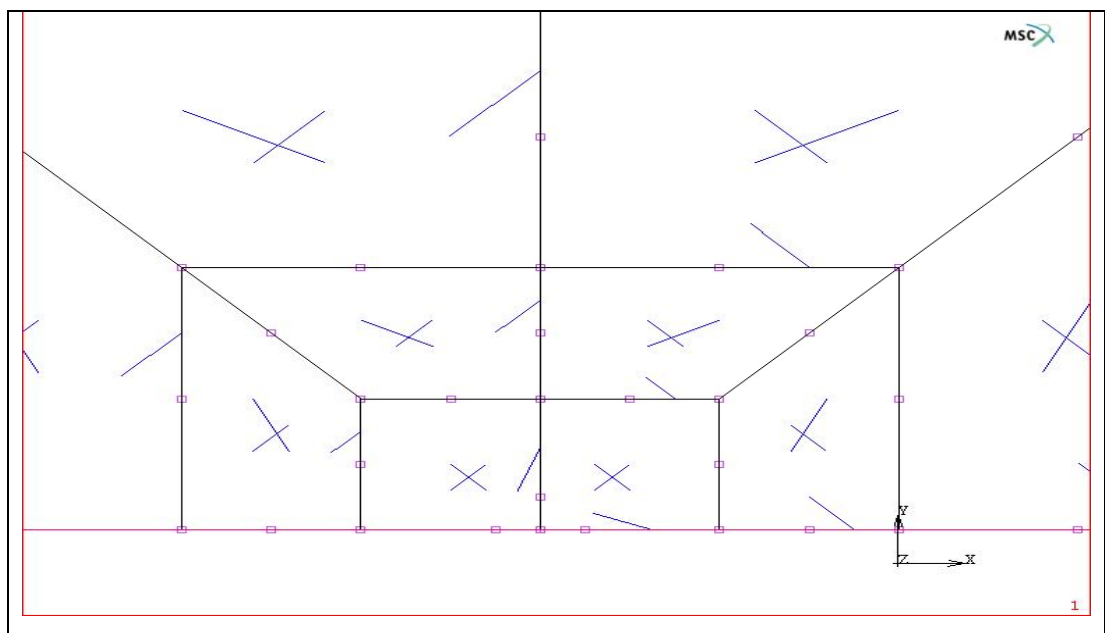
Figure.4.16. *Crack tip for 2-D model. Elements used at the crack tip are modified with one quarter technique.*

In order to determine J integral, a radius, r, of line integration must be specified. The value for the radius varied over a range. The smallest value was equal to the crack tip element size. The largest had a size covering nearly the whole of the uncracked ligament. A total on nine radii were used. Normally J integral increases with increase in r. Beyond a certain value of r, J is saturated. This value, i.e. far field J, is taken as the J integral value of the model.

4.2.2. Three Dimensional (3-D) Analysis

In 3-D analysis, the model was expanded version of 2-D model by introduction of z direction, Fig 4.17. The boundary conditions were the same, but applied along the symmetry planes rather than the lines. There is an additional symmetry plane shown by BB' placed at the midthickness of the 3-D model. Displacements at BB' plane in z direction were set to zero. Thus, only one fourth of the sample was analyzed.

The model is meshed with 20 node brick elements[2], Fig.4.18. The meshing is carried out automatically. A total of 900 elements with 5200 nodes were used in the analysis. The crack tip element size, smallest of all used in the model to crack size value was $5 \ 10^{-4}$. The crack tip was modified as before by " one quarter method ". Other details of analysis are the same as those given above.

J integral value evaluated as above varied across the thickness of the model. For a given r, the value was maximum value at the midthickness and decreased towards the surface. Thus to determine J integral for the model as a whole an averaging procedure is used. For this purpose, trapezoidal rule is used, i.e. J values are integrated from surface to the center and divided by the half thickness.

4.2.3. Three Dimensional (3D-L) Layered Analysis

3-D analysis given above refers to monolithic materials. To adopt this for layered materials, model depicted in Fig. 4.19 were used. In terms of boundary conditions, the model is identical to the 3-D. However, the model is made up of layers of different mechanical properties. The choice of element type and size were the same as the 3-D model. Typically, there were 10 elements across the thickness of each layer. Where the elements layers were in contact, the last elements in both sides

---

[2] Element 21 in Marc Pacakage program

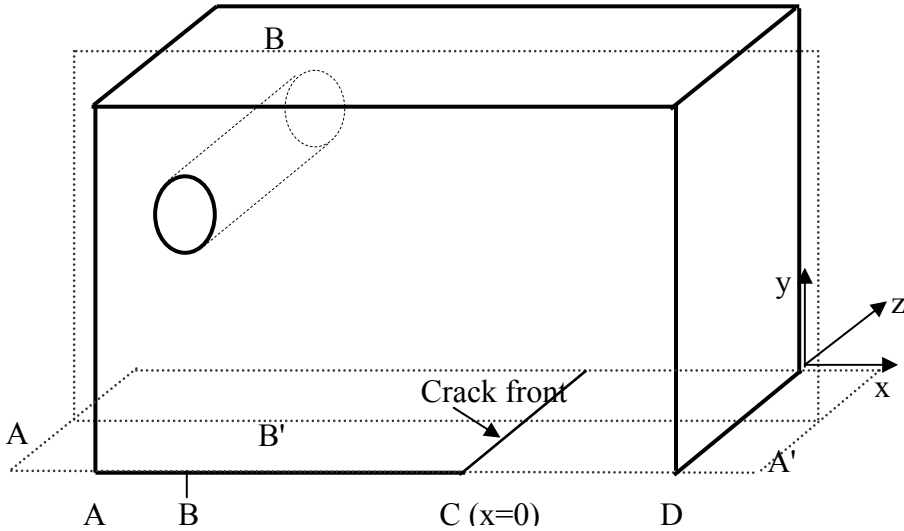were subdivided into 10 sub elements. The model had a total over of 1500 elements with 8000 nodes.

Figure 4.17. *Symmetry in 3-D modeling. AA' and BB' are the symmetry planes. Point B (x=-33.8) locates the position of load line, point C (x=0) and D(x=18.2) locate the crack front uncracked ligament respectively; a_o/W (BC/BD)=0.65.*
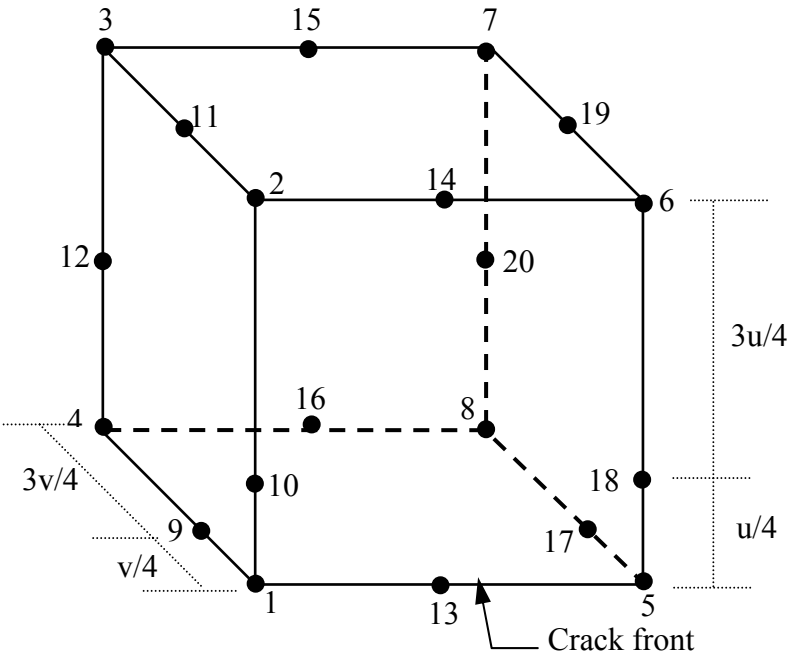

Figure 4.18. *20 noded birck elements used in 3-D modelling. The element shown above modified with one quarter technique are used at the crack front, the rest is meshed with unmidified brick elements.*
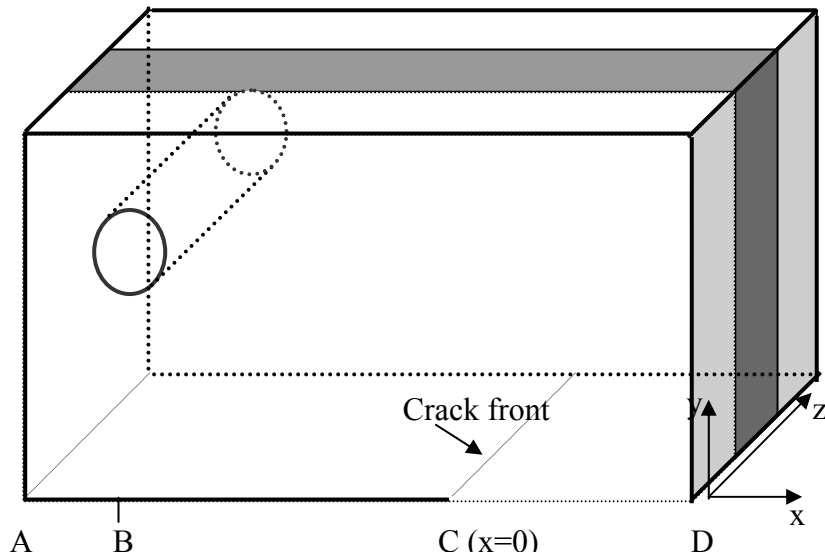
Figure 4.19. *Geometry of 3-D layered model. Dotted planes are planes of symmetry Point B (x=-33.8), C (x=0) and D (x=18.2) locate the position of load line, crack front and the end of the uncracked ligament respectively. a_o/W (BC/BD)=0.65. Gray and white layers depict materials of different property.*

The layers making up the model are attached to each other by "gluing". In this way nodes are attached and behave in the same way except when a specified value of interfacial stress or force is reached. When this stress is reached, the layers are separated and each node behaves independently. A value for "separation distance" must be specified below which the nodes glued are considered in contact and therefore behaves as one, and above which the separation occurs yielding two independent nodes.

Because separation of layers, i.e. delamination, is an important process in the failure of layered composite, a separate analysis were carried out for "separation distance", before the "gluing" is used in compact tension modeling. The model used for this purpose is shown in Fig. 4.19. The model is two dimensional and meshed with 8 node plane strain elements. With respect to centerline, lower part of the model has material properties of medium C steel, and that above have properties of low C steel. The model is continuous across the centerline expect for the region between A and

B. Here the nodes are "glued" together. Interfacial strength for the "glued region" is specified as what was measured experimentally (118 MPa, i.e. interfacial shear strength converted to tensile stress using Tresca criterion). The model is deformed by longitudinal displacements at the edges. Longitudinal normal stresses were monitored during loading at various values of separation distance. It is found that the delamination is predicted at the expected value of the normal stress when the separation distance was 5% of the smallest element size. Therefore, a separation distance of this ratio was used in 3-D layered analysis.
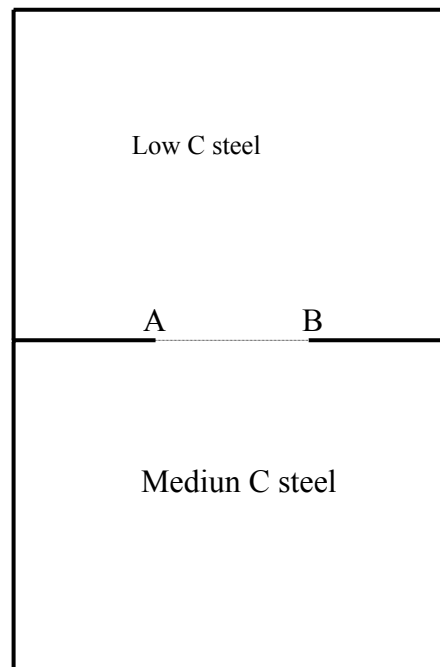
Figure 4.19. *Model used to calibrate separation distance in "glued" layers. In the model low –C and medium –C plates are continuous at the interface except for the portion in between A and B where they are "glued" together.*

J integral values vary across the thickness of the each layer as well as across the total thickness of the model. Although J values varied systematically from layer to layer depending on the mechanical properties of the layers, there were in general, severe oscillations at the interfaces, Fig 4.20. In deriving J integral value for the

layered model, the interface J values were ignored, and average value is calculated with the same procedure as that described for 3-D model.
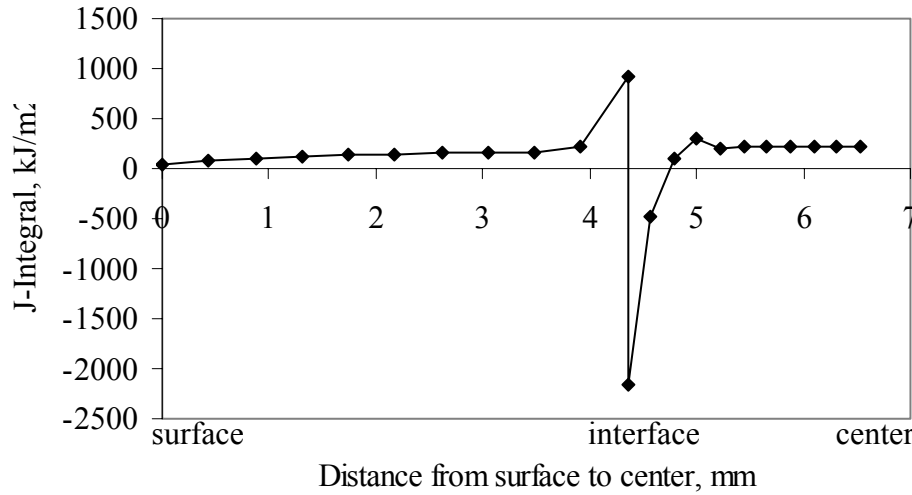

Figure 4.20. *Variation of J integral values from surface to center.*

4.2.4. Fracture Criterion

In the numerical analysis, J integral values were obtained as a function of load line displacement, i.e. displacements imposed at pinholes. To determine J_{IC}, i.e. critical value of J integral, a fracture criterion is needed.

In this study, a critical value is assumed for load line displacement. This value is selected as that corresponding to 0.2 mm crack extension based on the experimental data of the material in question.

CHAPTER V

RESULTS AND DISCUSSION

5.1. Experimental Results

The current study aims to determine whether or not J_{IC} of laminated composites could be predicted with FEM analysis. In order to determine this, experimental program has been devised to generate data that could be used to check the validly of the prediction. This involved the experimental measurement of J_{IC} for monolithic material as well as for steel laminates.

5.1.1. Fracture Toughness of AISI 1050 Monolithic Steel

Two compact tension samples of medium carbon steel, AISI 1050 were tested. Load versus load line displacement curves are shown in Fig. 5.1. J-crack extension curves are in Figs. 5.2 and 5.3. In addition, the test results are tabulated in Table 5.1. As seen from this table, the monolithic material has a fracture toughness of 139.7 kJ/m^2.

The test was not altogether reliable. Final crack extension as measured by heat tint method were smaller than those calculated by the partially unloading compliance method. For instance this value in one of the samples were 1.22 mm, the value predicted by the compliance was 2.079, Table 5.2. Such large differences have also been reported in literature (e.g. Gudas and Davis (1982))

Table 5.1. *Data for J_{IC} testing of monolithic AISI 1050 steel.*

Specimen	Critical value of crack extension mm	Corresponding LLD mm	J_{IC} kJ/m^2
1050-1	0.2	1.04	149.1
1050-2	0.2	1.14	130.2
		Average of J_{IC}	139.7

Table 5.2 *Comparison of crack extension data for monolithic 1050 steel. Data below refer to final values of crack extension. Δa (phys.) is physically measured data with heat tint method and Δa (cal.) is the value calculated from the partially unloading compliance method.*

Specimen	Δa (phys.) mm	Δa (cal.) mm	$\dfrac{\Delta a(phys)}{\Delta a(cal)}$
1050-1	1.222	2.079	0.588
1050-2	0.694	1.314	0.528
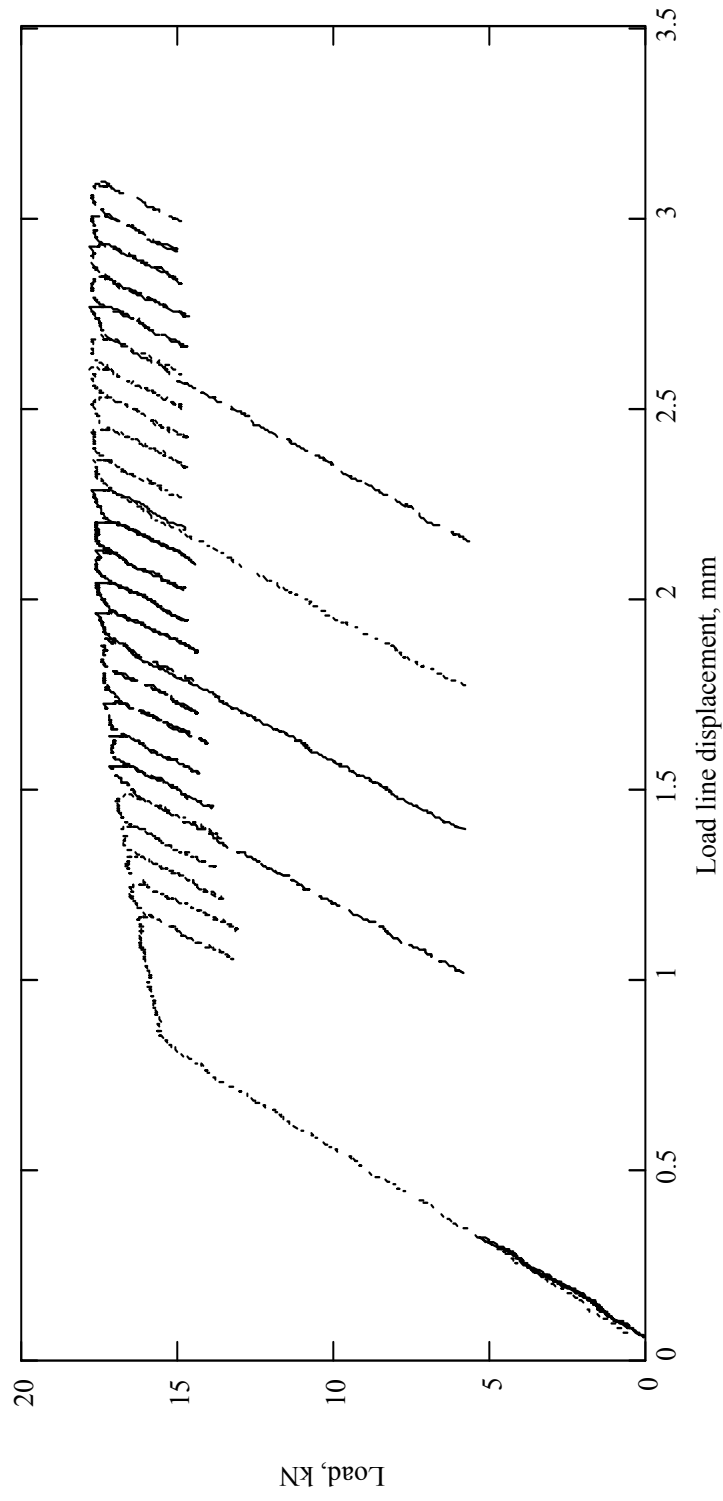
Figure 5.1. *Load versus load line displacement curve of 1050 steel. Specimen No. 1.*
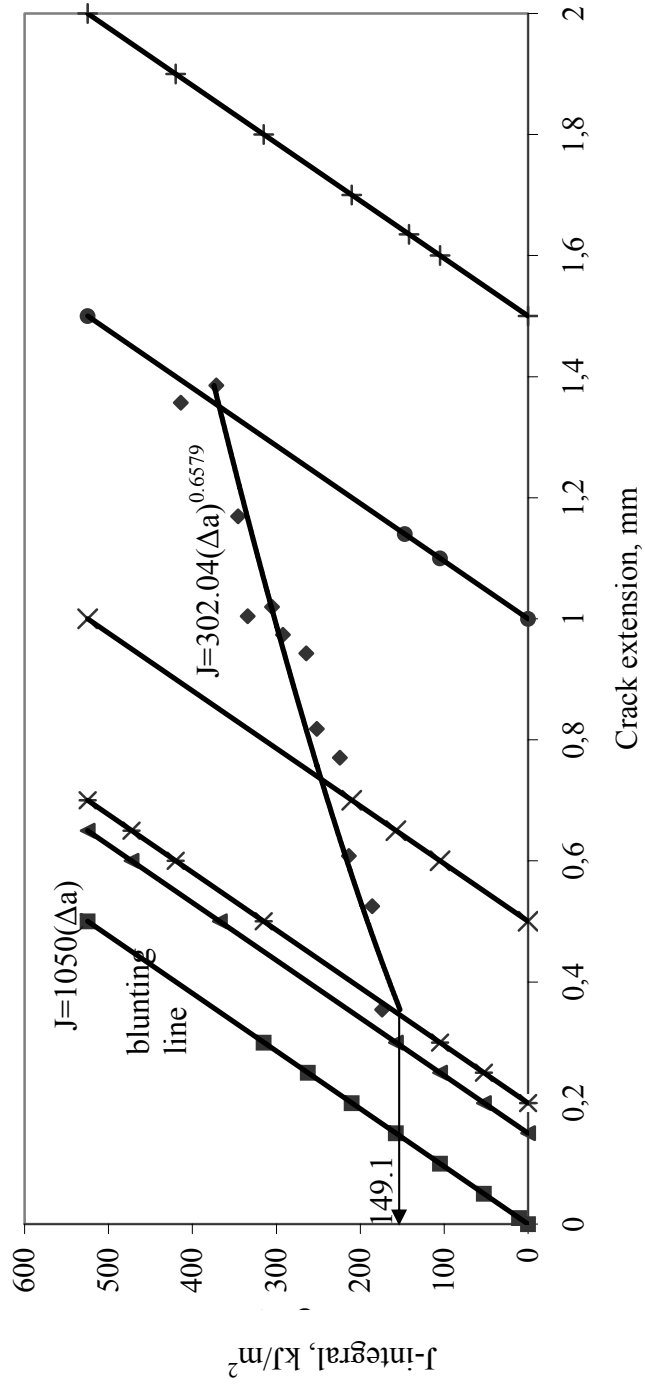
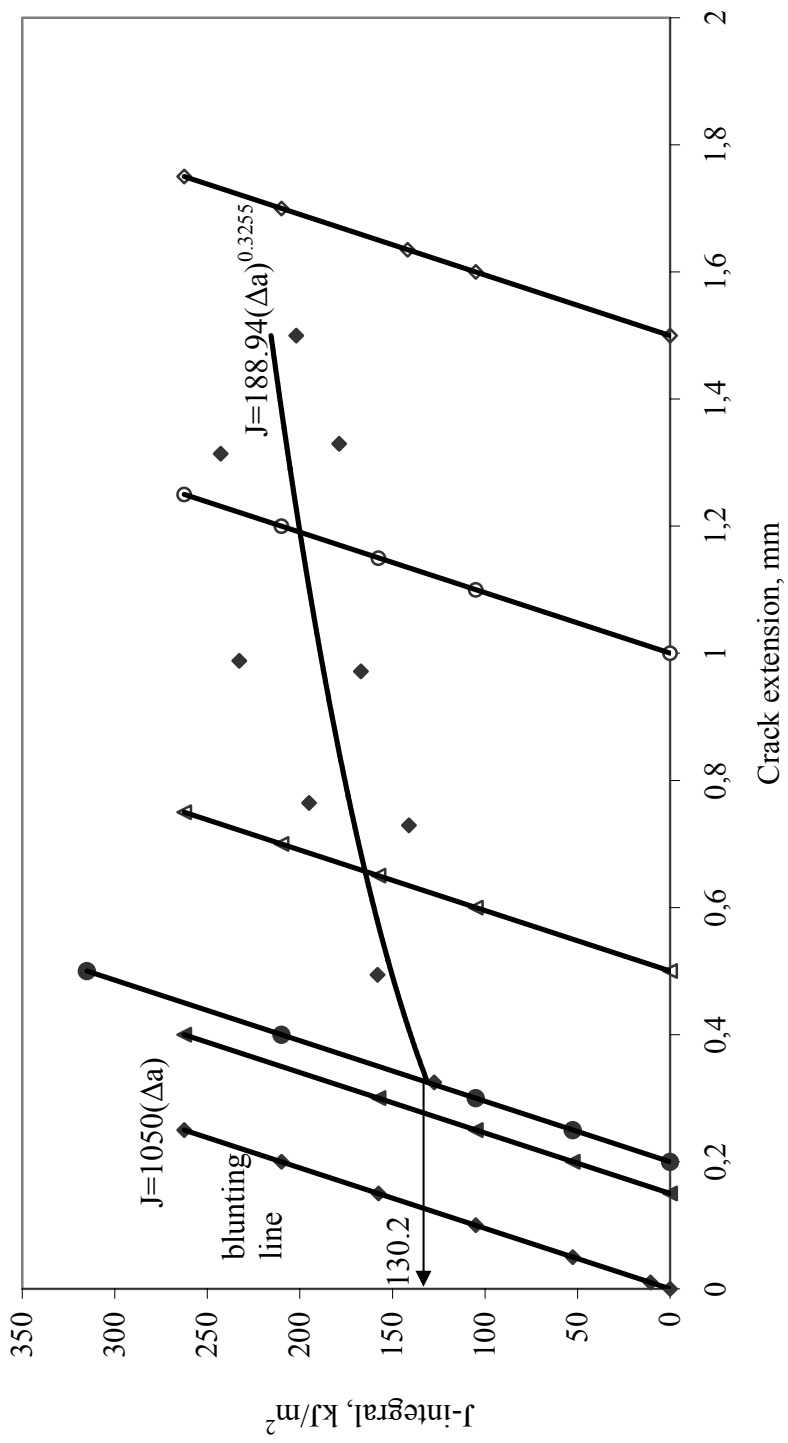**Figure 5.2.** *J versus crack extension curves of AISI 1050 Steel. Specimen No. 1.*

57

Figure 5.3. *J-integral versus crack extension curves of AISI 1050 steel. Specimen No.2.*

The figure contains axis labels: J-integral, kJ/m² (vertical axis), Crack extension, mm (horizontal axis); and the equations $J=188.94(\Delta a)^{0.3255}$, $J=1050(\Delta a)$, blunting line, 130.2.

Fracture surfaces of broken samples of AISI 1050 were examined and are shown in Figs. 5.4 (a and b). The crack extended on the same plane of crack front and Pop-in crack shape were observed. This means that the crack extended more at the center rather than at the external surfaces of samples. This observation is in agreement with the fact that plain-stress condition exists at the free surfaces of the samples.
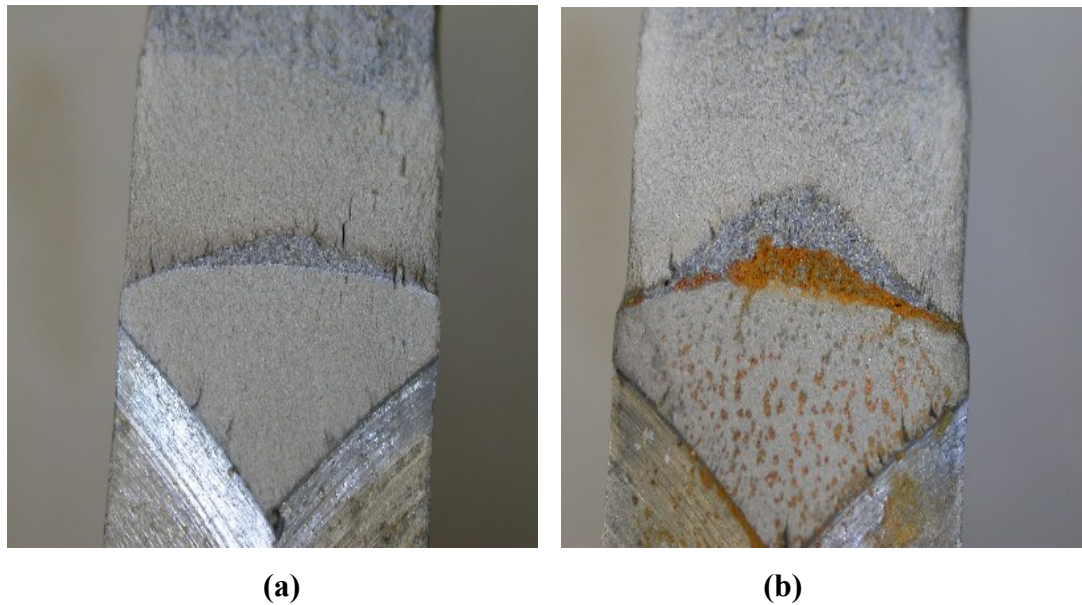

(a)   (b)

Figure 5.4. Fracture surface of Monolithic 1050 steel.
   a) Sample as fractured.
   b) Sample after heat tinting (at 300 ^{o}C for 10 min)

5.1.2. Fracture Toughness of Laminated Steel

Two steel laminates with the volume fraction (hard phase) of Vr= 0.41 and Vr=0.81 were tested (Table 5.3.). Load versus load line displacement curves are shown in Figs. 5.5. J integrals versus crack extension curves obtained for the same laminates are given Fig. 5.6 (a, b and c). J_{IC} was measured between 97-100 kJ/m^2 for Vr=0.41 and 148 kJ/m^2 for Vr=0.81. It was observed, that as the volume fraction of AISI 1060 steel layer increases, the fracture toughness of the laminate increases also.

Table 5.3. *Data for J_{IC} testing of laminates.*

Specimen, Vr	Critical value of crack extension mm	Corresponding LLD, mm	J_{IC} kJ/m²
0.41 -1	0.2	0.90	97
0.41 -2	0.2	0.93	100
		Average of J_{IC}	98.5
0.81	0.2	1.04	148

As seen from the Table 5.4, there are differences in physically measured crack length and those calculated by compliance method. The direction of this difference in Vr=0.41 is similar to that observed in monolithic sample, i.e. physically measured values are smaller than those calculated by the compliance method. In the case of Vr=0.81, however, the difference is in the opposite direction, i.e. physically measured values are greater.

Table 5.4 *Comparison of crack extension data for laminates. Data below refer to final values of crack extension Δa (phys.) is physically measured data with heat tint method. Δa (cal.) is the value calculated from the partially unloading compliance method.*

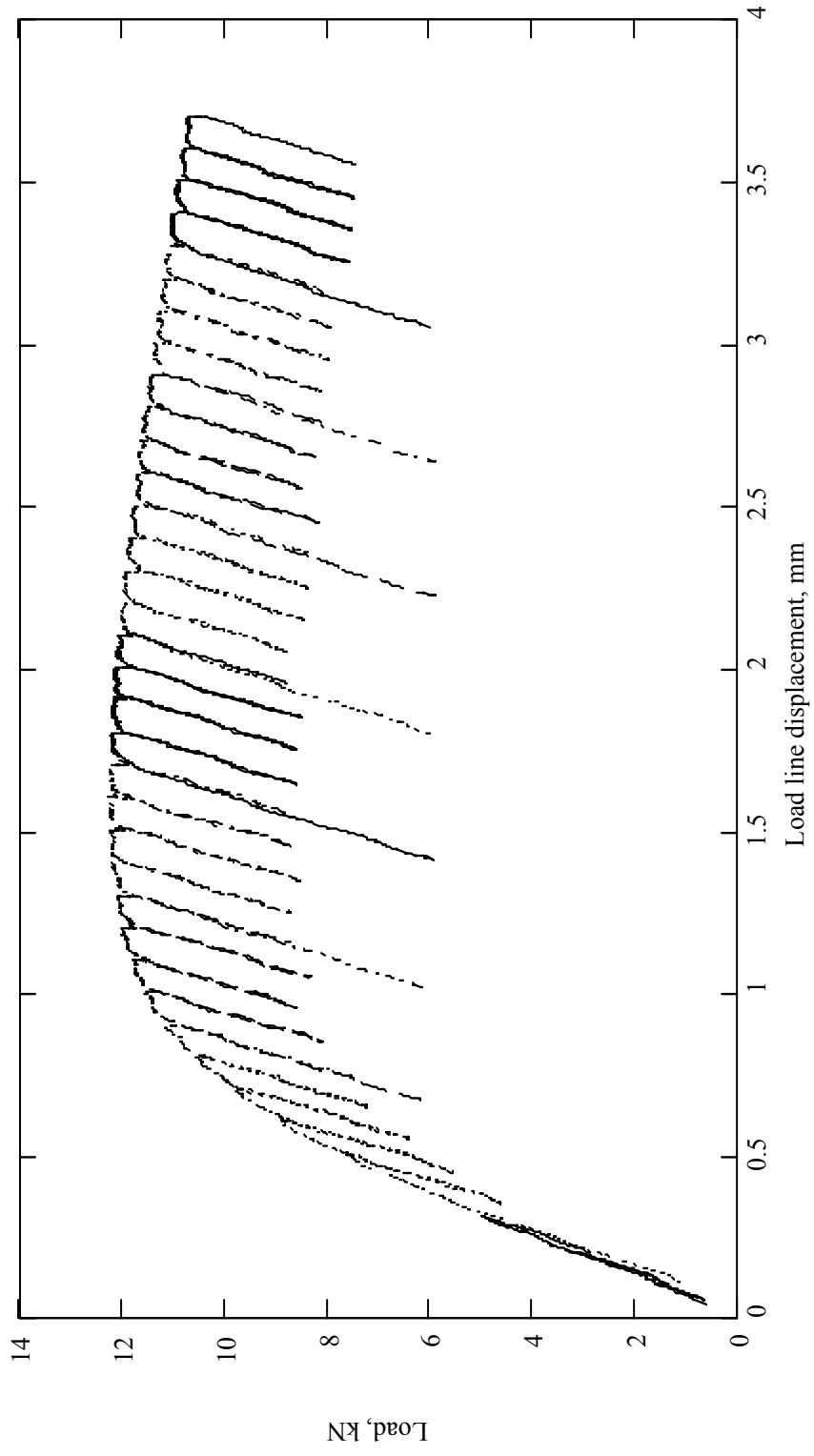| Specimen, Vr	Δa (phys.) mm	Δa (cal.) mm	$\dfrac{\Delta a(phys)}{\Delta a(cal.)}$
0.41 -1	1.6619	2.1536	0.7717
0.41 -2	1.0176	1.6869	0.6032
0.81	2.2256	1.5703	1.4173

Figure 5.5. Load - load line displacement of laminate for Vr=0.41-1

J-integral, kJ/m²

Crack extension, mm

exclusion lines parallel to blunting line

$J=251.34(\Delta a)^{0.07645}$

$J=1070(\Delta a)$

blunting line

97

(a)

exclusion lines parallel to blunting line

$J=271.65(\Delta a)^{0.8137}$

$J=1070(\Delta a)$

blunting
line

Crack extension, mm

J-integral,kJ/m^2

(b)
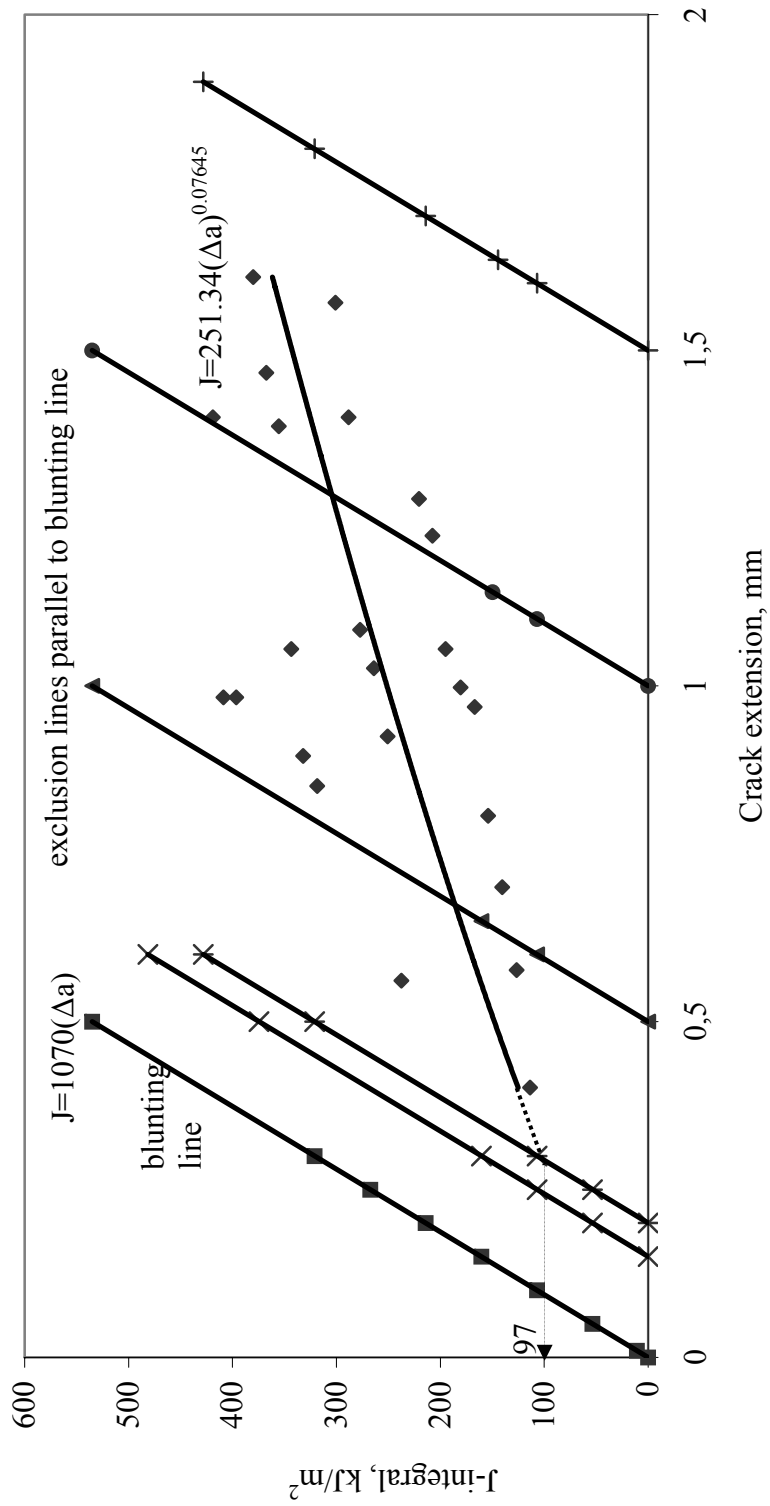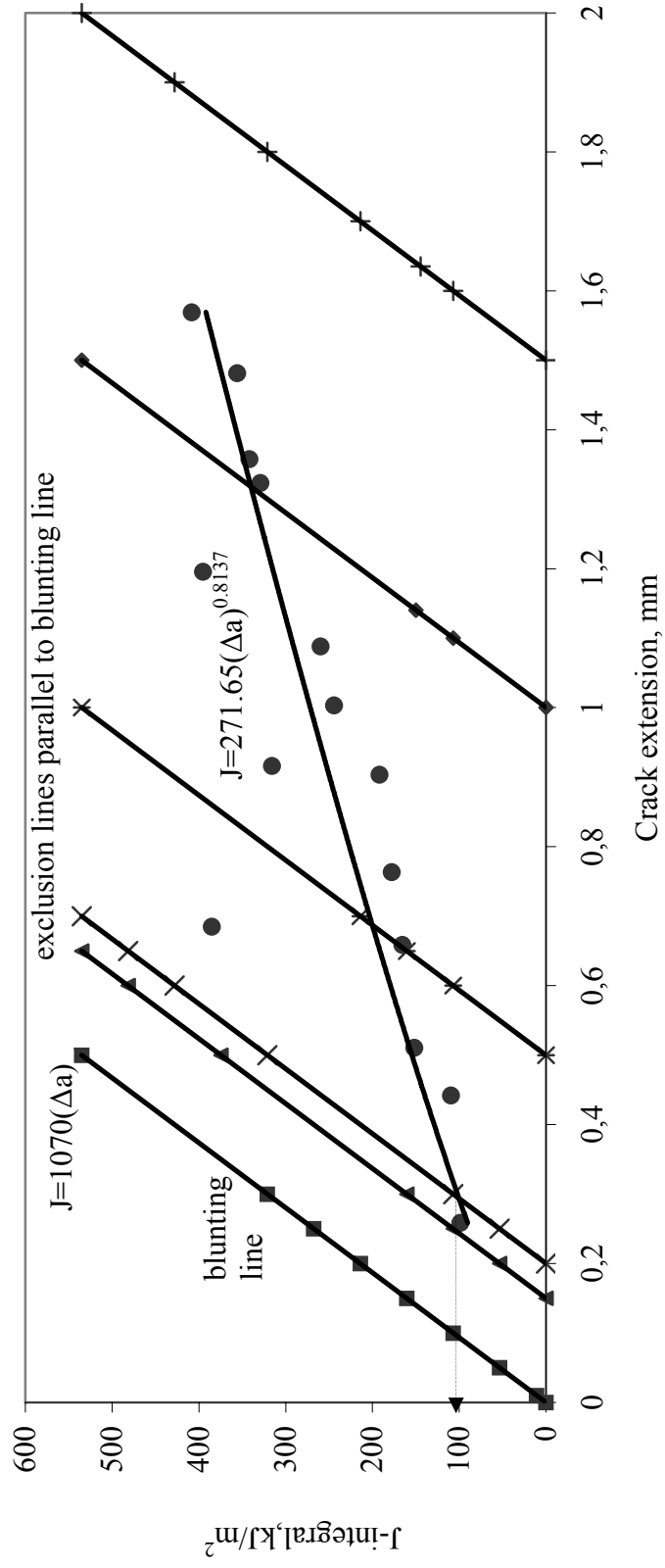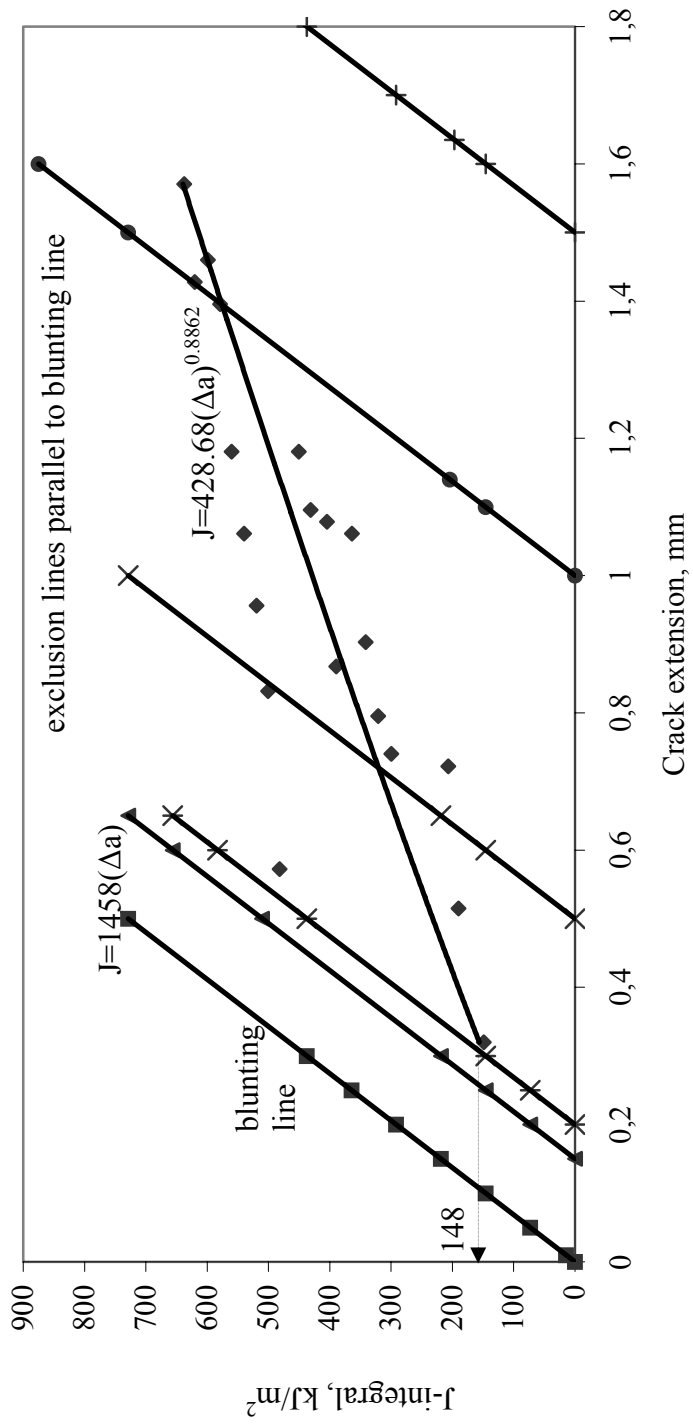
Figure 5.6. *J-crack extension curve of laminates for a) Vr=0.41-1 b) Vr=0.41-2 c) Vr=0.81*

Part of the reason for the differences between physically measured values and those calculated by the compliance method may be due to poor clevis design as well as due to the use of insufficient holding time. For instance with holding time of 10 sec. used in the current work, the load did not relax fully, as seen in Fig 5.7. Thus some improvements are possible by modification of experimental conditions. As reported in section 2.3, difference between physically measured crack length and those calculated by compliance method even in monolithic materials may differ from each other by a factor between 0.42 and 2.918 (Gudas and Davis, 1982). Considering these, the values found in this work are therefore quite acceptable.
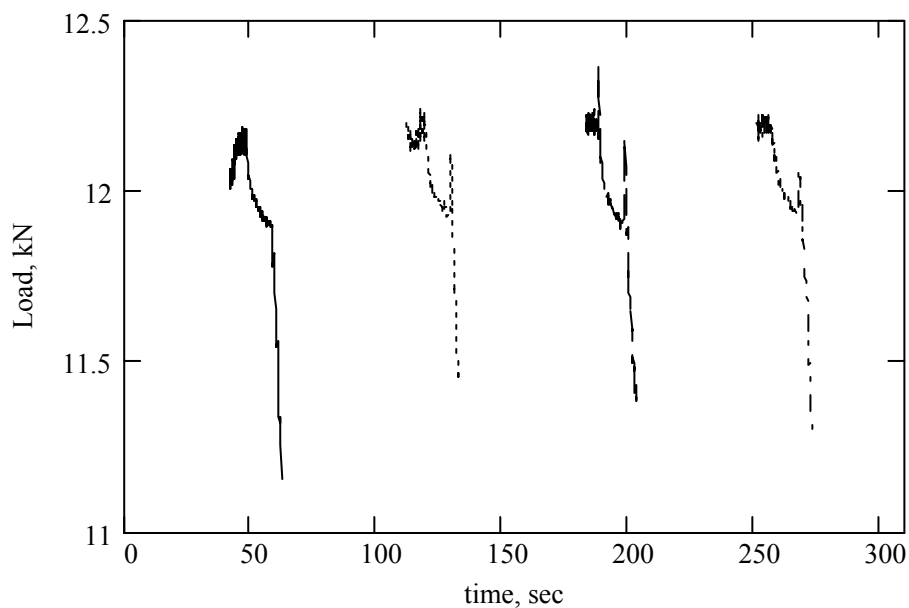

Figure 5.7. *Load versus time curve of laminate of Vr=0.41-1 for the third ramping during holding time before unloading*

Fracture surfaces in the laminates with Vr=0.41 and Vr=0.81 are shown in Figs 5.8-9. For the former the crack growth was not uniform across the hard and soft layers. The soft layers show signs of deformation without crack growth, whereas crack has advanced considerably in the hard layer. There are severe delaminations between soft and hard layers. Where two soft layers are in contact no delamination was observed.
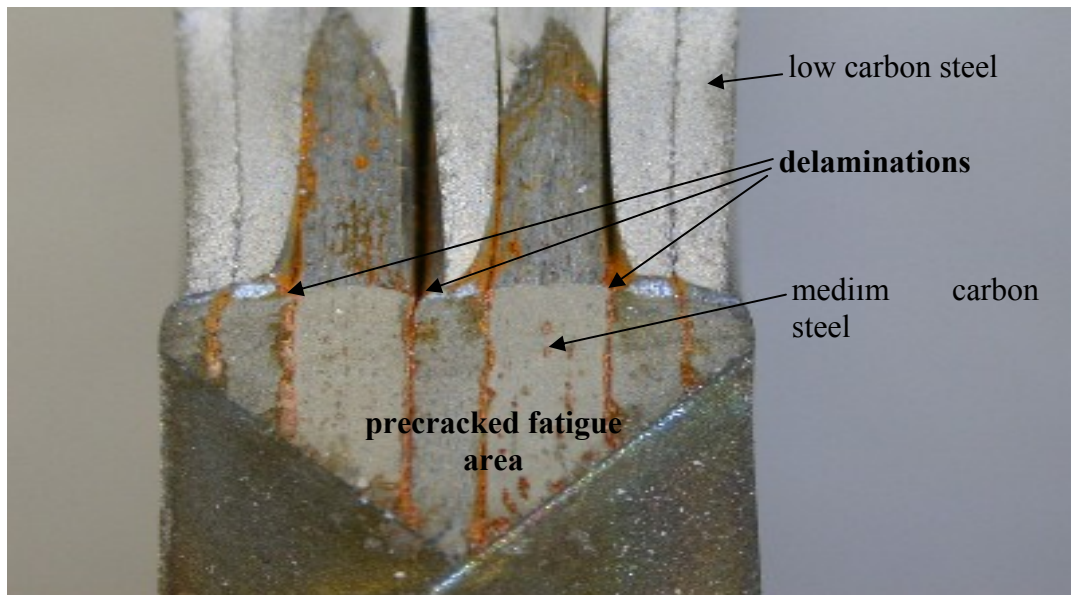
Figure 5.8. *Fracture surface of laminate for Vr=0.41-1; precracked fatigue area: no delamination, delamination of interface, the low carbon steel: no crack extension, the medium carbon steel: crack extension deep and parabolic.*

With sample with Vr=0.81, the case was similar. This sample contained alternate layers of soft and hard materials and as a result delamination occurred between all layers, Fig. 5.9.
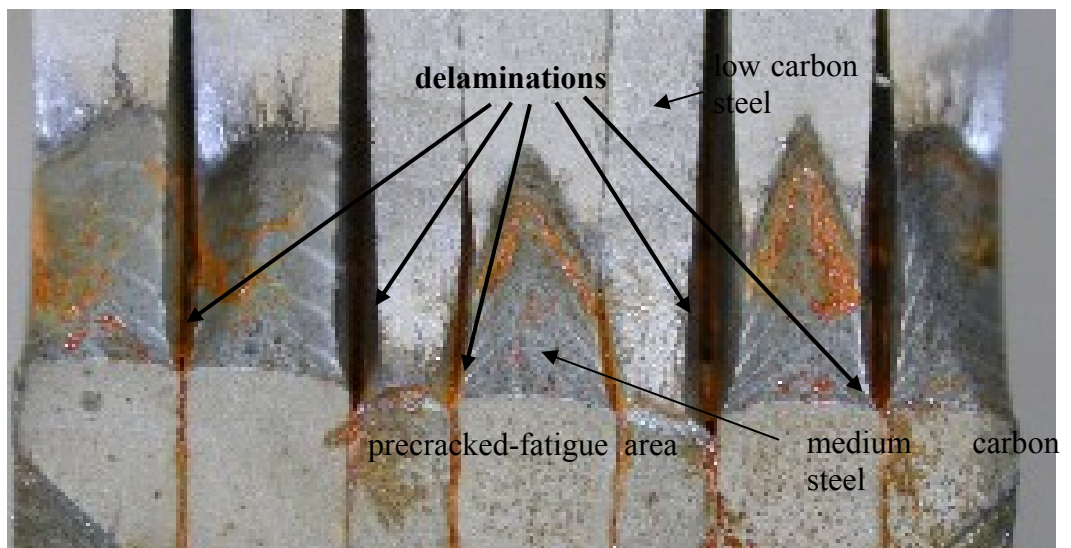

Figure 5.9. *Fracture surface of laminate for Vr=0.81; precracked fatigue area: no delamination, delamination of interface, low carbon steel: no crack extension, medium carbon steel: crack extension deep and parabolic.*

5.2. Numerical Analysis

In order to predict the fracture toughness of laminates, a methodology is employed starting from monolithic material. First 2D model was used to predict J_{IC} under plane strain condition. This is followed by a 3 D model in which the brick elements deformed freely. Then 3-D model is layered artificially to predict J_{IC}. Finally 3-D layered model is adapted for laminates. Greater portion of the analysis concentrated on verification of the model with monolithic materials, namely HY 130 steel for which extensive data is available from literature (Clarke et al. 1980), and medium carbon steel AISI 1050 used in the present study.

5.2.1. Fracture Criterion

In all prediction J values are determined as a function of load line displacement without crack growth. J_{IC} is determined by assuming a critical value for load line displacement (LLD). This value is taken from experimental measurements on crack extension- LLD relations. Crack extension of 0.2 mm was taken as the critical value and its corresponding LLD was taken as the critical value for the predictions.

5.2.2. Verification of the Model

2-D Model: Material properties as well as geometric data used for 2-D analysis are given in Tables 5.5 and 5.6. These are taken from Clark et al and refer to HY 130 steel, the material that was the subject of extensive cooperative program in the 80's (Clarke et al., 1980). J values as a function of LLD obtained with 2-D are summarized in Table 5.7. The corresponding experimental values are given in Table 5.7. Results are compared in Fig.5.11. The predicted values compare well with experimental results, the difference is lower than 3 %.

Table 5.5. *Mechanical properties for HY130 Steel taken from Kuang and Chen (1996)*

E GPa	σ_{ys} MPa	σ_{UTS} MPa	κ MPa	n	ν
200	975	1030	1140	40	0.3

Table 5.6. *J values as a function of crack extension, Δa for HY 130 steel taken from Clarke et al. (1980).*

B mm	a_o/W	Δa mm	J-integral kJ/m^2
22.86	0.65	0	71
22.86	0.65	0.05	111
22.86	0.65	0.13	146
22.86	0.65	0.25	168
22.86	0.65	0.66	208

Table 5.7. *J values as a function of load line displacement for HY 130 Steel predicted from 2D analysis. Experimental J values were taken from Clarke et al. (1980)*

Load line displacement mm	J-integral 2D kJ/m^2	J-integral experimental kJ/m^2
0.53	71	71
0.66	109	111
0.77	147	146
0.84	173	168
0.93	209	208

J-values are determined with 2-D analysis as a function of LLD. This enabled the determination of LLD versus crack extension curve, Fig. 5.10. It is seen that the crack extension of 0.2 mm corresponds to LLD of 0.82 mm. Using critical LLD of 0.82 mm, the fracture toughness of HY 130 was predicted to have a value of 165 kJ/m^2, see Fig.5.11. Experimental value reported for this material was 175±35 kJ/m^2. The values are in good agreement.
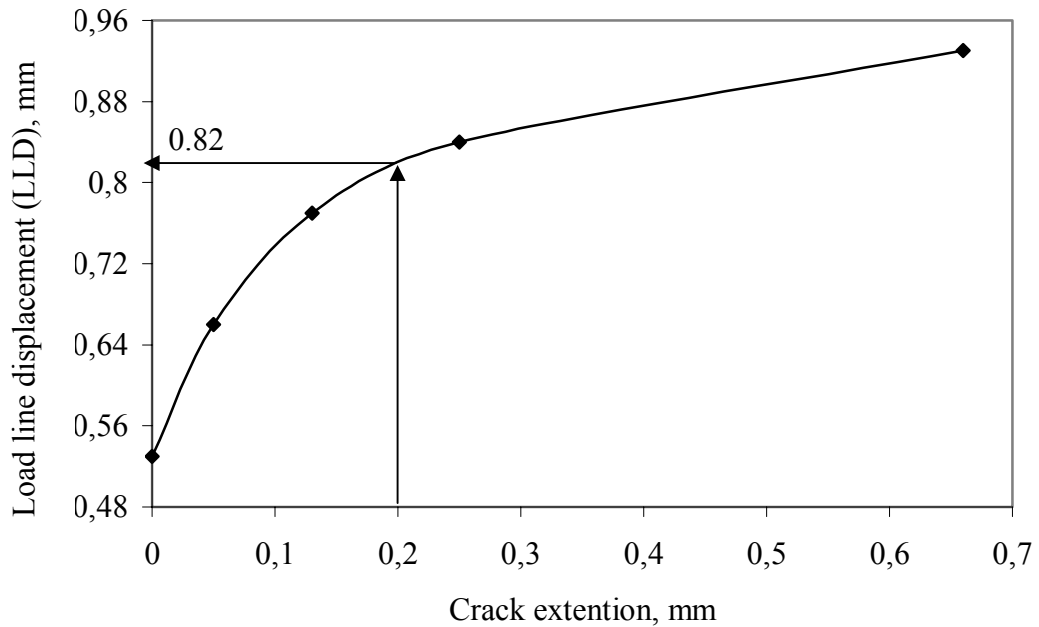

Figure 5.10. *Load line displacements predicted from 2D analysis versus those taken from Clarke et al. (1980). The critical load line displacement was determined for 0.2 mm crack extension.*
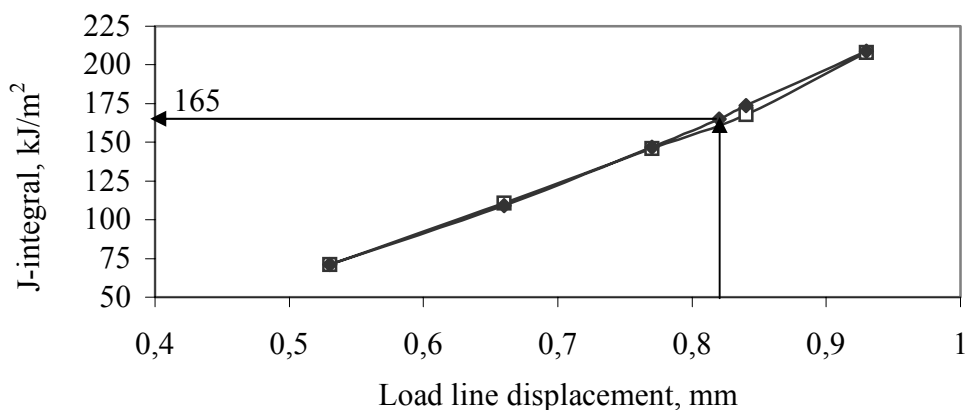

Figure 5.11. *J values for HY 130 steel. Solid symbols are those predicted with 2D analysis and open symbols show values taken from Clarke et al. (1980)*

3-D Model: J values versus LLD predicted with 3-D model are given in Table 5.8 and Fig. 5.13. J values across the sample thickness are shown plotted in Fig. 5.12. It is seen that J values are lower at the surface, where the conditions are plane-stress, but increases inside the sample reaching a plateau at 1/3 the thickness. Using the same approach, J_{IC} predicted for HY130 steel with 3D analysis, was 150 kJ/m^2. This is slightly less than the value predicted with 2-D analysis. This is the consequence of the variation of J across the sample thickness.
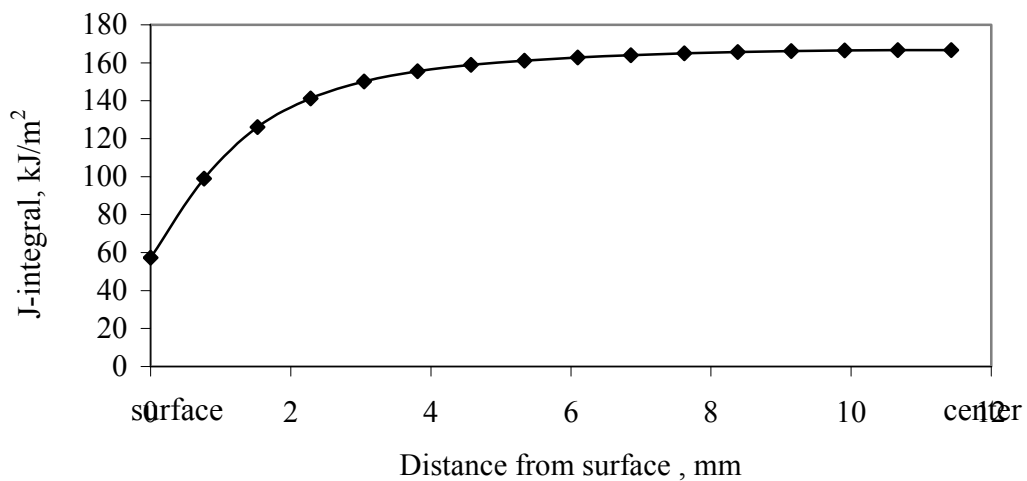

Figure5.12. *Variation of J Integral values (from 3D analysis) from surface to center for HY 130 Steel.*

Table 5.8. *J-values as a function of load line displacement for HY 130 steel predicted from 3D analysis. Experimental values are those from Clarke et al. (1980)*

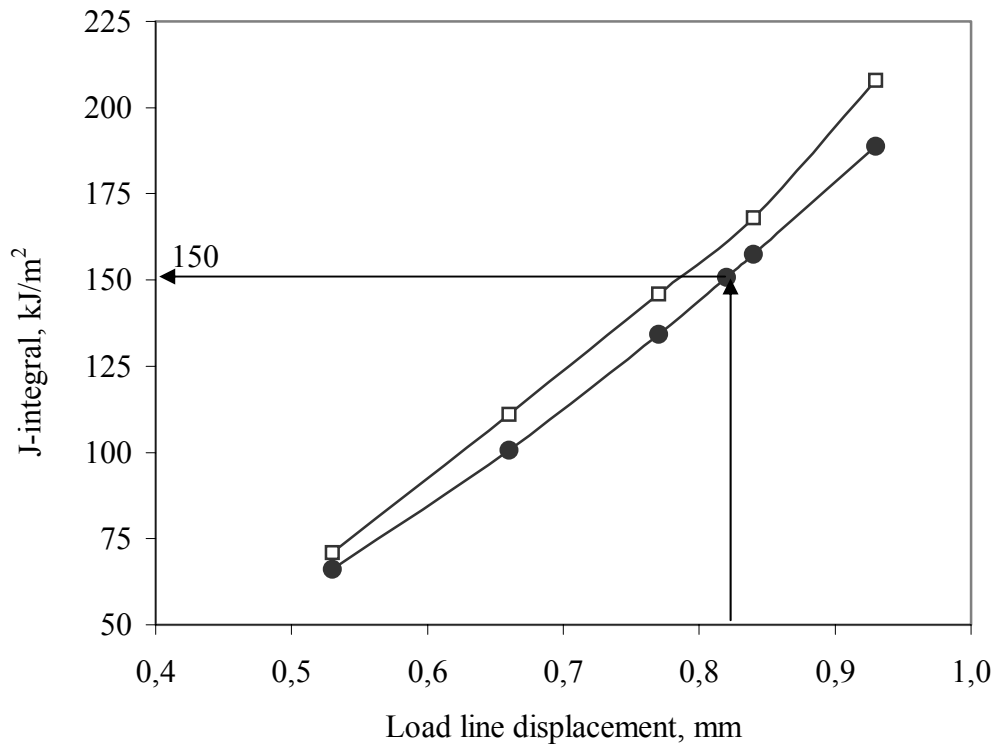| Load line displacement mm	J*-integral 3D kJ/m^2	J-integral experimental kJ/m^2
0.53	66	71
0.66	100	111
0.77	134	146
0.84	157	168
0.93	188	208

Figure 5.13. *J values for HY 130 steel. Solid symbols are those predicted with 3D analysis and open symbols show values taken from Clarke et al. (1980)*

3-D Layered Model: 3-D layered model is verified with HY 130 steel as before. This model is also verified with experimental measurements on monolithic steel (1050)

Across the sample thickness, J values vary as before. Additionally however, there were scatter at the J values very near the interface. A typical example is given in Fig. 5.14. As mentioned in section 4.2.3, these scatter were excluded from data and the values were averaged across the sample thickness. Variation of averaged J values as a function of LLD is given in Table 5.9 and Fig. 5.15. It is seen that using a value of LLD=0.82, the model yields a value of J_{IC}=154 kJ/m² for HY 130 steel.

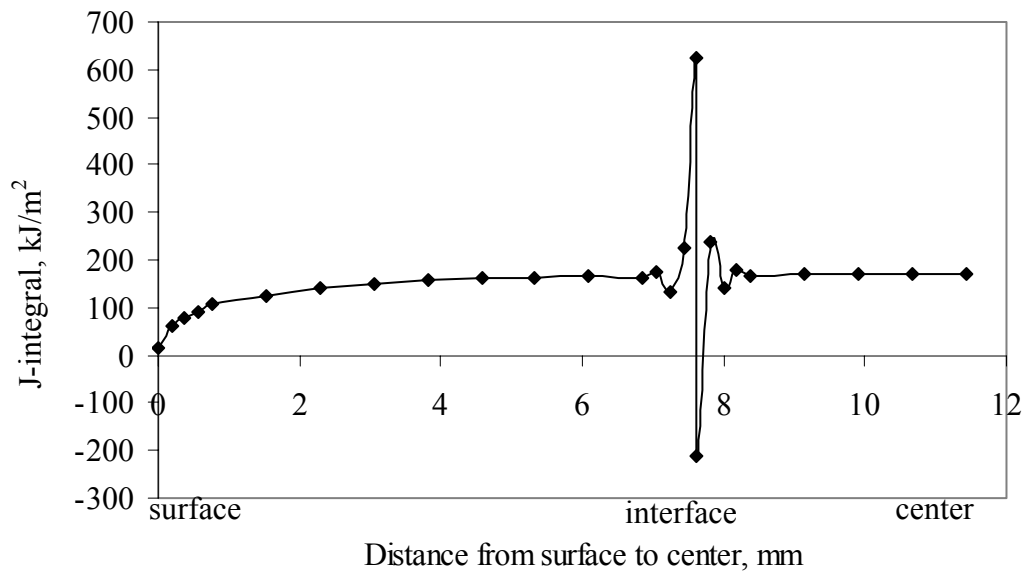***Figure 5.14.*** *Variation of J Integral values (from layered analysis) from surface to center for HY 130 Steel, with fluctuation at the interface*

Table.5.9. *J values as a function of load line displacement for HY130 Steel predicted from layered analysis. Experimental J values are those from Clarke et al. (1980).*

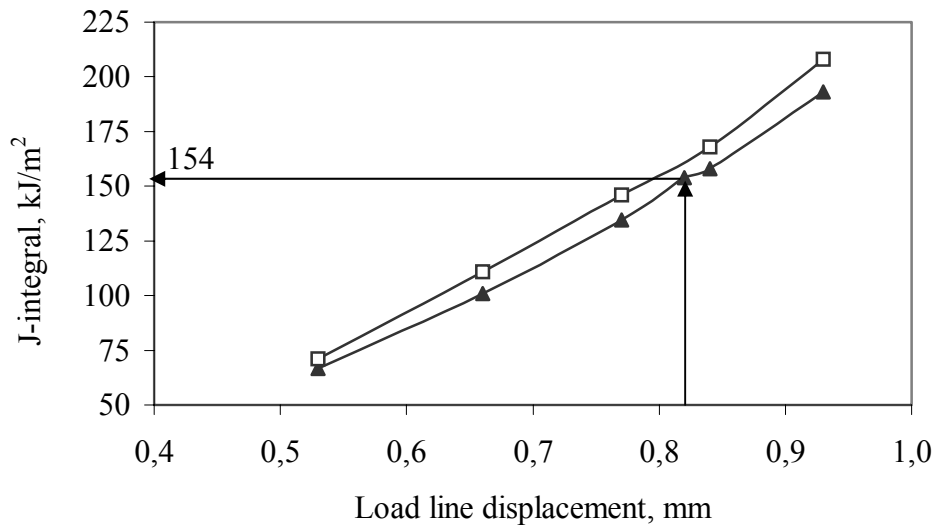| Load line displacement mm	J*-integral 3D-layered kJ/m²	J-integral experimental kJ/m²
0.53	66	71
0.66	101	111
0.77	134	146
0.84	157	168
0.93	193	208

Figure 5.15. *J values for HY 130 steel. Sold symbols are those predicted with layered analysis and open symbols show values taken from Clarke et al. (1980)*

The values obtained with 2-D, 3-D and layered 3-D model are collected together in Table 5.10 and Fig. 5.16. It is seen that J_{IC} has values of 165 kJ/m^2 for 2-D, 150 kJ/m^2 for 3-D and 154 kJ/m^2 for 3-D layered models. These values are quite close to one another, indicating that 3-D layered model can be applied safely for J_{IC} evaluation of steel laminates

Table 5.10. *J* values as a function of load line displacement for HY 130 steel. Predicted J values obtained from 2D, 3D and layered analyses. Experimental J-values are those from Clarke et al. (1980).*

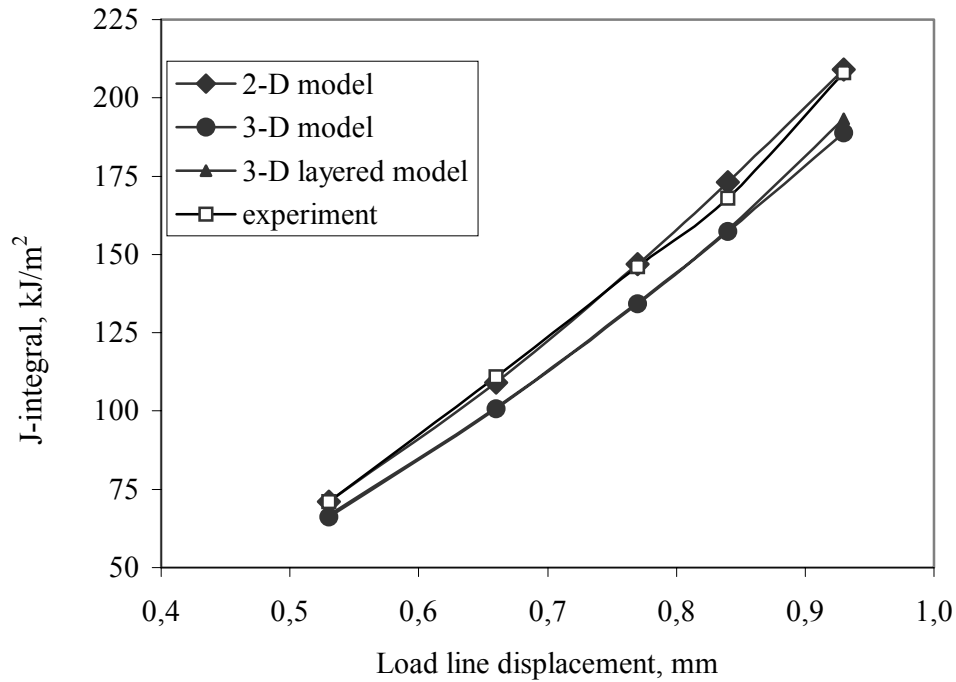| LLD mm	J*-integral 2D kJ/m^2	J*-integral 3D kJ/m^2	J*-integral 3D-layered kJ/m^2	J-integral experimental kJ/m^2
0.53	71	66	66	71
0.66	109	100	101	111
0.77	147	134	134	146
0.82	**165**	**150**	**154**	**175±35**
0.84	173.5	157	157	168
0.93	209	188	193	208

Figure 5.16 *Variation of J integral values as a function of load line displacement for HY130 Steel. Open symbols are those predicted with layered analysis and solid symbols show values taken from Clarke et al. (1980)*

As a further check whether or not 3-D layered model could be used for prediction similar evaluation is carried out for AISI 1050 steel. As reported in section 4.2.3, J_{IC} of this material was measured to have an average value of 136 kJ/m². Experimentally measured LLD versus crack extension data for this material averaged for two samples is given Fig.5.17. Again crack extension value of 0.2 mm was taken as the critical value. This corresponds to LLDs of 1.09 mm. 3-D layered model for the critical LLD of 1.09 mm yields a value 112.5 kJ/m². This value compares well with 136 kJ/m² i.e. experimental value measured for this material (see Table. 5.11).
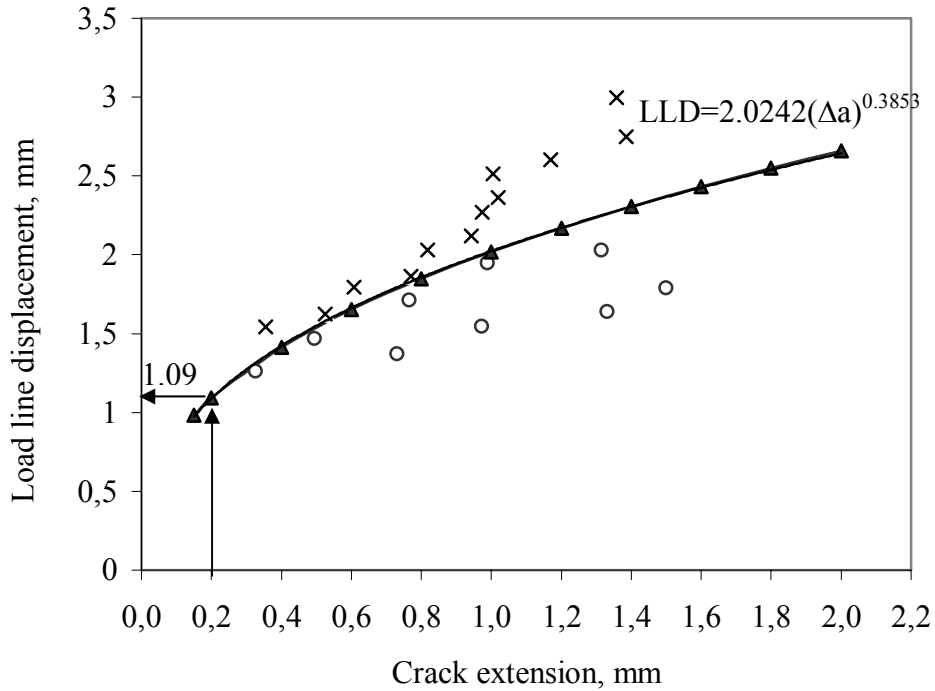
Figure 5.17. *Experimentally measured LLD versus crack extension data for AISI 1050 steel. Data shown with x and o are obtained from different samples, ▲ are the average values.* .

Table 5.11. *J values predicted from layered analysis of monolithic AISI 1050 steel. Experimental J values are those obtained from partially unloading compliance method.*

Specimen	J_{IC} experimental kJ/m2	J_{IC} 3D-layered kJ/m2
1050	136.0	112.5

5.2.3. Prediction of J_{IC} for Steel Laminates

Evaluation with respect to steel laminates is similar to 3-D layered model. This is with the difference that properties assigned to layers varied in accordance with properties measured for each phase (see section 4.1.1).

Critical value of LLD was determined based on experiment. The experimental relationship between LLD and crack extension is given in Fig 5.18 and 5.19 for the laminates with volume fraction of Vr=0.41 and Vr=0.81 respectively. These yield critical LLD values of 0.91 mm, and 1.04 mm in the same order.
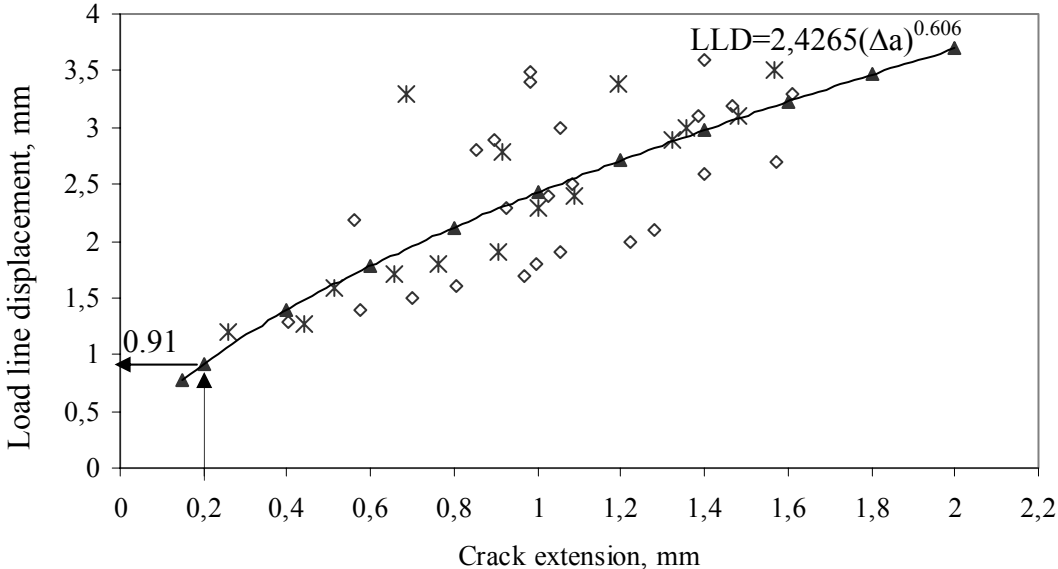

Figure 5.18. *Experimentally measured LLD versus crack extension data for Vr=0.41 laminate. Data shown with ✳ and ◊ o are obtained from different samples, ▲ shows the average values of LLD as a function of crack extension*

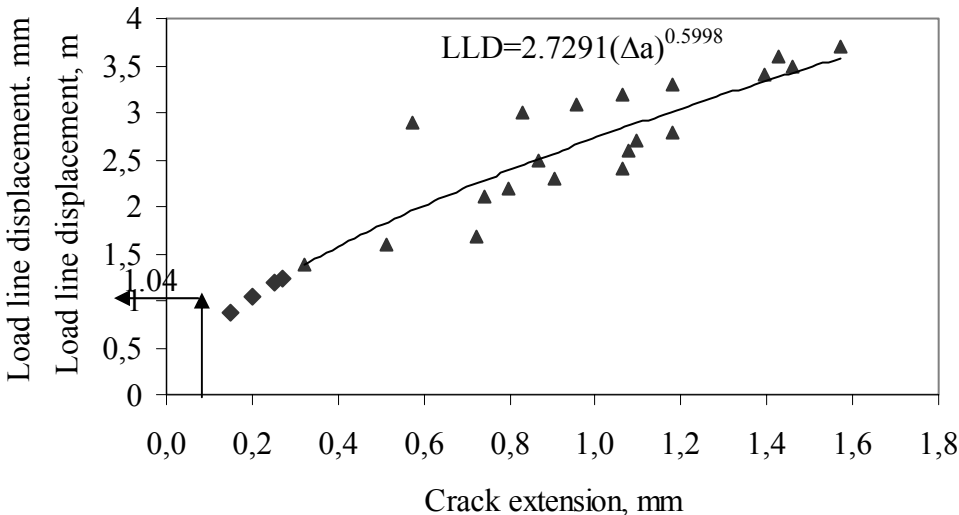**Figure 5.19.** *Experimentally measured LLD versus crack extension data for Vr=0.81 laminate. Data is extrapolated, shown ◆-with to values less than 0.32.*

Since the properties of layers are different, J values vary across the thickness of the sample in the expected manner. A typical example is given Fig.5.20. Here J values are lower in the softer layer and increases in the hard layer with an overall pattern of rising J as it is moved from surface of the sample to its center.
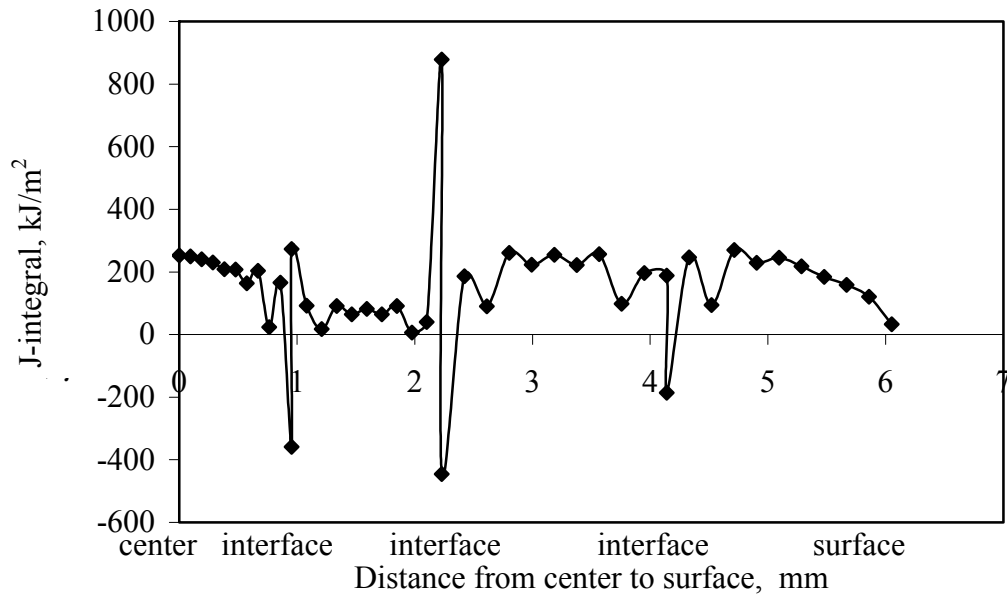

Figure 5.20. *Variation of J-integral values (from 3D-layered analysis) from center to surface for Vr=0.81 composite, with fluctuations at the interfaces*

Evaluation for steel laminates yield J_{IC} values of 98.3, and 156.6 kJ/m^2 for Vr=0.41 and Vr=0.81 respectively. For this evaluation no interface separation was permitted. Therefore the values are applicable where the interfacial strength is extremely high.

3-D layered model as implemented for the laminates enables the separation of layers, i.e. delamination, if the stress normal to interface is greater than a critical value (see section 4.2.3). This critical value based on the measurements was 118 MPa.

In order to check whether or not the model works for delamination, a separate simple model was used. The details of this model are given in section 4.2.3, and will

not be repeated here. Fig 5.21 shows the model after a macroscopic strain of 0.017. Bright region at the middle shows the delamination. The variation of normal stress was monitored as a function of displacement. It was noted that when normal stress exceeds the separation stress, the interface separates indicating that implementing the same procedure for 3-D layered model would enable the examination of delamination effect in the laminates.
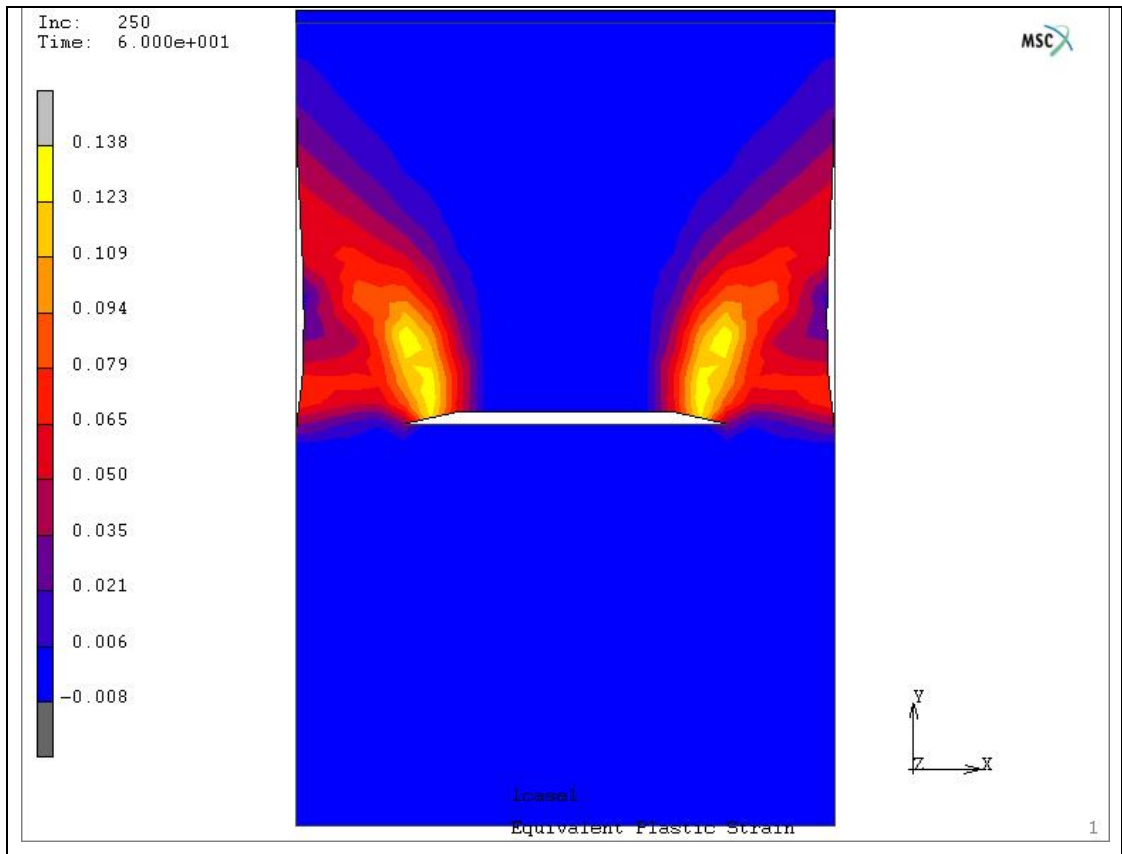

Figure 5.21. *Delamination in a joined plate after a macroscopic strain of εy= 0.017. The plate is made of two parts; one low carbon steel (upper half), one medium carbon steel (lower half). Middle portion of the interface is "glued together" with interfacial stress of 118 MPa. Figure shows equivalent plastic strain distribution. Bright region shows separation of the interface.*

At the critical values of LLD both samples Vr=0.41 and Vr=0.81 showed delamination. Examples of this for Vr=0.41 at distances of 0, 0.2, 0.8, and 1.6 mm are shown in Fig. 5.22. Here distances refer to location of the section with respect to

crack plane. It is found that delamination occurs within a volume whose length (in front of crack plane) is approximately 4.6 mm and with a height of approximately 1.6 mm. The values for Vr=0.81, Fig. 23, are 8.17 mm and 1.6 mm in the same order.

As reported above, delamination was also observed in the experiments. Only the depth of delamination was measured which had values of 0.6 mm and 0.7 mm for Vr=0.41 and Vr=0.81 respectively. Delamination observed larger in the model.

At the critical values of LLDs, values of J_{IC} derived for the laminates are 100 kJ/m^2 for Vr=0.41 and 165 kJ/m^2 for Vr=0.81 (Table 5.12). These values should be compared with earlier values of 98.3, and 156.6 kJ/m^2 which were obtained without delamination. Thus as expected when delamination is allowed, the prediction leads to higher values for fracture toughness.

The values with delamination are compared with experiment in Table 5.12. The value for monolithic material was also included into the table. It is seen that predicted J_{IC} show the same trend as the experiments. Differences between predicted values and the experiments are not more than 20%.

Table 5.12. *J values predicted from layered analysis for composite materials with Vr=0.41 and Vr=0.81. Experimental J values are those obtained from partially unloading compliance method.*

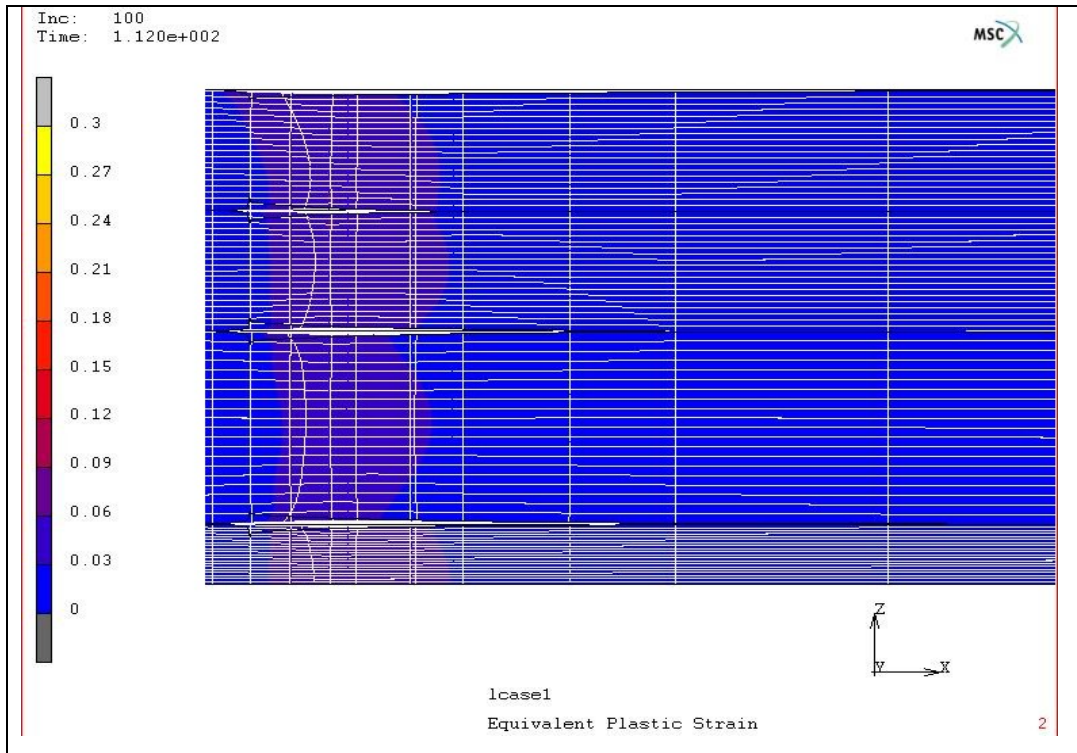| Materials	J_{IC} experimental Kj/m2	J_{IC} predicted Kj/m2
Steel laminate (Vr=0.41)	98.8	100.5
Monolithic	136.0	112.5
Steel laminate (Vr=0.81)	148.3	165.3
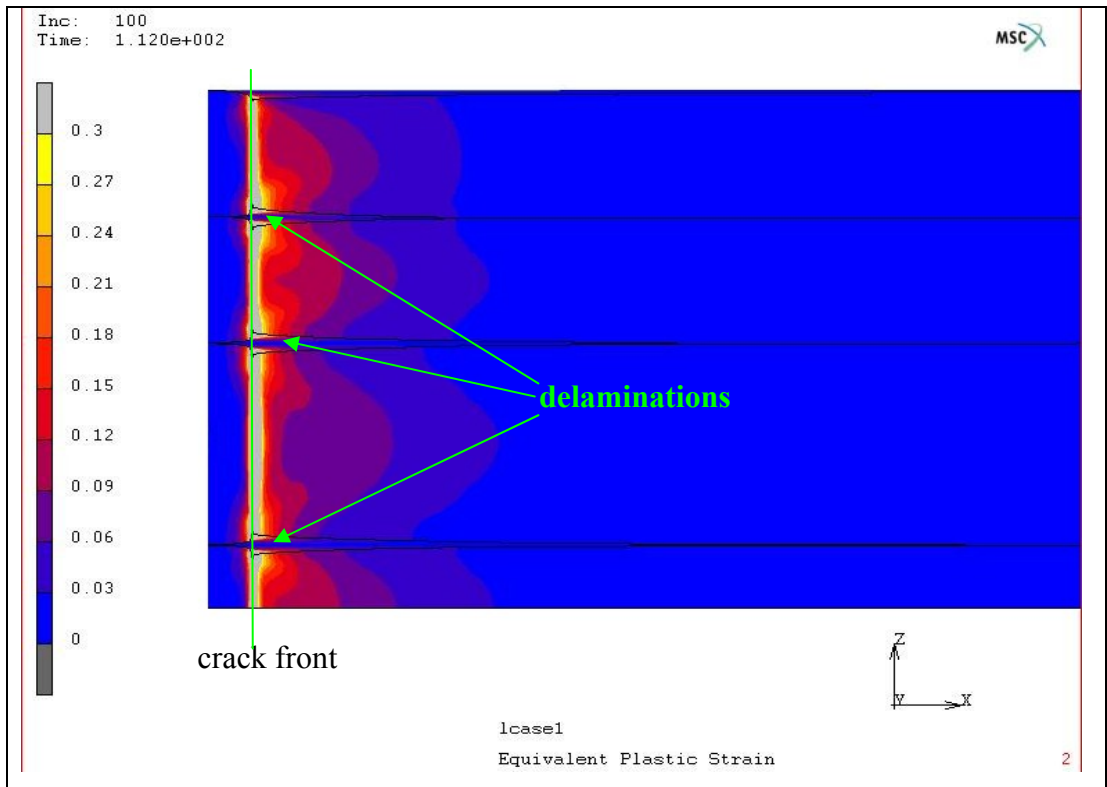
(a)
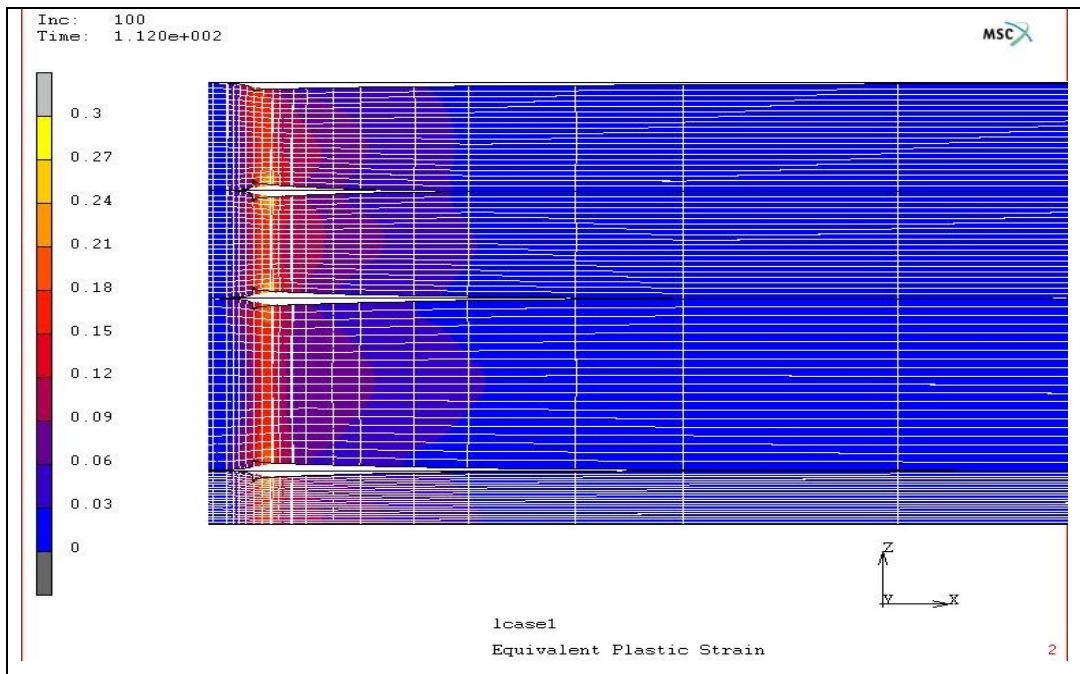
(b)

(c)
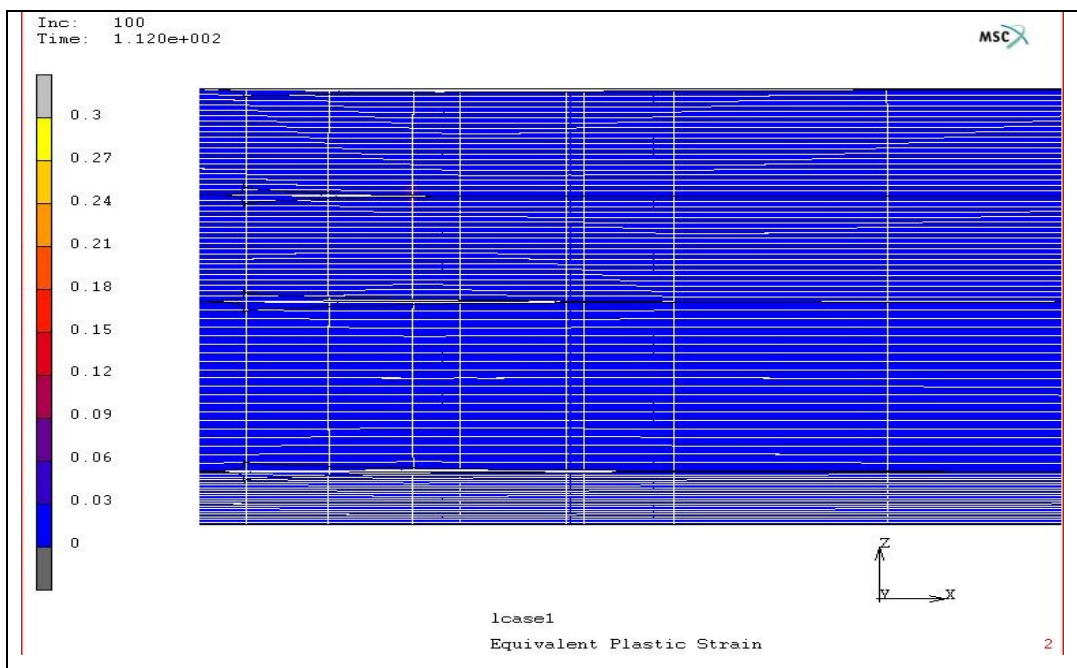
(d)

Figure 5.22. *Delamination in Vr=0.41. At sections parallel to the crack plane. Values indicated refer to equivalent plastic strain, only values up to ε_{eqv}=0. 3 are shown. Distance from the crack plane are; a) 0 b)0.2 c) 0.8 d) 1.6 mm.*
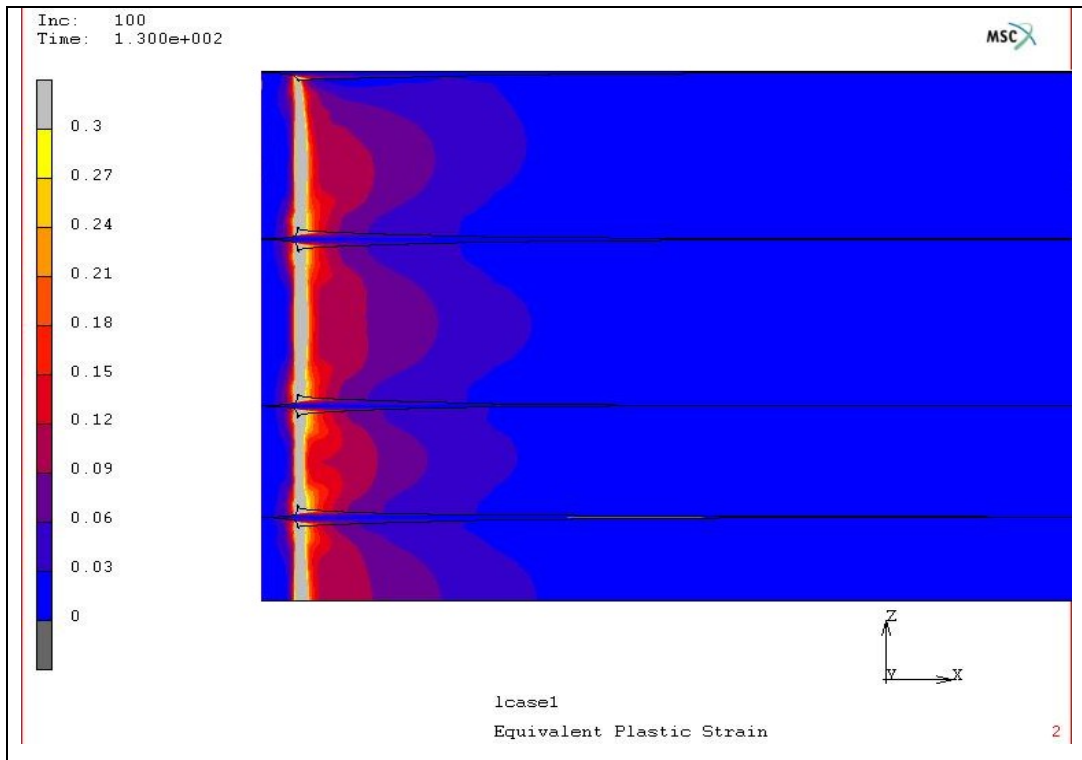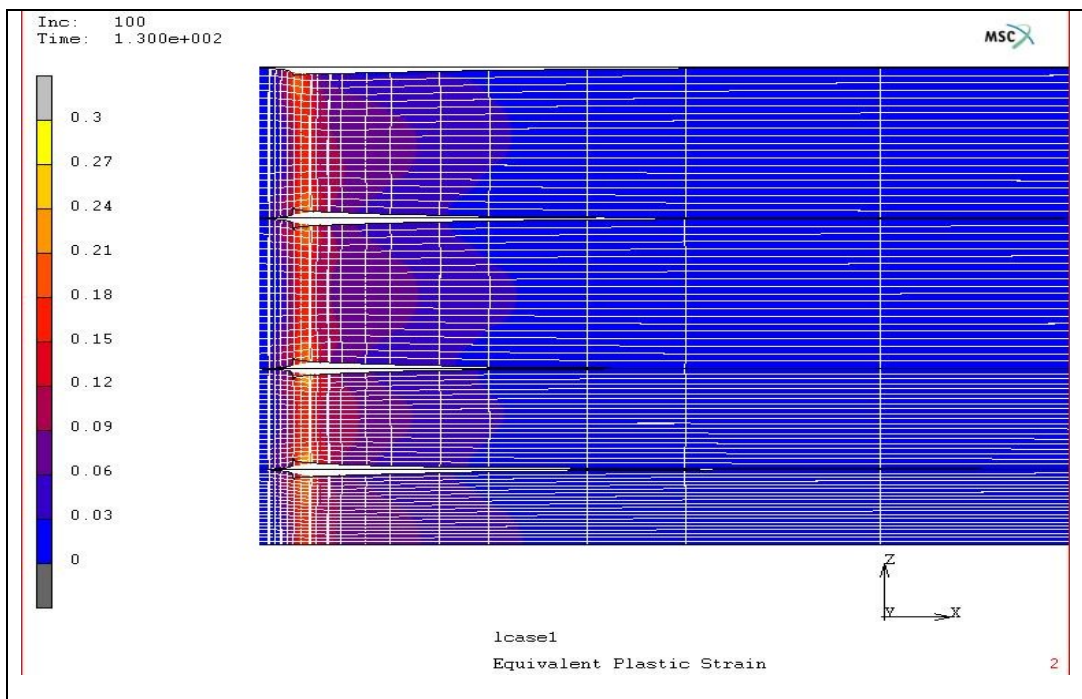
(a)
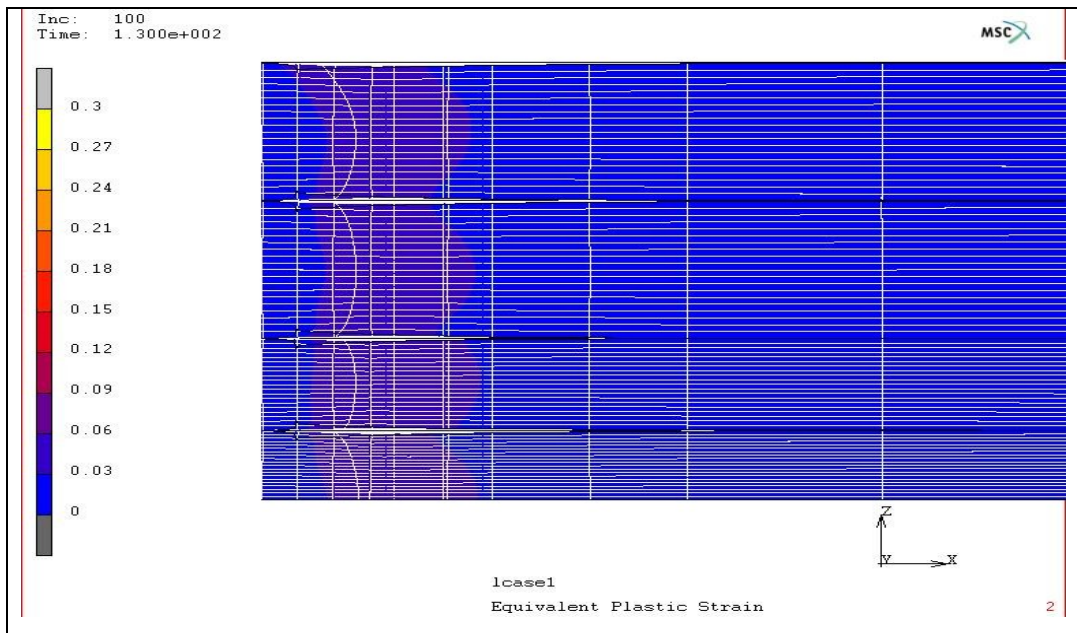

(b)

82

(c)

(d)

***Figure* 5.23.** *Delamination in Vr=0.81, at sections parallel to the crack plane. Values indicated refer to equivalent plastic strain, only values up to ε_{eqv}=0. 3 are shown. Distance from the crack plane are; a) 0   b) 0.2   c) 0.8   d) 1.6 mm.*
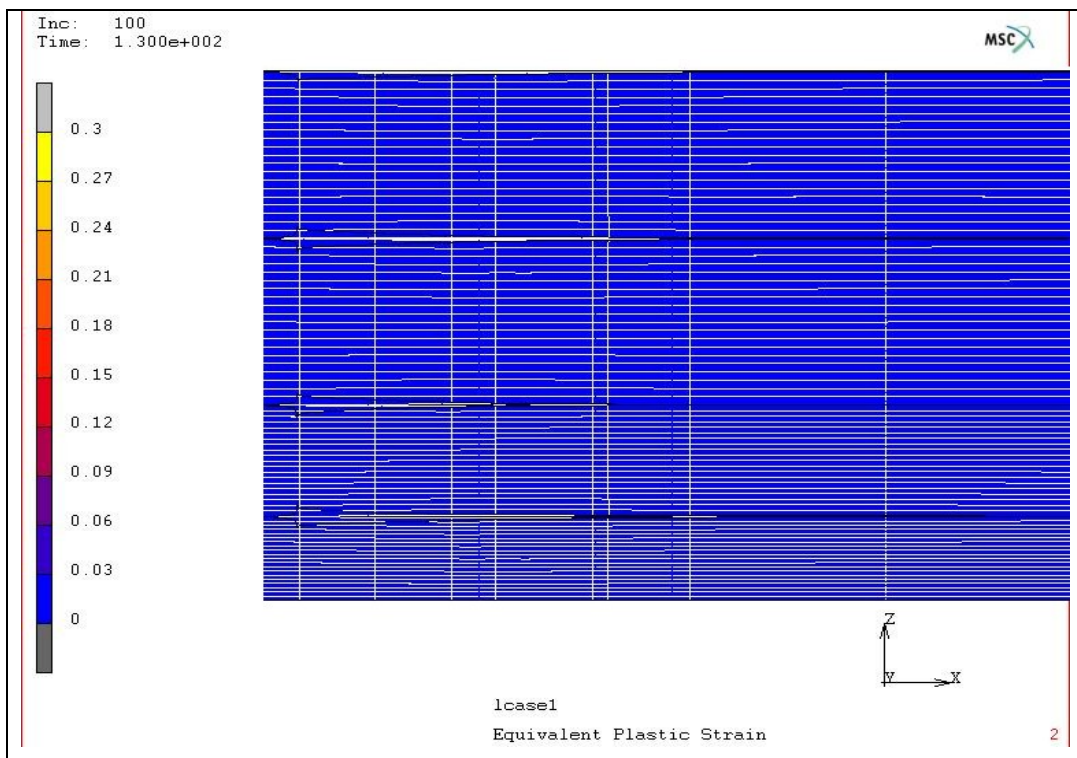
5.3. Discussion

Results show that   fracture toughness of laminates can be predicted successfully with finite element analysis. To be able to predict the toughness of laminates would be useful for structural optimization, i.e. volume fraction size and properties of layers. However a difficulty in the current approach is that critical value of LLD should be determined experimentally. Thus there is still a need for experiment. An alternative approach would be to base the fracture criterion on plastic zone size which could be predicted with FEM without the need for experiment.

Variation of plastic zone size with LLD in 2-D analysis for HY 130 and AISI 1050 steel is given in Fig. 5.24 (a and b). It is seen   that initially there is a rapid increase of plastic zone size with LLD. But after a certain value of LLD, the zone size reaches saturation. 95 % of the saturation value yields LLD values of 0.74 mm and 1.12 mm for HY130 steel and 1050 steel respectively. These values compare with critical values of 0.82 mm and 1.1 mm determined based on experimental crack growth-LLD data. It is seen that the values are quite close to each other.

Similar evaluation for the laminates are not carried out.   But it is likely that the evaluation based on experimental measurement of critical LLD may well be based on critical value of plastic zone size, with the advantage that the latter could be predicted directly without the need for experiment.
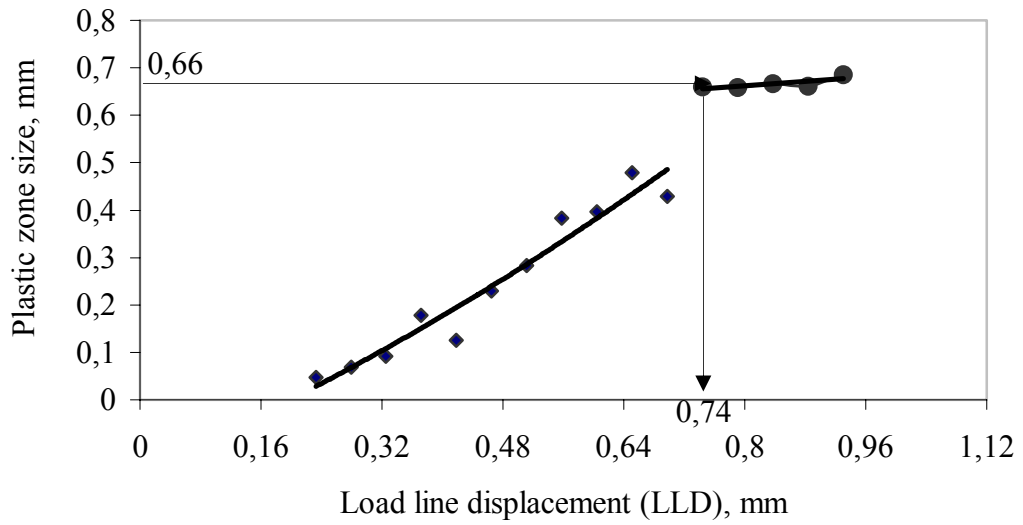
(a)
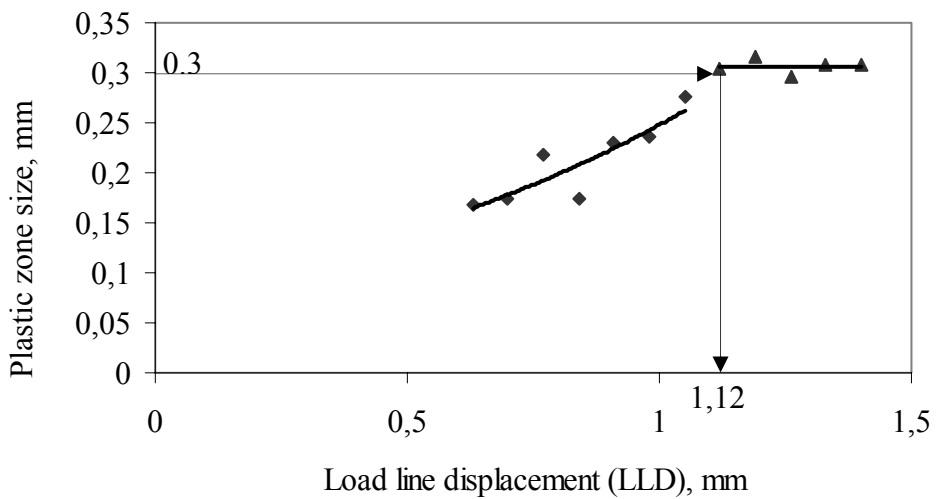
(b)

Figure5.24. *Variation of plastic zone size with LLD in 2-D analysis for
a) HY 130 steel   b) AISI 1050 steel*

CHAPTER VI

CONCLUSION

From experimental part of the current study on fracture toughness of steel and steel laminates the following can be concluded

i) J_{IC} of hot rolled 1050 steel determined with partial unloading technique has a fracture toughness value of $J_{IC}= 139.5$ kJ/m^2

ii) Steel laminates made up of low –C steel (yield stress: 232 MPa) and medium- C steel quenched and tempered (yield stress: 858 MPa) have fracture toughness values, measured again with partial unloading technique of $J_{IC}= 98.5$ kJ/m^2, and $J_{IC}= 148$ kJ/m^2 for volume fraction (hard phase) of Vr= 0.41 and Vr= 0.81 respectively.

The purpose of the current work is to determine the extent to which fracture toughness of laminates composites could be determined with finite element analysis. From the numerical part of the current study, the following can be concluded;

iii) Finite element package program, MARC, with details implemented in this work leads to successful prediction of J values reported in the literature for HY 130 and AISI 1050 steel. The critical value of J_{IC} can be determined based on a critical value of load line displacement determined experimentally.

iv) With the same approach J_{IC} of steel laminates can be predicted successfully with and without delamination.

v) It is found that with delamination fracture toughness of steel laminates are improved and have values of J_{IC}= 100.6 kJ/m^2 and J_{IC} =165 kJ/m^2 for Vr=0.41 and Vr=0.81 respectively.

vi) From prediction of load line displacement versus plastic zone size relationship it is found that a criterion for fracture may be based on a critical value of plastic zone size. This critical value may be predicted with finite element analysis without the need for experiment.

The current work, dealt with steel laminates in which the both phase are ductile. This was for the purpose of selecting a suitable system for J_{IC} evaluation, which is known to be applicable to cases where considerable plasticity is involved in the fracture process. Thus the finite element method as implemented in the work verified with ductile steel laminates may be used for structural optimization of other more useful composite systems, e.g. for intermetallic reinforced metal laminates.

REFERENCES

Alic, J. A., Danesh, A. Eng. Fracture Mechanics vol.10, pp177-186,1978.

Alic, J. A., International Journal of Fracture, vol.11, pp701-704, 1975.

Amini, B., Wunk, M.P., International Journal of Fracture Mechanics, vol.59, pp 245-264, 1993.

Andersson, H., in Computational Fracture Mechanics, E. F. Rybicki and S. E. Benzly, Eds., ASTM Special Publication, pp. 185-198, 1975.

Andersson, H., Journal of Mechanics and Physics of Solids, vol. 2, pp.285-2308, 1974.

Antolovich, S. D., Shete, P.M., Chanani, G. R. ASTM STP514, p114-134,1971(a).

Antolovich, S.D., Kasi, K., Chanani, G.R.,ASTM STP 514, p135-150, 1971(b).

ASTM D 2344-76 Standart Test Procedures for Interlaminar Shear Strength.

ASTM E 813 Standard Test Method for J_{IC}, A Measure of Fracture Toughness.

ASTM E399-90 Standard Test Method for Plain Strain Fracture Toughness of Metallic Materials.

Balton, J. D., Gant, A. J. Journal of Material Science, vol. 33, pp. 939-953, 1998.

Baron, R. P., Wert, J. A., Gerard, D. A., Wawner, F. E. Journal of Material Science, vol. 32, pp. 6435-6445, 1997.

Barsoum, R. S., International Journal of Numerical Methods in Engineering, vol.10,pp. 25-37, 1976.

Begley, J. A., Landes, J. D., in Fracture Toughness, ASTM STP 514, American Society for Testing and Materials, pp. 1-20, 1972.

Bleackly,M.H., Luxmoor, A.R., International Journal of Fracture, Vol.22, pp. 15-39, 1983.

Bloyer, D. R., Rao, K. T.V., Ritchie, R. O., Material Science and Engineering, A239, pp. 393-398, 1997.

Braess, D., Finite elements: theory, fast solver and application in solid mechanics, published by Cambridge University Press, 1997.

Buchholz, F. G., Accuracy, Reliability and Training in Finite Element Technology Proceedings of the 4th World Congress and Exhibition on Finite Element Methods. pp. 650-659, 1984.

Buchholz, F. G., Rikards, R., Wang, H., International Journal of Fracture, vol. 86, pp. 37-57, 1997.

CES, Cambridge Engineering Selector version 4, developed by Granta Design Ltd., 1999.

Chan, S. K., Tuba, I. S., Wilson, W. K., Engineerin Fractrure Mechanics, vol.2, pp. 1-17, 1970.

Chen, E. P., Sih, G. C., Engineering Fracture Mechanics,14, 195-204, 1980.

Chen, W. Y. C., Winchell, P.G., Scripta Metall. , vol.11 p.289-295, 1977.

Chen, W.H., Wu, C. W., International Journal of Fracture, vol.16, pp. R47-R51, 1980.

Chiang, C.R., Journal of Material Science, vol. 35, pp. 3161-3166, 2000.

Chung, D. S., Enoki, M., Kishi, T., Science and Technology of Advanced Materials, vol. 3, pp. 129-135, 2002.

Clarke, G. A., Journal of Testing and Evaluation vol. 8, pp. 213-220, 1980.

Clarke, G. A., Landes, J. D., Journal of Testing and Evaluation vol. 7, pp. 264-269, 1979.

Clarke, G. A., Andrews, W. R., Begley, J. A., Donald, J. K., Embley, G. T., Landes, J. D., McCabe, D. E., Underwood, J. H., Journal of Testing and Evaluation vol. 7, pp. 49-56, 1979.

Clarke, G. A., Landes, J. D., Begley, J. A. , J. of Testing and Evaluation Vol.8 pp.221-232, 1980.

Clausing, D. P., International Journal of Fracture Mechanics, vol.6, 1970.

Comninou, M, Journal of Applied Mechanics, vol. 44, pp. 631-636, 1977.

Cordes, J., Chang, A., Nelson, N., Kim,Y., Engineering Fracture Mechanics, vol.51, pp. 151-159, 1995.

Cordes, J., Yazici, R., Engineering Fracture Mechanics, vol.47, pp. 441-449, 1993.

Dadkhah, M. S., Kobayashi, A. S., Engineering Fracture Mechanics, vol.34, pp. 253-262, 1989.

Dattaguru, B., Venkatesha, K. S., Ramamurthy, T. S., Buchholz, F. G., Engineering Fracture Mechanics, vol.49, pp. 451-463, 1994.

Davidson, D. L., International Journal of Fracture, vol.96, pp. 359-370, 1999.

Demkowicz,L., Oden,J.T., International Journal of Engineering Science. vol. 24, pp. 55-68, 1986.

De Andres, A., Perez, J.L., International Journal of Solids and Structure, vol.36, pp. 2231-2258, 1999.

De Giorgi, V. G., Kirby III, G. C. Jolles, M.I., Engineerin Fractrure Mechanics, vol.33, pp. 773-785, 1989.

De Konig, A. U., 4th International Conference on Fracture, vol. 3, pp.25-31, 1977.

De Lorenzi, H. G., Shih, C. F., International Journal of Fracture, vol.13, pp. 507-511, 1977.

De Lorenzi, H. G., International Journal of Fracture, vol.19, pp. 183-193, 1982.

Dhar, S., Dixit, P. M., Sethuraman, R., International Journal of Pressure Vessels and Piping, vol. 77, pp. 335-344. 2000.

Dodds, Jr, R. H., Carpenter, W. C., Sorem, W. A. Engineering Fracture Mechanics, vol.29, pp. 275-285, 1988.

Elangovan, P.T., Engineering Fracture Mechanics, vol.40, pp. 433-463, 1991.

Freg, D. Z., Zhang, K. D., Engineering Fracture Mechanics, vol.46, pp. 481-489, 1993.

Fernando, G. M., Menandro,E. T., Moyer, Jr., Liebowitz, H., Engineerin Fractrure Mechanics, vol.50, pp. 713-726, 1995.

Fernando, G. M., Menandro,E. T., Moyer, Jr., Liebowitz, H., Engineerin Fractrure Mechanics, vol.50, pp. 703-711, 1995.

Fraisse, P., Schimit, F. International Journal of Fracture, vol.63, pp. 59-73, 1993.

Fu, S. Y., Lauke, B., Journal of Material Science, vol. 32, pp. 1985-1993, 1997.

Futato, R. J., Aadland, J. D., Van Der Sluy, W. A.,Lowe, A. L., ASTM STP 856 pp. 84-103, 1985.

Gdoutos, E. E., Giannakopoulou, A., Zacharopoulos, D. A., International Journal of Fracture, vol.98, pp. 279-291, 1999.

Gent, A. N., Wang, C., Journal of Material Science, vol. 27, pp. 2539, 1992.

Gent, A. N., Wang, C., Journal of Material Science, vol. 28, pp. 2494. 1993.

Gudas, J. P., and Davis, D. A., Journal of Testing and Evaluation, vol. 10, pp 252-262, 1982.

Han, T. S., Ural, A., Chen, C. S., Zehnder, A.T., Ingraffea, A. R., Billington, S. L., International Journal of Fracture, vol.15, pp. 101-123, 2002.

Hickerson, J., ASTM Committee Meeting E-24, 1976

Hollstein,T., Blauel, J. G., and Voss, B., ASTM STP 856, pp 104-116, 1985.

Hutchinson, J. W., Mear, M., Rice, J. R., Journal of Applied Mechanics, vol.54, pp 828-832, 1987.

Hwu, K. L., Derby, B., Acta Materialia, vol. 47, pp. 545-563, 1999.

Irwin, G.R. Handbuch der Physik, vol.6, p551-590,1958.

Jeng, S. M., Yang, J.-M. and Yang, C. J. Material Science and Engineering, A138, pp. 181-190, 1991.

Karlsson, A., Backlund, J., International Journal of Fracture, vol. 14, pp. R311-R314, 1978.

Kaufman, J. G., ASTM STP 632, pp.3-24, 1977.

Kishimoto, K., Aoki, S., Sakata, M., Engineering Fracture Mechanics, vol.13, pp. 841-850, 1980.

Kobayashi, A. S., Chiu, S. T., Beeuwkes, R., Engineerin Fractrure Mechanics, vol.5, pp. 293-305, 1973.

Krishnamurthy,T., Rammamurthy, T. S., Vijayakumar, K., Dattaguru, B., Finite Elements in Computational Mechanics, Edited by Kant,T., Pergamon Press, Oxford, pp. 891-900, 1985.

Kuang, J. H., Chen, Y. C., Engineering. Fracture. Mechanics, vol. 55, pp. 869-881 1996.

Lamain, L. G., Elastic –Plastic Fracture Mechanics, Edited by Larson, L.H., pp. 227-261, 1985.

Lee, C.K., Lo, S. H., Engineering Fracture Mechanics, vol.50, pp. 671-686, 1995.

Liebowitz,H., Engineerin Fractrure Mechanics, vol.50, pp. 595-600, 1995.

Light, M. F., Luxmoore, A. R., and Evans, E. T., International Journal of Fracture, vol.11, pp. 1045-1046, 1975.

Lou, J., Ye, F., Soboyejo, W. O., Journal of Material Science, vol.37, pp. 3023-3034, 2002.

Mac Neal, R., Finite element: their design and performance., published by M. Dekker, New York, 1994.

Macheret, J., Bucci,R. J., Eng. Fracture Mechanics,vol.45, p729-739, 1993.

Malyshev, B. M., Salganik, R. L., International Journal of Fracture, vol.1, pp. 114-127, 1965.

MARC 2001 volume A User Information Book.

McClintock, F. A., Journal of Applied Mechanics, vol.35, pp363-371, 1968.

McMeeking, R. M., Journal of Mechanics and Physics of Solids, vol. 2, pp.2285-2308, 1977.(p10)

Monaharan, M.G., Ellis, L., Lewandowski, J. J. Scripta Metall., vol.24, p1515-1519,1990 (b).

Monaharan, M. G., Sun, C. T., Composite Science and Technology, vol.39, pp. 99-116, 1990 (a).

Morozov, E. M., Engineering Fracture Mechanics, vol. 13, pp. 541-561, 1979.

Nagtegaal, J. C., Parks, D.M., Parks, D. M., Rice, J., Computer Methods in Applied Mechanics and Engineering, vol. 4, 1974.

Newman, Jr J.C., Elastic-Plastic Fracture Mechanics Technology, ASTM-STP 896, 1985.

Newman, Jr J.C., Booth, B.C., Shivakumar, K.N., ASTM-STP 945, pp. 665-685, 1985

Newman, T. C. and Armen H., Jr., American Institute of Aeronautics and Astronautics Paper No.74-366, AIAA/ASME/SAE Conference, Las Vegas, Nev., 1974.

O'Brien, T. K., Damage in Composite Materials, ASTM STP 775 pp. 140-167, 1982.

Ortiz, M., Pandolfi, A., International Journal for Numerical Methods in Engineering vol. 49, pp. 1267-1282, 1999.

Osman, T. M., Lewandowski, J. J., Lesuer, D. R., Material Science and Engineering, A229, pp. 1-9. 1997.

Pandey, A. B., Majumder, B. S., Miracle, D. B., Acta Materialia pp. 405-417, 2001.

Papanicolaou, G.C., and Bakos, D., Composites Part A, 27A,1165-173, 1996.

Parhizgar, S., Zacharry, L. W., Sun, C. T., International Journal of Fracture, vol. 20, pp. 3-15, 1982.

Parks,D. M., International Journal of Fracture, vol. 10, pp. 487-502, 1974.

Parks,D. M., Computer Methods in Applied Mechanics and Engineering vol. 12, pp. 353-364, 1977.

Qin, S., Zhang, G., Journal of Material Science, vol. 37, pp.879-883. 2002.

Raju, I. S., Engineerin Fractrure Mechanics, vol.28, pp. 251-274, 1987.

Raju, I. S., Crews, Jr. J. H., Aminpour, M. A., Engineerin Fractrure Mechanics, vol.30, pp. 383-396, 1988.

Rice, J. R., Trans. ASME. Journal of Applied Mechanics, 35, 379-386, 1968

Rice, J. R., Sih, G. C., Journal of Applied Mechanics, vol. 32, pp. 418-423, 1965

Rice, J. R., and Tracy, D. M., Journal of Mechanics and Physics of Solids, vol.17,pp.201-217, 1969.

Rice, J. R., Journal of Applied Mechanics vol. 55, pp. 98-103, 1988

Roeck,G. D., Wahab, M. M. A., Engineerin Fractrure Mechanics, vol.50, pp. 569-580, 1995.

Roeck,G. D., Wahab, M. M. A., Engineerin Fractrure Mechanics, vol.49, pp. 659-665, 1994.

Rohatgi, A., Harach, D. J., Vecchio, K. S., Harvey, K. P., Acta Materialia, vol.51, pp. 2933-2957, 2003.

Rybicki,E. F., Kanninen, M. F., Engineerin Fractrure Mechanics, vol.9, pp. 931-938, 1977.

Sakata, M., Aoki, S., Kishimoto, K., Takagi, R., International Journal of Fracture, vol. 23, pp. 187-200, 1983.

Sandhu, J.S., Liebowitz,H., Engineerin Fractrure Mechanics, vol.50, pp. 737-758, 1995.

Schwalbe, K.-H., Hellmann, D., Heerens, J., Knaack, J., and Müller-Roos, J., ASTM STP 856, pp 338-362, 1985.

Sethuraman,R., Maiti, S. K., Engineerin Fractrure Mechanics, vol.30, pp. 227-231, 1988.

Shan, G.X., Kolednik, D., Fischer, F.D., Stuewe, H.P., Engineerin Fractrure Mechanics, vol.45, pp. 99-106, 1993.

Shih, C.F., De lorenzi, H.G., Andrews, W.R., Elastic-Plastic Fracture Mechanics, ASTM STP 668, pp. 65-120, 1979.

Shivakumar, K. N., Newman Jr. J. C., Engineerin Fractrure Mechanics, vol.32, pp. 203-210, 1989.

Simha, N. K., Fischer, F. D., Kolednik, O., Chen, C. R., Journal of the Mechanics,and Physics of Solids, vol. 51, pp. 299-323, 2003.

Sivaneri,N.T., Xie, Y.P., Kang, B.S., Engineerin Fractrure Mechanics, vol.49, pp. 291-303, 1991.

Stump, D.M., and Zywicz, E., Engineerin Fractrure Mechanics, vol.45, pp. 61-77, 1993.

Sun, C. T., Jih, C. T., Engineerin Fractrure Mechanics, vol.28, pp. 13-20, 1987.

Sun, C. T., Monaharan, M. G. Journal of composite Materials, vol. 23, pp. 460-478, 1989.

Underwood, J. H., Winters, D. C., and Kendall, D. P., The Welding Institute, Cambrige, pp.31-39, 1976.

Williams, M.L., Bull. Seismoll. Soc. America. Vol.49, pp 199-204, 1959.

Xia, X., Mcqueen, H. J., Zhu, H. Applied Composite Materials, vol.9, pp.17-31, 2002.

Yagawa,g., Takahashi, Y., Kashima, K., Engineerin Fractrure Mechanics, vol.19, pp. 755-769, 1984

Yang, Q. S., Qin, Q. H., Composite Structures, vol. 53, pp. 403-407, 2001.

Zaho, D., Tuler, F. R., Engineerin Fractrure Mechanics, vol.47, pp. 303-308, 1994.

Zak, A. R., Williams, M. L., Journal of Applied Mechanics, vol.30, pp. 142-143, 1963.

Zheng, M., Wu, K., Yao, C. Material Science and Engineering, A318, pp. 50-56, 2001.

Zhang, J., Lewandowski, J. J., Journal of Material Science, vol. 32, pp. 3851-3856, 1997.

VITA

Mehmet Şimşir was born in Kaman on May 25, 1968. He received his B.S. and M.S. degrees in Metallurgical and Materials Engineering from the Middle East Technical University in July 1991 and January 1995 respectively. He worked in ÇEMAŞ, Kırşehir for two years. In 1994, he joined the Department of Metallurgical and Materials Engineering in the Cumhuriyet University. He has been a member of the UCTEA Chamber of Metallurgical Engineers since 1991. His main areas of interest are fracture mechanics, laminated composites, modeling of fracture toughness with finite element analysis and nondestructive testing.

PUBLICATIONS

M. Şimşir, 'Determination of sensitivity and reliability of NDI techniques on damage tolerance based life prediction of turbine discs', M.S. Thesis Middle East Technical University, January 1995.